Modeling and Implementation of Solder-activated Joints for Single Actuator, Centimeter-Scale Robotic Mechanisms

by

Maria J. Telleria

Sc.B. Mechanical Engineering
Massachusetts Institute of Technology, 2008

Submitted to the Department of Mechanical Engineering
in Partial Fulfillment of the Requirements for the Degree of
Master of Science in Mechanical Engineering

at the

Massachusetts Institute of Technology

May 19th, 2010
[June 2010]

Signature of Author.....
Department of Mechanical Engineering
May 19th, 2010

Certified by.....
Martin L. Culpepper
Associate Professor of Mechanical Engineering
Thesis Supervisor

Accepted by.....
David E. Hardt
Professor of Mechanical Engineering
Graduate Officer

Report Documentation Page

Form Approved
OMB No. 0704-0188

1. REPORT DATE	2. REPORT TYPE	3. DATES COVERED
JUN 2010		**00-00-2010 to 00-00-2010**

4. TITLE AND SUBTITLE	5a. CONTRACT NUMBER
Modeling and Implementation of Solder-activated Joints for Single Actuator, Centimeter-Scale Robotic Mechanisms	5b. GRANT NUMBER
	5c. PROGRAM ELEMENT NUMBER
6. AUTHOR(S)	5d. PROJECT NUMBER
	5e. TASK NUMBER
	5f. WORK UNIT NUMBER
7. PERFORMING ORGANIZATION NAME(S) AND ADDRESS(ES) **Massachusetts Institute of Technology,77 Massachusetts Avenue,Cambridge,MA,02139**	8. PERFORMING ORGANIZATION REPORT NUMBER
9. SPONSORING/MONITORING AGENCY NAME(S) AND ADDRESS(ES)	10. SPONSOR/MONITOR'S ACRONYM(S)
	11. SPONSOR/MONITOR'S REPORT NUMBER(S)

12. DISTRIBUTION/AVAILABILITY STATEMENT
Approved for public release; distribution unlimited

13. SUPPLEMENTARY NOTES

14. ABSTRACT

This thesis explains when, and why, solder-based phase change materials (PCMs) are best-suited as a means to modify a robotic mechanism's kinematic and elastomechanic behavior. The preceding refers to mechanisms that possess joints which may be thermally locked and unlocked via a material phase change within the joint. Different combinations of locked and unlocked joints yield different one-DOF mechanisms states. A single actuator is used to control motion allowed by the different states. By reducing the number of required actuators, solderlocking joints enable the creation of compliant centimeter-scale mechanisms that can perform a multiplicity of tasks. Herein, this thesis presents physics-based design insights that provide understanding of how solder-based material properties and joint design dominate joint performance characteristics. First order models are used to demonstrate selection of suitable PCMs and how to set initial joint geometry prior to fine tuning via detailed FEA models and experiments. The first order models result in order-of-magnitude estimates of the locking and unlocking times for the joints. The insights and models are discussed in the context of two case studies. Squishbot1 is a crawling robot that uses a single spooler motor and three solder-locking joints to crawl and steer. Squishbot 1 is able to reconfigure its joints in approximately 10 seconds. SquishTendons utilizes solder-locking joints to actuate a compliant structure with a single motor. The second robot used the complete set of models and rules to improve on the performance of Squishbotl. SquishTendons can unlock and lock its joints in less than 6 seconds.

15. SUBJECT TERMS

16. SECURITY CLASSIFICATION OF:			17. LIMITATION OF ABSTRACT	18. NUMBER OF PAGES	19a. NAME OF RESPONSIBLE PERSON
a. REPORT **unclassified**	b. ABSTRACT **unclassified**	c. THIS PAGE **unclassified**	**Same as Report (SAR)**	**149**	

Modeling and Implementation of Solder-activated Joints for Single Actuator, Centimeter-Scale Robotic Mechanisms

by

Maria J. Telleria

Submitted to the Department of Mechanical Engineering
on May 19th, 2010 in Partial Fulfillment of the
Requirements for the Degree of Master of Science in
Mechanical Engineering

ABSTRACT

This thesis explains when, and why, solder-based phase change materials (PCMs) are best-suited as a means to modify a robotic mechanism's kinematic and elastomechanic behavior. The preceding refers to mechanisms that possess joints which may be thermally locked and unlocked via a material phase change within the joint. Different combinations of locked and unlocked joints yield different one-DOF mechanisms states. A single actuator is used to control motion allowed by the different states. By reducing the number of required actuators, solder-locking joints enable the creation of compliant centimeter-scale mechanisms that can perform a multiplicity of tasks. Herein, this thesis presents physics-based design insights that provide understanding of how solder-based material properties and joint design dominate joint performance characteristics. First order models are used to demonstrate selection of suitable PCMs and how to set initial joint geometry prior to fine tuning via detailed FEA models and experiments. The first order models result in order-of-magnitude estimates of the locking and unlocking times for the joints. The insights and models are discussed in the context of two case studies. Squishbot1 is a crawling robot that uses a single spooler motor and three solder-locking joints to crawl and steer. Squishbot1 is able to reconfigure its joints in approximately 10 seconds. SquishTendons utilizes solder-locking joints to actuate a compliant structure with a single motor. The second robot used the complete set of models and rules to improve on the performance of Squishbot1. SquishTendons can unlock and lock its joints in less than 6 seconds.

Thesis Supervisor: Martin L. Culpepper
Title: Professor of Mechanical Engineering

ACKNOWLEDGEMENTS

I am very grateful for Prof. Culpepper's mentorship throughout my academic career. Under his guidance I have become a better researcher, student, and mentor to other students. I look forward to continuing working and learning in his laboratory.

This material is based upon work supported by the U. S. Army Research Laboratory and the U. S. Army Research Office under contract/grant number W911NF-08-C-0055.

To my SQUISHbot team members, this project would not have been the same without any of you. It was a pleasure to work with all of you on this challenge. To everyone in the Precision Compliant Systems Lab, thanks for your help. I look forward to continuing working with you. Finally, I want to thank my family and friends who have always helped me every step of the way. I specially want to thank those who took the time to read and review this thesis.

I am so thankful for everyone's support and friendship throughout the entire project.

CONTENTS

FIGURES

TABLES

CHAPTER

1

INTRODUCTION

1.1 Introduction of Research

The purpose of this thesis was to understand what dominates and limits the behavior of solder-activated mechanism joints. This information is presented as design guidelines and modeling methods that enable engineers to effectively create joints that are locked using a phase change material (PCM) [1]. The concepts produced by this thesis make it possible to design, optimize, and fabricate a solder-locking joint to achieve a desired performance. Figure 1.1 presents a solder-activated joint that was designed while developing these design rules. The figure highlights the different components of a typical solder-locking joint.

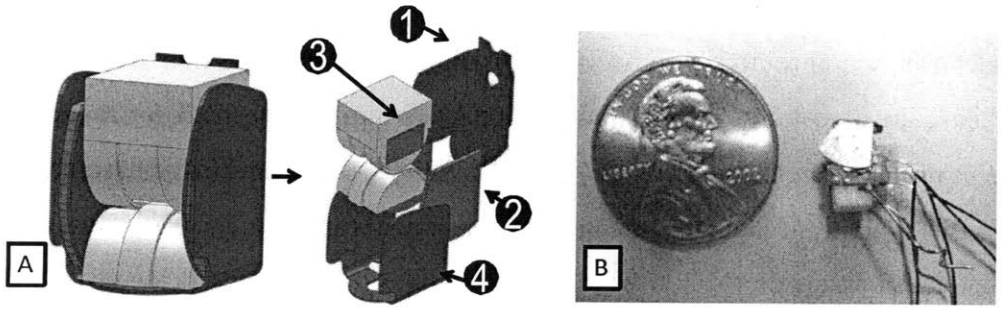

Figure 1.1: Sample solder-activated joint. (A)The joint, in light grey, uses flexures to keep the top and bottom half-cylinders in contact. Rolling of the top half-cylinder over the bottom is constrained when the solder (2) between the two copper pieces (1 & 4) is solidified. Current is run through a strain gage (3) within the joint to melt the solder. (B) Picture of an actual solder activated joint designed and built using this thesis.

The design of PCM activated joints involves the use of mechanical, kinematic, and thermal domains. The joint design problem is highly coupled, therefore modeling and experimentation rather than intuition and iteration are the fastest means to achieve useful performance. This thesis provides the basis to understand (i) the physics that dominate and limit

joint performance, (ii) how to select and design the PCM, and (iii) how to rapidly use 1st order models to set an initial joint geometry for specific performance characteristics.

PCM activated joints allow for the creation of single actuator, cm-scale, multi degree-of-freedom (DOF) robots. Joints are locked in combinations that enable different one-DOF mechanism states. All of the mechanism states are actuated with a single motor. The multi-DOF nature of the resulting robots allows them to be more flexible in the variety of tasks that they may perform. This actuation approach enables the creation of robots using compliant components. Compliant components and robots are defined as having a multiplicity of DOF, which may be locked using PCMs to perform different functions. Compliant robots are necessary in applications requiring the mechanism to travel through restricted paths.

1.1.1 Motivation

A troublesome problem in multi degree-of-freedom (DOF), centimeter-scale (cm) robot design is the need for multiple sub-cm actuators. It is often impossible to find off-the-shelf actuators that exhibit the requisite force or torque, power, and speed characteristics in a sub-cm package. Even if one could find suitable actuators, there are other practical issues associated with miniaturization. For example, it is difficult to create suitably small, stiff and strong mounting points for many small actuators upon a small mechanism. Also, the packaging of requisite electronics and routing of power lines to multiple actuators is non-trivial.

Solder activated joints enable the creation of compliant mechanisms that are capable of exhibiting several different, single DOF outputs with a single mechanical actuator input. An example of this type of mechanisms is Squishbot1, shown in Figure 1.2. The reduction in number of actuators leads to a smaller robot, which in turn makes it possible to design robots that exhibit reduced: (i) power consumption, (ii) weight, (iii) control complexity, (iv) size, and (v) cost. Achieving the proceeding is possible if the mechanism's joints may be turned on and off, via solder melting-solidification, in combinations that modify kinematic behavior of the mechanism. One actuator may be used to control motion allowed by a first state, then a new combination of locked/unlocked joints may be set and the same actuator then controls motion allowed by the new state.

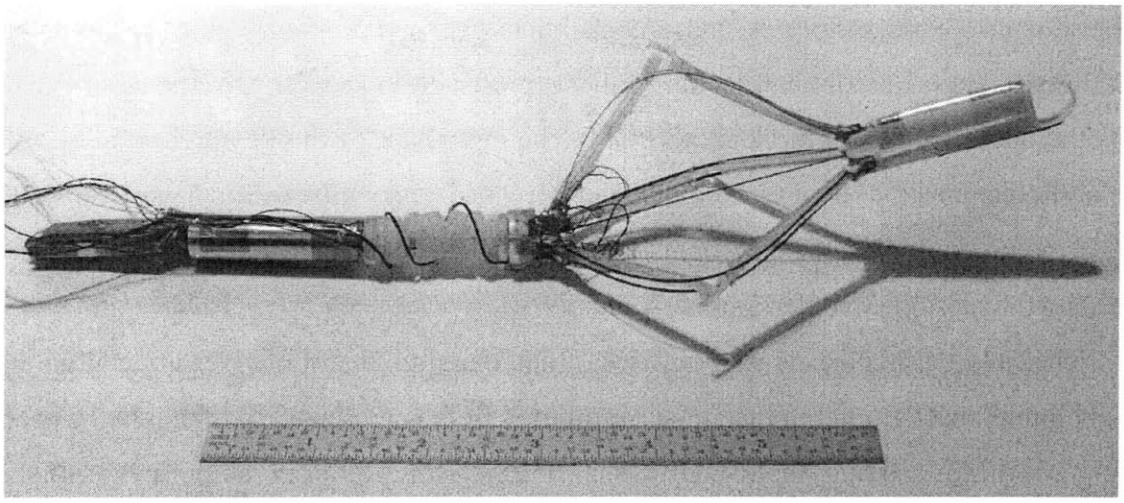

Figure 1.2: Squishbot1, a single actuator robot that is able to achieve multiple single DOF mechanism states through solder-activated joints.

Single actuator, cm-scale mechanisms fill a gap in the robotics field. Traditional robots are limited by the amount of actuators that the design may afford to carry or power, which in turn limits their DOF. The ability to design single actuator machines with more DOF leads to the creation of cm-scale robots that may perform tasks impossible to current small-scale robots. The large amount of actuators required in current mechanisms limits their flexibility. This thesis may be used to create compliant robots that have new and expanded functionality.

The applications for small compliant robotics are broad. Search and rescue, as well as military operations, would benefit from robots that could gain access to restricted and hard to reach places. Current robots used in military and rescue operations have limited mobility and are often size-limited in the places they may reach. Another application is medicine. It has long been envisioned to use small-scale robots to perform procedures inside the body [2]. Multi-DOF, compliant, single actuator robots would be ideal in many medical applications. The use of a single motor would reduce the mechanism's cost enabling the design of disposable robots. The machine's compliance would allow for it to be less invasive. Another application that could benefit from robots with increased articulation and reduced actuation is pipe system exploration.

1.2 Scope

This thesis focused on single actuator, multiple DOF robots with active joints that enable miniaturization for cm-scale robotic mechanisms. The author's research has explored how to use

a variety of active fluids to lock and unlock joints [3]. A discussion on active fluids and the selection of solder as an optimal locking fluid is presented in section 1.5. The rest of the thesis details the use of solder as the locking PCM. The end result of this research is guidelines and models that demonstrate how to design solder-activated joints effectively. Two case studies, of single-actuator, multiple-DOF mechanisms are provided to demonstrate the use of the thesis results and the feasibility solder-locking joints.

The field of small scale robotics is vast and therefore, hard to cover in detail in a single work. A limited background of the cm-scale robotics field is presented to highlight the need for a new approach to creating multi-DOF small mechanisms. A brief summary of the solder knowledge that has been gathered by the electronics packaging industry is included. There is a wealth information available on solders in a variety of works [[4]-[6]], however it is too large and not the main focus of this thesis and is therefore better explored as required by the reader.

1.2.1 Work Organization

The core of the thesis focuses on presenting the guidelines and models that have been developed to design and optimize solder-activated joints. These insights are presented in two sections (i) solder design and (ii) joint design. The first case study, Squishbot1, is shown in Figure 1.2. Squishbot1 was created while the design rules were being developed. The second case study, the locking tendons application shown in Figure 1.3, was developed using the completed guidelines and models. Consequently, its joint performance is superior to that of the joints in Squishbot1. The two examples are used to demonstrate the efficacy of the rules and models.

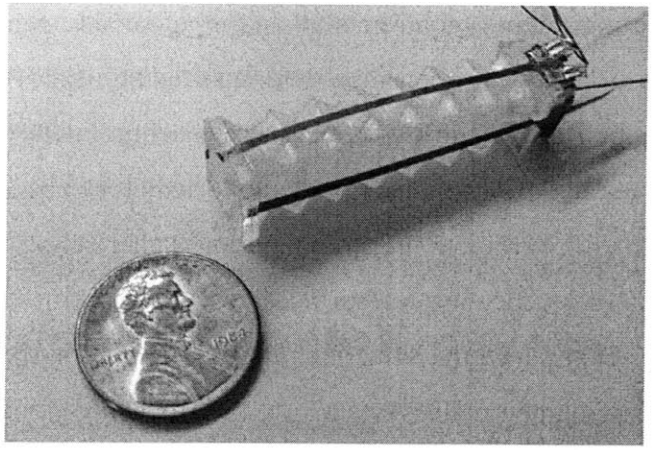

Figure 1.3: The SquishTendons locking mechanism, which was designed with the full set of rules and insights for effective solder-activated joint design.

1.3 Knowledge and Technology Gap

1.3.1 Challenges of cm-scale Robotics

The state-of-the-art in cm-scale robotics is largely limited by the size and weight of actuators and energy sources. Advances in miniature motors and batteries are ongoing [[7]-[9]]. However, they are not yet practical; in addition, there will always be the desire to make smaller mechanisms. The combination of active joints and single actuators is a powerful technology that enables small-scale compliant robots.

Un-tethered mechanisms must carry their own energy source. The smaller the mechanism, the smaller the battery it may carry, and the less energy available for actuation and other tasks. Available energy is the main limitation on the design of cm-scale mechanisms. As a result, it is important that cm-scale robots make efficient use of their limited power supply. The constraint is amplified when trying to create multi-DOF robots. The power available limits the number of actuators that may be used. It is also a salient issue when trying to use active joints. If the active fluid is not chosen carefully, the actuation energy will be too high. The active fluid and the joint must be carefully co-designed to yield viable designs. Available power is the largest limitation in cm-scale robots. The design of the mechanism must use the energy available efficiently to enable multiple-DOF.

The choice of actuator is limited, in part, by the energy source. The actuator must be able to provide enough force or torque to move the weight of the battery. The motor must also be able to produce this output with minimal power input. Therefore, vetting of actuators must include

criteria such as size, weight, output requirements, and input requirements. Appendix A shows a comparison of the motors that were considered for use in Squishbot1. This information was collected by Don Campbell of Boston Dynamics. The list highlights that actuators with more than one Newton of force are too large for more than one actuator to be used in a cm-scale robot.

Problems with traditional joints, e.g. revolute and spherical, arise when they are scaled down. Coulomb friction is independent of surface area; therefore, two geometrically identical joints at different scales experience the same amount of friction. On the other hand, the inertial effects on the joint scale volumetrically. As a result, the smaller joint experiences a higher ratio of frictional to inertial effects [10]. Essentially, energy loss in the joints may outweigh energy required for locomotion. As such, frictional effects may be prohibitive at small enough scales. Another disadvantage of miniaturized traditional joints is backlash. Backlash scales with clearance which is approximately the same for small and large joints. In mm-scale devices the backlash may be a large percentage of the joint's motion. As a result, mm-scales joints may be difficult to control. Flexural joints do not suffer from these limitations at any scale, because they rely on compliance of members as opposed to sliding and rolling. Therefore, flexural joints are better suited for cm-scale robots.

Most traditional robot designs require one actuator per DOF. The limitations of small-scale energy sources, actuators, and joints compound to limit a robot to use a few actuators. Therefore, the mobility of robot is limited to a few DOF. New concepts are necessary to enable cm-scale robots to increase their mobility. The ultimate goal for roboticists is to have small-scale compliant robots that have many DOF, so that they may perform a variety of different tasks. This thesis achieves multiple-DOF, circumventing the limitations of cm-scale robots, by using a single motor in conjunction with active flexural joints. The resulting mechanisms are able to perform a multiplicity of functions with a simple control scheme, advancing the field one step closer to compliant small-scale robots.

1.3.2 Small, Multi-DOF Robot Approaches

1.3.2.1 Linking of multiple mechanisms

The constraints on cm-scale mechanisms have led to the generation of concepts that enable increased mobility of small-scale robots. One of these approaches is to link multiple small-scale mechanisms together to perform tasks that a single robot cannot perform by itself.

The Carnegie Mellon University Millibot train is a good example of this approach [11]. The train is composed of cm-scale semiautonomous sensing and communication modules, referred to as Millibots. The modules use caterpillar tracks to drive and steer. The individual modules are unable to translate out of the terrain plane and therefore have limited performance. Investigators argue that by allowing the Millibots to couple to one another, both mechanically and electronically, they create a train that may control its shape in two dimensions. This train may then perform an increased number of tasks that any individual robot would be unable to perform [11].

In this approach, each module remains constrained by the size and weight of the required actuators and the energy sources. Each module has a couple DOF because it can only contain a couple actuators. Therefore, a train of building blocks is essentially a larger scale robot that requires multiple actuators, at each module, to control separate DOF.

1.3.2.2 Multiple Small Actuators

Shape memory alloys (SMA) are part of new class of actuators, known as 'soft' actuators [12]. SMA actuators diameter, 0.2-0.85mm, is orders of magnitude smaller than traditional actuators; therefore, a cm-scale robot may encompass hundreds of SMA wires within its volume [13]. These alloys are not without drawbacks. The force produced by SMA actuators is proportional to the applied voltage. To generate one Newton forces may require hundreds to thousands of volts [12]. The Carnot efficiencies for SMA actuators have been calculated to be below 10% [14]. Higher efficiencies are desired given the limited available power. The motor used in Squishbot1 has an efficiency of 54%.

SMA's have been used to control the shape of compliant structures that enable locomotion over different terrains. In these mechanisms, a compliant structure is deformed by extending and contracting different SMA wires. The structure is deformed in such a way to enable it to perform different tasks, such as crawl and jump [12]. This type of approach to cm-scale mechanisms is limited by the performance of the SMA actuators.

1.3.2.3 Single Actuator

Under-actuated mechanisms have fewer inputs than DOF. These types of robots often require complex control schemes to achieve the desired outputs using a single input [15]. A

locking joint approach enables different, one-DOF mechanism states that respond to the same input without the complicated control systems because the actuator control is independent of the desired mechanism task. The joints constrain the motion leading to different mechanism states. Using active joints avoids the complex control schemes of other under-actuated mechanisms, making easier for the designer to achieve the desired functions.

1.4 Research Approach

This research seeks to avoid the limitations of cm-scale actuators by reducing the number of actuators in the robot design. Locking/unlocking joints are used to achieve different one-DOF mechanism states with a single motor. The joints may be locked in various combinations to achieve a range of mechanism states. Active fluids are proposed as the best way to lock mm-scale joints because they may be used to lock the joints without any moving mechanisms. Therefore, the resulting joint has reduced complexity making it easier to fabricate and assemble. Active fluids have field-tunable rheological properties. This thesis focuses on thermo-rheological fluids (TR), which experience a phase change due to temperature. TR fluids were selected because these are the strongest active fluids, the most widely available, and they scale down favorably. Solder is the ideal PCM because of its high diffusivity, which enables it to adjust its temperature quickly. Quick temperature adjustments of the locking material are necessary in order to achieve short joint activation times.

PCM's have been used for mechanism fixation within MEMS and in micro-optical alignment [16]. In these prior works, the mechanism was fixated by the PCM, thereby enabling locking of position and orientation without powered actuation. This concept differs from the presented approach as it does not change the mechanism's kinematic or elastomechanic behavior. The mechanism approach presented herein encompasses the use of PCMs that lock and unlock joints, thereby altering the mechanism's kinematic and elastomechanic behavior. The use of PCM joints was first suggested and experimentally verified via bench-level experiments (using hot glues) by Boston Dynamics.

1.5 Active Fluids

In general, joint locking and unlocking may be achieved with a variety of active fluids. This thesis focuses on PCMs. An overview of competing materials is provided as a basis for arguing why solder-based PCMs are well-suited for small-scale robotics applications.

1.5.1 Introduction

Active fluids possess tunable rheological properties. They are classified by the means used to cause a change in state within the fluid. For example, the resistive shear stress within magneto-rheological (MR) fluids is proportional to the magnetic field within the fluid. Failure stresses of 50kPa (7.25 psi) have been reported for this type of fluid [17]. MR fluids have been used in vibration dampers and locking spherical joints [17],[3]. The failure stress within electro-rheological (ER) fluids is controlled by the electric field within the fluid. Failure stresses of 130 kPa (18.9 psi) have been reported [18].

The imposition of a field in MR and ER fluids forces nanoscale particles to align within the fluid thereby enabling the fluid to resist deformation [17],[18]. This alignment mechanism endows them with millisecond response times but places fundamental limits on failure stresses (at practical field strengths). The failure stress determines the strength of a locked joint and therefore the strength of the mechanism.

The change in state of photo-rheological (PR) fluids is caused by exposure to ultra violet light. The UV light induces a chemical change within the fluid that leads to a change in deformation resistance characteristics. Viscosity changes of four orders of magnitude have been reported, however, the highest absolute viscosity is comparable to that of honey, 10 Pa-s [19]. For robotic applications, the fluid must be reversible, meaning it needs to be able to switch between soft and hard states. Most PR fluids are non-reversible, and therefore cannot be returned to their original soft state once activated. This non-reversability would result in PR-activated joints that could not be unlocked. There are a limited number of newly-available reversible PR fluids; however, their response time is slow, around four minutes [20]. A favorable characteristic of PR fluids is that they do not require constant energy input to maintain a locked state, unlike MR and ER fluids.

Thermo-rheological (TR) fluids achieve a change in state via temperature change. For practical purposes, the discussion is limited to those TR fluids which change phase within

temperatures, a few 100°C above room temperature, that are reasonable for robotics applications. This thesis considers TR fluids to be in their off-state at room temperature.

Common TR fluids - solders (~ 40 MPa), and hot glues (~ 5 MPa) - exhibit failure stresses that are well above those of MR, ER and PR fluids. For a given joint geometry, they provide higher strength; however, they are impractical if the fundamental issues governing the (i) energy requirements and (ii) lock/unlock speed are not addressed. Phase change is inherently energy intensive, which is problematic given the limited energy that may be stored on-board a small robot.

The thermal characteristics of the PCM – specific heat capacity, latent heat of fusion and melting temperature – must be selected in order to minimize melting energy. It is critical to use the available power efficiently as there are no suitable small-scale heat recovery devices, e.g. thermoelectrics, which could recapture heat energy. It is important to note that the limits of solidification/lock and melting/unlock speeds equate to robot speed. The activation speeds are defined in-part by the thermal characteristics of the TR fluid. Melt time is inversely proportional to power, which is in limited supply. The length of cooling time is determined in-part by the PCM's thermal diffusivity (varies widely between TR fluids) and the convection of heat out of the PCM.

The Pugh chart in Table 1.1 contains a qualitative comparison of the different types of active fluids. The table contains two types of TR fluids to better represent the wide range in properties that may be seen in TR fluids.

Table 1.1: Active Fluid Comparison Pugh Chart Based on Common Considerations in Robotic Design* [2,4-9].

	PR	MR	ER	Wax	Solder
Activator	UV light	Magnetic Field	Electric Field	Temperature	Temperature
Speed	0	+ +	++	0	+
Activator Weight	0	-	+	+	+ +
Strength	0	+	+	+	+ +
Power	0	0	0	0	+
Scalability	0	- -	-	0	0

*PR is used as a baseline for qualitative comparison. A "+" signifies that the fluid has a better performance in that category than the PR fluid. While "-" signifies that the fluid has a worse performance in that category than the PR fluid.

1.5.2 The Case for Solder as an Active Fluid in Robotics

The strength of solder in its locked state is at least an order of magnitude larger than that of other active fluids. Solders have a high thermal diffusivity, which is typically at least an order

of magnitude larger than that of waxes and glues. Their diffusivity enables solder to quickly spread thermal energy throughout its volume, thereby speeding melting and solidification. Thermal diffusivity is the relevant thermal property to obtaining short response time in TR fluids. Glues and waxes have low diffusivity and are, therefore, slow to melt and solidify. In contrast, anyone who has soldered wires for electronics knows how rapidly solders may be melted and cooled.

The electronics packaging community has created many different solders, and characterized their melt energy, melt times and solidification times. Therein lays a wealth of knowledge regarding material properties of solders and guidance on customizing properties. When thermal and mechanical requirements are not satisfied by off-the-shelf solders, it is possible to modify their composition through alloying and thereof obtain the desired characteristics. The solder design process is covered in detail in Chapter 2 of this thesis.

1.6 Summary

Many applications for small-scale mechanisms require that the robot be able to perform different tasks, which requires a multiplicity of DOF. The ultimate goal is to create compliant robots which have many DOF enabling them to accomplish functions that state-of-the-art, limited-DOF robots cannot perform. Available power and size of usable actuators limits the number of actuators in cm-scale mechanisms. Active joints make it possible use a single actuator to achieve a multiplicity of DOF. Active fluids are used to lock the joints because they may be used to lock the joints without any moving mechanisms. The moving mechanisms would increase the complexity of the joint design. Solder is the best active fluid to use because it provides a quick, strong, and scalable way to lock active joints.

The rest of this thesis presents the insights and models necessary to efficiently and effectively design and implement these solder-activated joints. Chapter 2 presents models and insights for how to design the solder, through alloying, to optimize activation times. The design insights, methods, and rules for the kinematic, thermal, and mechanical design of the active joint are covered in Chapter 3. Chapters 4 and 5 detail two case studies of mechanisms that use solder-activated joints. The first case study, Squishbot1, was designed as the models and insights of this thesis were being developed. The second example, SquishTendons, uses the full set of rules to create a mechanism with active joints with improved performance over those in Squishbot1.

CHAPTER

2

SOLDER DESIGN

2.1 Solder as a Joint Locking Mechanism

Solder is an excellent joint locking mechanism because of its locking strength and thermal properties. Its yield stress is orders of magnitude higher than other active fluids and its thermal properties make it possible to cycle it faster than other thermo-rheological fluids. Solder refers to a broad category of fusible metal alloys which are used to join two surfaces [4]. The alloy composition of a solder determines its mechanical and thermal properties, therefore, one may tune the characteristics of a solder by changing its composition. When designing solder-activated joints, the material's tuning ability allows the designer to achieve the desired joint performance. This chapter describes the solder parameters that determine the performance of the joint and explores how these parameters change depending on the composition of the solder. The scope is limited to discussing only the properties that play a role in joint performance, as opposed to all mechanical and thermal properties of solders.

The solder composition discussion is limited to lead-tin base solders. These particular solders are the most common and well-studied. Lead-tin solders have excellent wetting and strength properties for their low-cost [5]. The analysis presented herein for choosing a solder composition may be applied to any base composition given the designer has access to data on the performance of the solders. Lead-free solders are growing in popularity given environmental and health concerns. As more information becomes available one should consider these as they are non-toxic. The focus here is to present the guidelines for designing solder-activated joints, not to investigate different compositions of solder. Lead-tin solders provide a good starting point thanks to the wealth of information available on their thermal and mechanical performance.

2.2 Important Mechanical Properties for Joint Locking

2.2.1 Yield Strength

When working with cm-scale mechanisms the size of the active joint is most likely on the order of millimeters. At this scale the solder is often stronger than the mechanism components themselves, and therefore solder strength is not a limiting factor. It is important that the designer understand what parameters affect the yield strength of a solder and how to calculate the locking strength of a joint. This strength may be traded off to obtain more favorable thermal properties when tuning the solder composition.

There are several concepts for joint designs where locking could be implemented, and they are classified by the solder loading mechanism. Shear and tension are the most common loading modes, but torsion, compression, and combinations are possible as well. The shear and tension modes are shown in a generalized geometry within Figure 2.1. The yield stress of the solder depends on the loading mechanism. The tensile strength of lead-tin solders is generally higher than the shear strength [6].

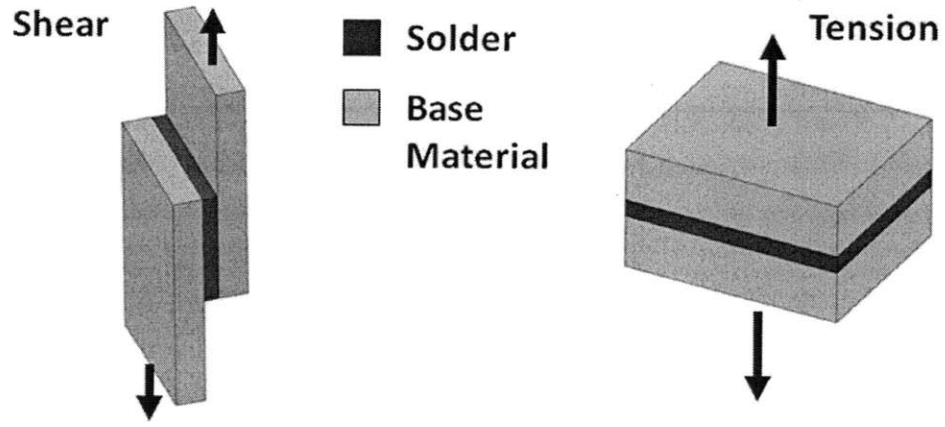

Figure 2.1: Generalized Shear and Tension Solder Joint Geometries.

The strength of a TR, thermo-rheological, joint may be calculated using the appropriate failure stress (shear or tension) of the solder and the surface area of the joint. Equation (2.1) links failure load, F_{yield}, to failure stress, σ_{yield}, via the area, A_{load}, over which the solder resists load. Equation (2.1) gives a good approximation of the failure load [5].

$$F_{yield} = A_{load} \cdot \sigma_{yield} \tag{2.1}$$

The failure stress values of solders are readily obtained from standard electronics handbooks [4]-[6] or from manufacturers. Most solders are metal alloys, and changing the mass fraction of alloying elements induces changes upon thermal and mechanical properties, including yield strength. Other properties of the joint may also affect its locking strength. Changes in the locking gap, ideally 10-100 micrometers, may affect the strength of the joint [4]. It is also known that the mechanical and thermal properties of the base material require consideration. For example copper-tin/lead joints generally have the highest shear strength. The joining and operating temperatures may also affect strength [5]. As presented in Table 2.1, there are several factors that may affect strength, therefore, it is optimal to use standard failure stress data to obtain a first approximation for joint strength and to follow best practices [4]-[6] for other factors. If other factors become relevant, experimentation is used to quantify their effect on joint performance.

Table 2.1: List of general factors that affect solder joint locking strength [4]-[6].

Solder Composition
Solder Loading Mode
Joint Geometry
Joint Gap
Base Material Composition
Joining Temperature
Operating Temperature

Creep strength of the joint is important if the joint is going to be loaded for an extended period of time. The creep of a material is highly temperature dependant [6]. In this research, energy efficiency demands that joints not be held at high temperatures for long times. This thesis, therefore, assumes that joints are not loaded at temperature and stress beyond creep limits for long periods of time, therefore, creep did not play a major role.

2.2.2 Ease of Soldering

The compatibility between the solder and the base material must exists for a joint to be locked. This compatibility is often quantified by the contact angle between the two materials. Figure 2.2 illustrates the contact angle and the surface tensions involved when a liquid comes into contact with a solid. The liquid spreads over the solid surface to balance the surface tensions between the liquid solder, the solid base material, and the atmosphere [4]. A contact angle less

than 90° corresponds to an imbalance of surface tensions which results in the solder spreading over the surface [4]. The smaller the contact angle the larger the area the solder spreads over. Joints that use solders and base materials with low contact angles have increased wetting [4].

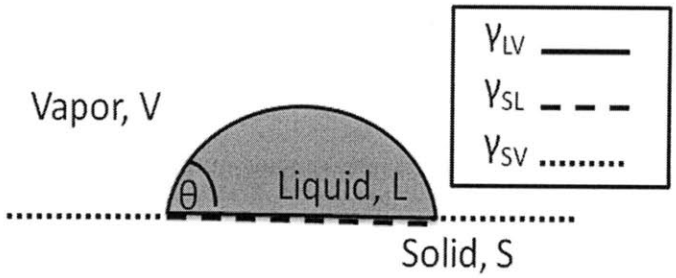

Figure 2.2: Solder Wetting Model. Surface tension forces act on the solder droplet. The variable γ_{SV} represents the surface tension between the solid and the vapor, γ_{LV} liquid vapor surface tension, and γ_{SL} solid liquid surface tension. Theta, θ, denotes contact angle. [4]

The contact angle equation provides insight as to how to improve the wetting of the solder. As Equation (2.2) shows, the contact angle, θ, may be decreased by increasing the solid-vapor surface tension, γ_{sv}, and/or decreasing the solid-liquid surface tension, γ_{sl}, and/or liquid-vapor surface tension, γ_{lv}.

$$\cos\theta = \frac{\gamma_{SV} - \gamma_{SL}}{\gamma_{LV}} \tag{2.2}$$

The solid-vapor surface tension may be maximized by cleaning the solid surface, as is often done with a flux. The other two surface tensions may be varied by changing the composition of the solder. The solid-liquid surface tension is also dependant on the soldering temperature. The liquid-vapor surface tension may be reduced by altering the pressure of the atmosphere [4]. Table 2.2 summarizes the factors that influence the surface tensions. Putting this information in the context of joint locking, it is clear that ambient conditions on a robot are hard to control when the mechanism is being deployed in different environments. The temperature of the joint may be raised to achieve better wetting, however this greatly increases the energy consumption. It is, therefore, best to choose the solder composition and base material carefully, in order to achieve a low contact angle.

Table 2.2: Factors that may be modified to decrease the contact angle between liquid and solid. [4].

Decrease Contact Angle	Soldering Properties
Increase γ_{SV}	Clean solid surface Flux
Decrease γ_{SL}	Solder Composition Soldering Temperature
Decrease γ_{LV}	Solder Composition Soldering Pressure

2.2.3 Solder Composition

There are many alloying elements that may be added to a common lead/tin solder to tune its material properties. Table 2.3 shows the trends in several key properties of the solder when a few common alloying elements are added [4]-[6]. Table 2.3 portrays general trends that are appropriate as guidelines for first order design. More details may be found in the table's references [4]-[6].

Table 2.3: Trends in solder properties with addition of alloying Elements [4]-[6]+

Element	Strength	Ease of Soldering	T_{Melt}	Creep Strength
Indium	↓	↓	↓	↓
Bismuth	↓	↓	↓	↓
Antimony (<6%)	↑	↓	≈	↑
Silver (<5%)	↑	↑	↑	↑

+Symbols indicate whether adding the element to lead-tin solders increases (↑), decreases (↓), or has little effect (≈) on the properties [1-3].

The effect on the melting temperature of the solder has been included in Table 2.3. This change in melting temperature is important because the melting point plays a large role in the performance of the joint. Once the thermal constraints on the solder design are understood, it may be found favorable to sacrifice solder strength for improved thermal properties, in particular, melting point.

2.2.4 Importance of Cycling

A thermally activated joint must be able to withstand multiple cycles before de-wetting, de-lamination or crack formation occur. These types of failures are not deterministic and

therefore should be investigated via experimental thermal cycling. Unfortunately, there is only modest information available given most solder joints are only cycled once; as a result experiments are often necessary. There is some information available that indicates how solder composition may affect cycling. For example, Indium base solders may fail because of phase segregation when there is an extreme and unidirectional thermal gradient across the joint. Bismuth may become brittle if it solidifies rapidly [4]. From experience, it is known that the best means of ascertaining the risk associated with these failures is to conduct failure tests.

2.2.5 Rules, Trade-offs, and Caveats

Solders typically mechanically over perform as mm-scale joint locking mechanisms. The mechanical constraints on solder design are locking strength and the ability of the solder to wet the locking mechanism material. Although these design constraints may seem trivial because of the high solder strength, the joint is likely fail if they are not taken into consideration. In particular, the wetting ability may be an issue due to the cycling imposed on the joints. The main mechanical insights that should be considered when choosing a solder are:

(1) Understand how the solder is loaded, and its yield stress. Use this information to determine how much strength may be sacrificed for improved thermal properties without risking locking failure.

(2) Creep strength may be an issue if the joint is submitted to large loads for extended periods of time. Energy limitations typically make creep a non-issue.

(3) Follow well-established soldering practices to achieve maximum strength for a given solder composition.

(4) Solder composition must be chosen with the locking mechanism material in mind. The wetting ability of a solder is especially important because of joint cycling. Cycling may lead to problems involving: oxidation, de-lamination, and contaminants.

(5) Experimentation is the best way to address cycling concerns. Time should be devoted to investigating how the mechanical properties change with cycling.

2.3 Important Thermal Properties

The thermal performance of a joint is measured by (i) the amount of energy required to activate the joint and (ii) the locking/unlocking cycle time. Solder's thermal properties influence

this performance, and as such require understanding. This understanding enables the designer to choose the best solder for optimizing performance. This chapter discusses the properties affecting energy consumption: melting point/range, specific heat capacity, and latent heat of fusion. In addition, thermal diffusivity is covered as it speaks to the time constant of the problem.

2.3.1 Melting Point/Range

Pure metals transition from solid to liquid at a single temperature, above which they are liquid and below which they are solid. Alloys melt over a temperature range. There is a solidus temperature which is the highest temperature at which the solder is entirely solid, and a liquidus temperature, the lowest temperature at which it is entirely liquid [6]. The best method for understanding this concept is to examine the phase diagram for the alloy. Figure 2.3 shows the basic parts of a simplified phase diagram for an alloy. The solidus temperature and liquidus temperature vary depending on the alloy composition. At the eutectic composition, the alloy behaves as a pure metal, melting at a single temperature. The melting range increases as composition moves away from the eutectic point [6]. For lead-tin solders, the eutectic composition is approximately 63% tin and 37% lead. This composition is commonly referred to as 63/37 solder. Its melting point is 183°C [6]. For any other lead-tin composition, the joint temperature will have to be raised above 183°C for the solder to be completely liquid.

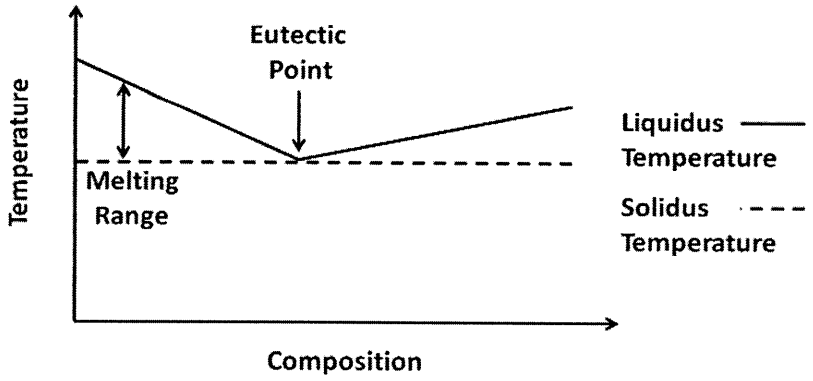

Figure 2.3: Simplified phase diagram for an alloy.

In terms of joint design, the designer should choose a solder with a low melting point and a small melting range. The liquidus temperature determines the minimum temperature required to heat the joint. The melting range comes into play in the cooling cycle. The joint must be

cooled from its liquidus temperature to its solidus temperature to lock the joint. A good starting point is to pick 60/40 solder; this solder is near the eutectic composition and is widely available.

The lowest melting point of pure lead-tin solders is 183°C, which is for practical purposes hard to achieve with mm-scale heaters and with a limited power supply. As mentioned earlier, other elements may be added to lead-tin alloys to lower their liquidus temperatures. When a new element is added to the solder, the phase diagram becomes more complex. If the solder is bought from a manufacturer they will often provide the liquidus and solidus temperatures, thereby enabling the designer to compare different compositions. Another approach is to mix two different alloys to create a new alloy, in which case, experimentation is the best method for determining the liquidus and solidus temperatures. This approach is examined in detail in Chapter 6 during the case study of Squishbot1.

2.3.2 Specific Heat Capacity

The specific heat capacity of a material, c, refers to the amount of energy required to raise the temperature of a certain mass of the material by one unit of temperature. In SI units it is measured as the number of Joules required to raise the temperature of 1 kilogram of material by 1°C. Equation (2.3) is used to calculate the total energy required to raise the temperature, Q_{temp}, from a starting temperature, T_i, of a piece of solder with a given mass, m, to the solder's liquidus temperature, T_l.

$$Q_{temp} = m \cdot c \cdot (T_l - T_i) \tag{2.3}$$

As Equation (2.3) shows the specific heat capacity of the material determines the amount of energy required to raise its temperature. The specific heat capacity of a solder should be considered alongside its melting range. The material's ability to store and release heat depends on the material's specific heat capacity. For optimal joint performance, a solder with a low liquidus temperature, a short melting range, and a low heat capacity is desired. These properties reduce the amount of energy required to unlock the joint.

2.3.3 Heat of Fusion

Equation (2.3) calculates the amount of energy required to heat a material to its liquidus temperature, not the energy required to melt the material. The heat of fusion of the material refers to the amount of energy required for a mass of a material to change states from solid to

liquid. The total energy required to melt the solder, Q_{solder}, in a joint is given by Equation (2.4), where H_f represents the heat of fusion of the solder.

$$Q_{solder} = m \cdot c \cdot (T_l - T_i) + m \cdot H_f \tag{2.4}$$

2.3.4 Thermal Diffusivity

The time constants associated with locking and unlocking the joint are important to robot speed. The thermal diffusivity of the solder affects how quickly the joint may be cycled. Overall solders diffuse heat well because they are metal alloys. The next chapter shows that joint material properties are the determining factor in the heating and cooling time calculations. The thermal diffusivity of the solder should be understood to demonstrate that the thermal joint design is extremely important.

The thermal diffusivity of a material, α, is the ratio of the material's thermal conductivity, k, to the product of its density, ρ, and its specific heat capacity, c. The thermal diffusivity equation is given in Equation (2.5).

$$\alpha = \frac{k}{\rho \cdot c} \tag{2.5}$$

Diffusivity compares the material's ability to conduct heat to its surrounding to its ability to store heat [21]. Materials with high thermal diffusivities adjust quickly to changes in temperature, making them ideal for cycling. Decreasing the heating time calls for a solder that adjusts quickly to the temperature of the heater and then promptly cools once the heater has been turned off.

2.3.5 Choosing a Solder based on its thermal properties

2.3.5.1 Energy Consideration

In choosing a solder, the energy to melt the solder must be considered given the limited power supply concerns. The total energy required to melt the solder is calculated using Equation (2.4). It depends on the solder's liquidus temperature, its specific heat capacity, the latent heat of fusion and the mass of solder. In general, it is good practice to reduce the amount of solder required in the joint as this reduces energy consumption, cooling time, and heating time.

From Equation (2.4), it may be seen that one wants to use a solder with the lowest liquidus temperature, heat capacity, and latent heat of fusion. It is likely that different solders

will be the best choices in the different categories. A good starting point is to consider the heater's maximum temperature; this determines the upper limit of the liquidus temperature. Next, compare the melt energies of the different solders that meet this limit. A rapid estimate of the energy tells which solders have the lowest melt energies. Table 2.4 shows a comparison of the thermal properties for five Bismuth Lead-Tin solders.

Table 2.4: Comparison of total melt energies for 1g of different bismuth-lead-tin solder compositions from room temperature (23 °C) [6].

Solder Composition Bi- Bismuth, Pb- Lead, Sn- Tin, Cd- Cadmium, In- Indium	Liquidus Temp. (°C)	Solidus Temp. (°C)	Heat Capacity (J/g°C)	Latent Heat of Fusion (J/g)	Total Melt Energy 1 gram of solder. (J)
Bi45%, Pb23%, Sn8%, Cd5%, In19%	47	47	.146	14	17.5
Bi50%, Pb27%, Sn13%, Cd10%	70	70	.167	32.5	40.3
Bi 55%, Pb 45%	124	124	.126	16	28.7
Bi 58%, Pb 42%	138	138	.188	46.5	68.1
Bi42%, Pb38%, Sn11%, Cd9%	70	88	.167	23	30.8

The cooling and heating times for the solder must be considered before making the final decision on which solder to use.

2.3.5.2 Heating Time

The factors that determine the heating time, $t_{heating}$, required to melt the solder are the melt energy and the power of the heater, P_{heater}. Equation (2.6) lists the relationship between these factors.

$$t_{heating} = \frac{Q_{solder}}{P_{heater}} \tag{2.6}$$

For a given heater power, the heating time is reduced by decreasing the melt energy. In general cm-scale mechanisms are power limited by the heater and/or the on-board power supply.

2.3.5.3 Cooling Time

The cooling time calculation takes into consideration the required energy loss that induces solidification. This calculation is rate limited by the heat transfer rate out of the solder. The heat transfer methods within the joint are examined in detail in Chapter 3. The important thing to note here is that the heat transfer rate out of the solder is limited by the joint materials and the convection coefficient, not the solder. The diffusivity of the solder should be checked as it may play a limiting factor if it is abnormally low for a solder and/or if it is lower than the diffusivities of all other joint materials. The total energy loss necessary to solidify the solder, Q_{solid}, is given by Equation (2.7). The solidification energy is composed of the energy associated with the latent heat of fusion, as well as the energy loss required to reduce the solder's temperature down from its liquidus temperature to its solidus temperature, T_s. Ideally, the solder has a low latent heat of fusion, low specific heat capacity and a short melting range.

$$Q_{solid} = m \cdot c \cdot (T_l - T_s) + m \cdot H_f \tag{2.7}$$

2.3.6 Rules, Tradeoffs, and Caveats

There are several solder thermal properties that must be considered when choosing a solder. Understanding the effects of each solder property yields the solder for best joint performance. The following insights should be kept in mind when making this decision:

(1) Minimize the amount of solder used in the joint.

(2) Lead-tin solders alloyed with Indium and Bismuth additions have lower melting temperatures.

(3) Minimize the solder's specific heat capacity, liquidus temperature, melting range, and latent heat.

(4) Maximum heater temperature limits the selection to those solders with liquidus temperatures below maximum temperature output.

(5) Comparing the total melt and solidification energies of the solders highlights solders with best joint locking performance.

(6) Heating time is determined by the melt energy and the power output of the heater.

(7) Cooling time is determined by the solidification energy and the heat transfer within the joint, this is covered in more detail within Chapter 3.

(8) The diffusivity of the solder sets its ability to adjust to temperature changes. A low diffusivity compared with other solders may be a problem as this limits the rate of heat transfer.

There are other factors that must be considered during solder selection such as toxicity, cost, and availability. These parameters might negate the use of the best solder available. Nonetheless, the analysis yields the best solder to use for the specific application considering all mechanical, thermal, and external parameters.

CHAPTER

3

JOINT DESIGN

3.1 Multi-Physics Problem

Using phase change materials, PCM, to lock/unlock a joint increases the complexity of the joint design. Mechanical and kinematic functional requirements and constraints must be considered during joint design. In a locking joint, thermal requirements and constraints must be taken into account as well. Figure 3.1 illustrates the multi-physics nature of this problem, listing some of the major functional requirements for each domain.

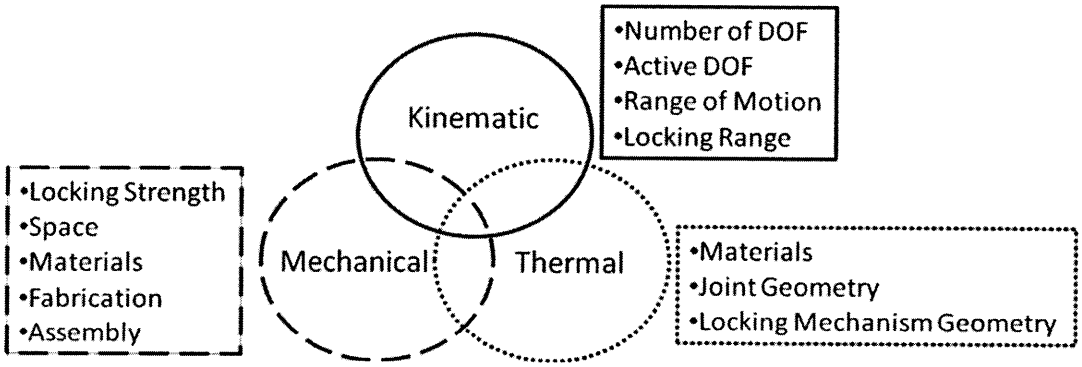

Figure 3.1: Venn diagram illustrating the multi-physics nature of the joint design problem, listing the major functional requirements for each domain.

The following sections highlight how to design a joint while addressing all design constraints and requirements. Particular attention is placed on the thermal domain as this is specific to PCM locking and unlocking. The discussion herein focuses on those kinematic and mechanical functional requirements that dictate the design of the locking mechanism. This chapter shows that the thermal constraints play the biggest role in the design of the joint, as they are often the limiting factor in (i) material choices, (ii) geometry, and (iii) size.

3.2 Kinematic Functional Requirements

3.2.1 Important Parameters: Scope

The kinematic parameters that influence joint design depend on the design of the mechanism. These have been studied in detail in the past and are not the focus of this research. The function of this section is to understand what parameters influence the design of mm-scale PCM joint locking mechanisms. Once the kinematic constraints/requirements on the locking mechanism have been identified, their role in the design of the joint is explored.

The four mechanism kinematic requirements that affect the design of a PCM locking joint are: (i) the DOF of each part of the mechanism, (ii) which DOF have to be locked and unlocked to perform the desired tasks, (iii) the range of motion of each joint, and (iv) the range over which the joint must be able to lock.

Squishbot1 is a robot that was designed while developing the insights and rules that are presented in this thesis. As such it serves as a good example to highlight the steps in the design process. This chapter presents the general design of PCM joints. This chapter does not touch on the specific constraints of Squisbot1. Chapter 4 discusses Squishbot1 and its joint design in detail.

3.2.1.1 Degrees of Freedom: Passive and Controlled

The mechanism design and the mechanism functions dictate the number of DOF that each joint must possess. A single-actuator approach dictates robot tasks be accomplished through a series of one-DOF mechanism states. A kinematic diagram is a graphic representation of the kinematics of a mechanism [22]. The diagram represents the type of connections and their placement within the robot. The complete kinematic diagram should include the number of DOF each joint must possess. A complete diagram for Squishbot1 is shown in Figure 3.2. The designer must understand which DOF must be locked to achieve the different one-DOF mechanism states. Each one-DOF mechanism state may be achieved by locking different joints. The question then becomes "what is the optimal combination of locking joints?"

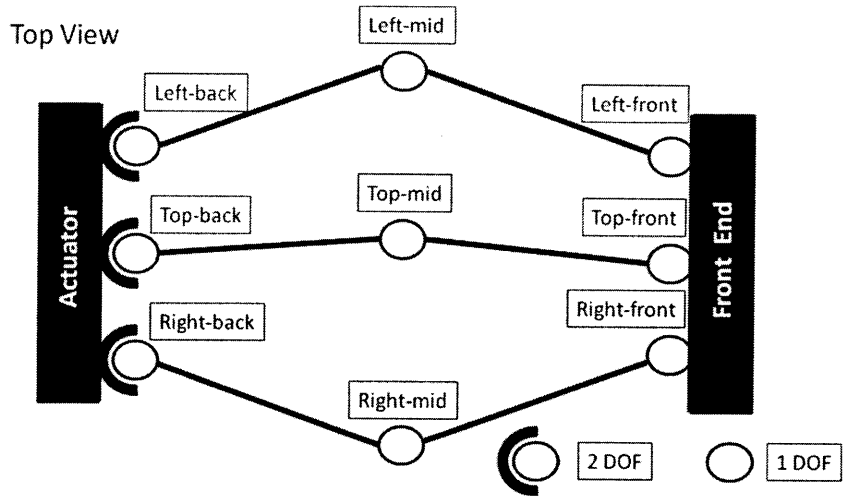

Figure 3.2: Squishbot1 mechanism kinematic diagram. Diagram specifies the required DOF of the mechanism's joints.

The first step is to identify which joints could lock the mechanism in the desired configurations. A good approach is to create a table which lists the different one-DOF mechanism states, the mechanism part that must be locked to achieve them, and which joints could be locked to achieve this. Table 3.1 shows these details for the mechanism in Figure 3.2. There are several guidelines that the designer should consider in order to decide which joints to lock. The first rule is to minimize the number of joints that have to be controllable; this reduces the weight of the mechanism and simplifies the entire robot design. The designer should try to find which combination of joints requires the least amount of locking joints to achieve all the mechanism states. Other factors to consider include the joint position within the mechanism and the particular requirements for that joint. The location of the joint should be considered because this dictates how much space is available for the locking mechanism, how far the power cables must be routed, and the moment arm on that joint. The moment arm on the joint determines how much torque the joint must sustain when locked. Finally the joint requirements, including range of motion, vary with joint location; these joint specific requirements are discussed in the next section. It is important to keep in mind that they affect locking mechanism design and may influence the decision of which joints to lock.

Table 3.1: Squishbot1 one-DOF mechanism states and the possible active joints required to achieve these states.

One DOF State	Description	Possible Locked Joints
Right Turn	Right Leg Locked Compressed	Right: back, mid, OR front
Left Turn	Left Leg Locked Compressed	Left-back, mid, OR front
Lift Front End	Top Leg Locked Compressed	Top-back, mid, OR front
Crawl	No legs locked	No locked joints
Locked - Extended	All Legs Locked Extended	Three Joints must be locked: • Right: back, mid, OR front • Left: back, mid OR front • Top: back, mid OR front

Once the locking joints have been identified, the designer must decide how to address the DOF of each joint. For those joints that require multiple DOF, a single joint with multiple DOF or stacks of multiple one-DOF joints may be used. For PCM locking joints, mechanical and thermal constraints must be considered. At first glance it seems convenient to try to use one single joint to address multiple DOF in one component. If these DOF must be controllable, then using a multiple-DOF joint complicates the thermal and mechanical design. The need for a simple design is especially true in the cm-scale mechanisms, where the joints are in the millimeter scale. Fabrication and assembly of these joints is non-trivial.

Isolating the locking mechanisms ensures that the joint has all the desired controllable DOF. Trying to lock only one DOF of a multiple DOF joint with PCM is complicated. This approach requires complex joint design to (i) allow motions in one direction while locked in the other directions and to (ii) ensure that locking/unlocking one DOF does not cause the other DOF to lock/unlock. Isolating the heat to a small region may be exceedingly difficult. It is likely that the entire joint will see at least some temperature rise when trying to unlock a single DOF. Consequently, it is recommended that the designer use separate joints for each controllable DOF. If the mechanism requires that a joint have multiple DOF, and those DOF are all locked and unlocked at the same time, then a single joint may be feasible. Otherwise, it is better to use one-DOF joints together to achieve multiple DOF. This 'keep it simple' approach is important as manufacturing and assembly at this scale is a challenge. On revisiting Figure 3.2 with the preceding information, the diagram evolves to indicate where multiple joints are used and which joints are locked as shown in Figure 3.3.

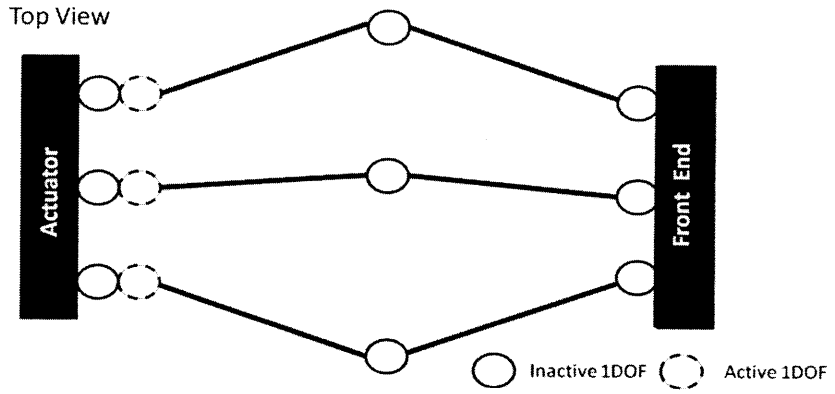

Figure 3.3: Squishbot1 final mechanism kinematic diagram. Diagram shows active joints with dotted circles. It indicates where multiple joints are used.

3.2.1.2 Joint Range of Motion and Locking Range

The other kinematic parameter that influences the thermal and mechanical design of an active-joint is the joint's range of motion and its locking positions. The range of motion required dictates the types of joints that may be used, as well as guide the design of the locking mechanism. In PCM locking, joint range of motion affects the general geometry of the locking plates and the amount of PCM that is required. The later affects the unlocking energy and unlocking/locking times.

The designer should understand which positions the joint must be able to lock in. It may be desirable for the joint to be unable to lock at a certain position to ensure correct positioning or to avoid stressing a component. The locking plate geometry should enable the joint to solidify throughout the range of desirable locking positions. Ideally the joint may be activated at any of these positions with the same heater.

There are many approaches to ensure locking along the desired range of motion including extending the locking section and including multiple locking spots at the desired locking positions. Figure 3.4 shows three different possibilities for locking mechanism design. At this point the designer must not finalize the locking mechanism design as the design is influenced by the mechanical and thermal constraints; however, he must be aware of how the design is constrained by the locking range.

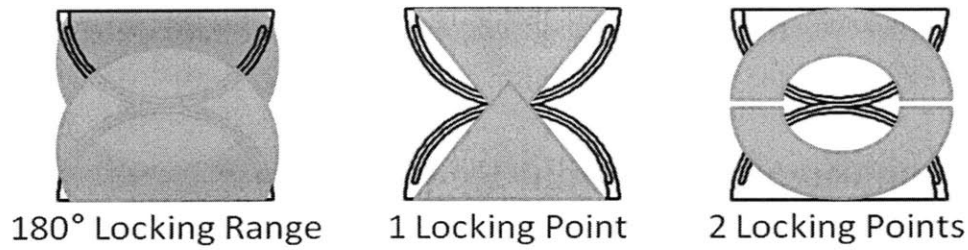

Figure 3.4: Schematics of three different locking mechanism shapes for locking a joint similar to the joints used in Squishbot1.

3.2.2 Kinematic Rules, Tradeoffs and Caveats

The kinematic constraints of the robot that affect the design of the PCM locking joint must be considered first as they set how to create a single actuator mechanism. The kinematic functional requirements dictate the number of locking joints, their position within the mechanism, and finally the constraints on the locking mechanism design. Once the kinematic requirements have been addressed, the next step in the locking joint design is to address the mechanical and thermal constraints.

The main insights to consider when approaching the kinematic functional requirements of a mechanism are:

(1) When dealing with PCM activated joints, it is recommended that the designer address different DOF with different joints. This point is important due to the millimeter-scale of the joints which makes it difficult to fabricate and assemble multi-DOF joints. At this scale isolating the activation heat to a single DOF is non-trivial.

(2) Minimize the number of locking joints. This point seems obvious but it is important to stress the impact that unnecessary joints have on the mechanism design. The extra joints increase the weight of the mechanism, the number of controlled heaters, and the number of locking mechanisms. At the millimeter-scale it is necessary to keep designs as simple as possible.

(3) Carefully choose which joint(s) to lock. Careful selection helps reduce the number of joints and the complexity of the mechanism design. Which joints are locked determines the required locking strength for that joint.

(4) Understanding the required locking range is important as the range is the first constraint on the locking mechanism design.

3.3 Mechanical Functional Requirements

3.3.1 Important Parameters: Scope

Joint design is driven by many mechanical functional requirements and design constraints. This section focuses on the mechanical design constraints of a PCM locking mechanism design. There are three main mechanical factors that need to be considered when designing the locking mechanism: (i) locking strength, (ii) space and material constraints, and (iii) fabrication and assembly of the joint and locking mechanism.

3.3.1.1 Locking Strength

The locked joints must be able to remain locked during actuation in order to achieve separate one-DOF mechanism states. The locking strength necessary to maintain the different configurations must be calculated to ensure functionality. Two factors determine the necessary locking strength mechanism weight and actuator force. The robot must be able to support itself in its different configurations. Identifying the loading on the joints throughout the application helps determine the minimum holding strength of the joint.

The second thing to consider is the actuator for the mechanism. The actuator determines how much torque a locked joint must sustain while remaining locked. In addition, the motor sets a boundary on the friction of the unlocked joint, as the actuator must be able to move an unlocked joint. As mentioned in the kinematic design section, one must consider the moment arm between the loading point and the joint's center of rotation. Equation (3.1) is used to determine the locking torque, Γ_l, on a joint based on the actuator force, $F_{actuator}$, and the moment arm, r.

$$\Gamma_l = F_{actuator} \cdot r \tag{3.1}$$

The locking strength of a joint depends on the solder shear/tension stress and the contact area. As discussed in Chapter 2, the solder's yield stress depends on loading, material properties, and joint properties. At this point the designer should know the average yield stress of the solder they wish to use. Then contact area may be tuned. Solder's relatively high yield stress leads to a

relatively small contact area. This is a key advantage of solder activated joints. The solder is strong enough so that holding torque is usually not a problem in a cm-scale mechanism. The designer should always try to minimize the contact area as this decreases the required mass of solder. A reduction in mass in turn reduces the unlocking energy as well as the activation time. There are other factors that influence a lower limit for the contact area. These factors are discussed in section 3.4.

3.3.1.2 Space and Material Limitations

In cm-scale mechanisms, space is a determining factor in many design decisions. If the robot has a functional requirement that limits its size, this limits the size of all of its components including, joints and their locking mechanisms. The designer must be aware of these limitations as the locking mechanism adds to the volume of the joint. Space limitations also yield pressure to reduce component spacing, which in turn affects the thermal performance of the joints. The effect on thermal performance is discussed in greater detail in section 3.4. Finally, the size limitation should be considered when deciding on the complexity of the locking mechanism. When dealing with these scales, it is recommended to make things as simple as possible.

In a purely mechanical sense, there are a few factors to consider when choosing the locking mechanism material, including but are not limited to solder and locking material compatibility and fabrication constraints. It is important to note at this point that the material choice plays a role in the thermal performance of the joint. The focus of this section is on the interaction between the solder and the locking material. The wetting ability of the solder to the base material limits the material options for the thermal design.

As discussed in Chapter 2, a solder's wetting ability depends on the contact material's surface properties. The compatibility of the solder with the base material is especially important given the cycling that the solder endures. Cycling may exacerbate oxidation and lead to joint failure. In general copper is a good choice for lead/tin solders; however, there may be problems when dealing with alloys. The literature, or bench-level experiments, may provide insight into wetting issues. Often, problems with wetting ability may be addressed by coating the copper with a thin layer of a material that enhances solder alloy wetting. Copper is a good starting point for lead-tin solders because it has favorable thermal properties and it is widely available in many forms. Copper's use with solders in the electronic industry has led to a wealth of information on

solder's compatibility properties and on methods that may be used to improve wetting ability with different coatings.

3.3.1.3 Fabrication and Assembly

Component fabrication and assembly is of particular importance for millimeter-scale locking joints. At this scale, one is limited to certain fabrication techniques. For milling procedures, the tools are often in the millimeter or sub-mm scale. These tools require high spindle speeds. A laser cutter and a 3D printer may be close to their resolution limits at this scale.

Assembly may be particularly tedious at this scale, making a simple design all that more appealing. During Squishbot1, it was found that assembling in layers simplifies this process. A design with tight tolerances is not recommended as these are hard to achieve. This relates back to the size of the locking area. In terms of strength, small contact areas suffice; however, a small contact requires tighter feature and assembly tolerances. Designers must be prepared to increase the contact area to ensure that the locking parts contact with sufficient area overlap. The magnitude of tolerances depends on the locking mechanism design. Increased contact area is a good practice in this case to avoid failure. To decide on the dimensions of the locking area, the designer must understand how increased contact area affects the joint's locking strength and its thermal performance.

3.3.2 Importance of Joint Cycling

Some of the failure modes observed during cycling include (i) separation of locking plates leading to locking failure and (ii) scraping of solder during its melted phase by the wiping of the locking plates. It is highly recommended that designers plan to conduct cycling tests early on in the prototyping phase in order to discover changes that preserve expected performance or yield improvements in performance.

As part of the Squishbot1 development, the joints were cycled 20+. During this testing, practical issues with respect to other failure modes were discovered. For example, wiping of the solder off the locking surfaces occurred when the joint slid into/out of contact. The wiping prevented the joints from locking in later cycles. Smaller gaps and blunting modifications to the 'wiping' edges of the joint removed this failure mode.

3.3.3 Mechanical Rules, Tradeoffs, and Caveats

There are many mechanical issues that affect the design of a joint. Few are particularly important and/or specific to a PCM activated joint. It is important to realize that the three domain constraints are not independent, and in most cases, design iterations are required.

For the mechanical design of the locking mechanism, the key insights are as follows:

(1) The locking strength of solder is usually 'overkill' in cm-scale mechanisms that have cm-scale actuators. The strength of the joint is usually not a problem; and though it should be assessed, other factors are more important in determining the locking contact area of the joint.

(2) Size constraints in this scale must be considered early in the design as they affect the size and therefore the design of the joints and their locking mechanisms.

(3) The solder/locking material interaction is important in the choice of locking material. The electronic industry is a great source of information on the wetting ability of solder to different materials. Given its thermal properties, availability, and use in the electronics industry, copper is a good starting point when dealing with lead-tin solders.

(4) At the mm-scale of the joints, fabrication and assembly considerations are key. They must be kept in mind when making the design decisions. The fabrication constraints play a role in the selection of the joint materials. The difficulty of assembly may require an increased solder locking area.

3.4 Thermal Functional Requirements

A more detailed account of the joint's thermal design is given in this section. This information is specific to PCM activated joints. The aims of this section are to highlight the key parameters that play a role in the thermal performance of a solder-activated joint and teach an elegant way to efficiently compare design choices. The goal is to provide the models and insights necessary to design and optimize the joints and their locking components. These tools highlight the role of two major parameters that must be considered in the thermal design of the joint (i) material choices and (ii) geometry of the joint and the locking mechanism.

3.4.1 Thermal Circuits

Complex thermal models are time and resource intensive, especially for phase change and transient problems. In locking joints, model accuracy depends upon the accuracy of convection coefficients, which may vary with joint design and joint orientation during operation. FEA-type models are limited by the accuracy of the inputs, the mesh size, and the length of the time step. It is, however, possible to use first principles to obtain rapid, practical estimates of melting energy, melt time, and solidification time. This information may be used to set the initial design of a joint, which may then be finely tuned via experiments or more detailed thermal FEA. The focus areas in this section are the methods used to (i) understand how performance scales with geometry/material properties, (ii) select desired materials and (iii) set initial design parameters for joint geometry.

A convenient way to approach modeling heat transfer is via thermal circuits. Each joint component is assigned a thermal resistance. Equation (3.2) calculates the conductive thermal resistance, R_{cond}, where k is the thermal conductivity of the material, L_{heat} is the length the heat must travel and A_k is the conduction area, perpendicular to the heat flow.

$$R_{cond} = \frac{L_{heat}}{A_k \cdot k} \tag{3.2}$$

Equation (3.3) is used to estimate convective thermal resistance, R_{conv}, where h is the thermal convection coefficient (~10W/m^2 in air) and A_h is the convective surface area exposed to the air.

$$R_{conv} = \frac{1}{A_h \cdot h} \tag{3.3}$$

The act of modeling a joint as a thermal circuit forces the designer to think in terms of joint geometry and material properties that govern heat flow. A high thermal resistance indicates a low heat transfer rate. The heat transfer rate, q, depends on the thermal resistance and the temperature difference, ΔT, between two points of interest. Specifically:

$$q = \frac{\Delta T}{R} \tag{3.4}$$

The first step in this modeling approach is to 'break' the joint into elements of a thermal circuit. Figure 3.5 shows the thermal circuit for half of a joint in Squishbot1. Heat flows from the heater through the copper and solder layers via conduction before dissipation to the ambient via convection. Heat also flows from the heater into the Teflon via conduction. To represent the

joint as a thermal circuit, one begins by identifying the power source (the heater); then recognizing the different paths through which heat may travel. As shown in Figure 3.5, one should choose to focus on the main paths. Treating these paths as one-dimensional elements simplifies the modeling. In reality, some heat travels perpendicular to the heater and out of the page. As a practical matter, the resistances to this flow are much higher, as indicated by (3.2), given the conduction area is much smaller. In general one can focus on the path of least resistance which is in the direction perpendicular to the surface area of the heater. Given this is the direction of least resistance, the designer should ensure that the solder surface area lies along this path.

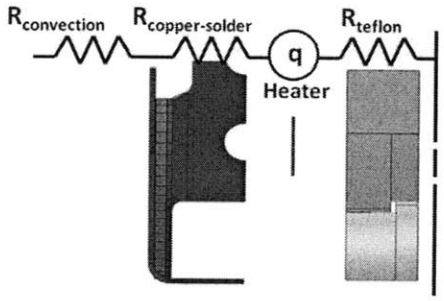

Figure 3.5: Half Squishbot1 joint with corresponding thermal circuit.

The equivalent resistance for each of these paths is calculated by adding the resistances of the components following the principles of electric circuit theory. As Table 3.2 shows, in Squishbot1 the low thermal resistance of the copper and solder layers indicates that they quickly adjust temperature. The high convection resistance, due to the product of small surface area and small convection coefficient, indicates there should be a low heat transfer rate to the environment. The resistance of heat flow through the Teflon is lower than convection resistance to the environment. The lower Teflon resistance is important to note as it plays a role in the heating and cooling time calculations.

Table 3.2: Thermal Resistances for Components of Squishbot1 Joint

	$R_{convection}$	$R_{copper\text{-}solder}$	R_{teflon}
Resistance (K/W)	4.34×10^{3}	2.15×10^{-3}	3.68×10^{2}

Thermal circuits are powerful tools that quickly yield information as to how the heat flows within the joint. More importantly, by understanding the thermal resistances of each of the elements the designer (i) understands how to change the geometry to reduce or increase the heat

flow to an element and (ii) is able to compare different material choices effectively. The rest of this section highlights how these thermal resistances influence the energy required to activate the joint as well as the unlocking/locking times.

3.4.2 Lumped Thermal Capacity Model

3.4.2.1 Biot Number

The lumped thermal capacity model is used in transient analysis. This model assumes that the temperature within a component is uniform, and approximates the temperature gradient within a component to be negligible. This assumption is typically valid if the Biot number of a component is less than 0.1. A Biot number below 0.1 indicates that the temperature within the system does not differ from that at the surface by more than 5%. A higher Biot number translates into a higher temperature gradient and as a result a decrease in the model's accuracy. The Biot number is a ratio of the internal conduction resistance to external convection resistance. The biot number is calculated using Equation (3.5) [22]. The ratio compares the convection coefficient, h, to the conductivity of the material, k, and the length of the conduction path, L_{heat}.

$$Biot = \frac{h \cdot L_{heat}}{k} \tag{3.5}$$

One must calculate the Biot Number of each of the components in a joint to determine whether the lumped thermal capacity model is appropriate. At the millimeter-scale, Biot numbers are often low due to the small associated length scales. Given that the joint is exposed to forced convection, the convection coefficient is also usually small. Unless the joint material has extremely low conductivity, the lumped thermal capacity is often a good model. If the designer finds that one of the components has a high Biot number, then he or she must be aware that the quick calculations done using thermal circuits are not accurate. In this case FEA modeling might be more appropriate.

3.4.2.2 Characteristic Time and Fourier Number

Another parameter to consider is the characteristic time for conduction within each component. Equation (3.6) shows the formula used to calculate the characteristic time, t_c, which depends upon the distance heat must travel, L_{heat}, and the material's diffusivity, α. The characteristic time indicates how quickly the temperature may be adjusted within the component.

It is important to understand the characteristic time because it gives the designer an idea of what temperature the component reaches during the heating process. To unlock the joint, the solder must be heated to its melting temperature. If a component has a characteristic time similar to or shorter than that of solder, then the melting temperature of the solder may be achieved during heating.

$$t_c = \frac{L_{heat}^2}{\alpha} \tag{3.6}$$

It is important to understand how these numbers affect the joint's thermal performance. Materials with low Biot numbers and short characteristic times adjust quickly to temperature changes. Low Biot numbers and short characteristic times translate to shorter heating and cooling cycles, however a material with a higher characteristic time may be used to store heat, thereby keeping the joint close to melting temperature between cycles. As such, there is no one solution, the best design is application specific.

The Fourier number is a dimensionless variable that compares the length of time to the time constant of interest. In other words, it is the ratio of heat conduction rate to the heat storage rate within a solid [21]. A low Fourier number, usually below 0.05 but this depends on the problem, indicates that the temperature of the material changes only on the surface. Large Fourier numbers, usually larger than 0.2 but again this depends on the problems, indicate that the entirety of the solid experiences a temperature change. Together with the Biot number, the Fourier number characterizes the heat conduction problem within the scope of interest of this thesis. Equation (3.7) relates the times of interest to the Fourier number, specifically the characteristic time for the solid, t_c, and the time length of the problem, t.

$$Fourier = \frac{t}{t_c} \tag{3.7}$$

3.4.3 Heating Step

As previously mentioned, minimizing the amount of energy required to melt the solder is important given the limited power available in cm-scale robots. During the heating step, the thermal energy that enters the joint is distributed between (i) raising the temperature of the joint components, (ii) heat loss during melting (typically a fraction of the melting energy and may assumed to be small), and (iii) the energy, i.e. latent heat of fusion, that is required to induce the

phase change in the solder. Figure 3.6 shows the heat flow paths during the heating step for a Squishbot1 joint. Equation (3.8) may be used to calculate the energy that is required to melt the solder in the joint. The total heat required to melt the solder in the joint, Q_{liquid}, is estimated from first principles using the specific heat capacity for the materials, c, the mass of the materials, m, and the change in temperature of each component during the heating cycle, ΔT. The energy required to achieve the phase change is calculated using the material's latent heat of fusion, H_f, and the mass of the material.

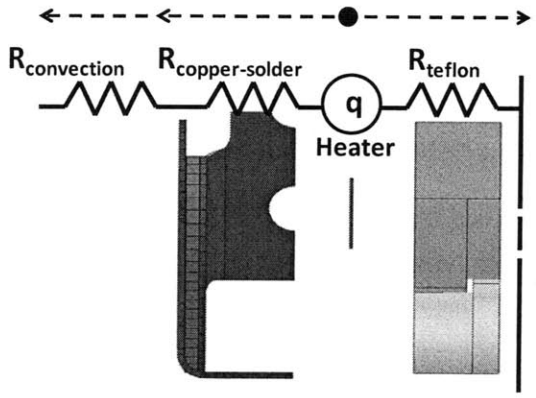

Figure 3.6: Squishbot1 heat paths through thermal circuits during joint heating.

$$Q_{liquid} = (m \cdot c \cdot \Delta T + m \cdot H_f)_{solder} + (m \cdot c \cdot \Delta T)_{components} \tag{3.8}$$

The temperature rise in each material depends on its characteristic time scale. Those with time scales that are shorter than the cycle time are heated to at least the melting temperature of the solder during the heating time. The temperature reached by components with longer characteristic times depends upon heat flow within the joint and is therefore difficult to obtain without complex FEA/experimentation. Given the mix of time scales, a full temperature distribution is difficult to achieve. One can, however, rapidly obtain a lower bound upon the required energy by calculating the energy required to melt the solder, Q_{solder}. The melt energy may be estimated via Equation (3.9). The results provide insight into what is required to reduce the lower bound. For example a reduction in the solder mass leads to a proportional reduction in energy. In addition, one desires to select a solder that exhibits a low melting temperature, as well as low specific heat and low latent heat of fusion.

$$Q_{solder} = (m \cdot c \cdot (T_l - T_i) + m \cdot H_f)_{solder} \tag{3.9}$$

A lower estimate on the heating time may be obtained using the energy required to melt the solder. Given the heater power, P_{heater}, and the total melt energy, Q_{solder}, it is possible to estimate melting time, t_{melt}, via the relation in (3.10).

$$t_{melt} = \frac{Q_{solder}}{P_{heater}} \tag{3.10}$$

These two lower bounds yield useful information about the performance of the joint. For a given solder they indicate: (i) how many times a joint may be activated with a single battery charge, and (ii) an estimate of how long it takes to melt the solder. At this point, given the power available, the designer can make a decision as to whether his initial solder choice is acceptable. If it is not, then one can alloy the solder and thereby tune its thermal properties for better performance. The alloying process was discussed in Chapter 2.

The time calculation in Equation (3.10) assumes that 100% of the heat is used to melt the solder. In practice, heat is lost to the adjacent joint materials; therefore, this estimate is a lower bound on the unlocking time. A more detailed model would consider the energy required to raise the temperature of each component. A better estimate of the energy required may be obtained by considering the temperature rise in each of the components. Those components with characteristic time scales on the order of magnitude of that of solder, or shorter, are heated to at least the melting temperature of the solder. Transient temperature simulations may be used to determine temperature rise in components with characteristic time scales that are approximately the same as, or larger than, the length of the heat cycle. A characteristic time longer than the heating time indicates that the component does not reach the melting temperature of the solder during the heating process.

3.4.3.1 Heating Insights

First the designer must understand the heat paths and decide the desired heat path. With this understanding there are a few rules of thumb to follow:

(1) Minimize the thermal resistance of the path to the solder. The path to the solder is considered the critical heat transfer path.

(2) Minimize heat flow to paths other than the solder path. This reduces the temperature rise in components outside the critical path and therefore maximizes the heat flow through the solder/critical path. Maximizing the heat flow to the solder in turn reduces the energy required to activate the solder. It is important to keep in mind that

the resistances of the components affect the cooling cycle. The designer must find a balance between designing for heating and for cooling.

(3) Minimize the amount of solder in the joint to reduce the energy required to melt the solder. This reduction results in a faster heating cycle.

(4) The critical path should have components with low characteristic times. A low characteristic time ensures that the components along the critical path respond quickly to changes in temperature.

3.4.4 Cooling Step

The cooling part of the thermal analysis is more complex given that the heat transfer rate out of the solder depends upon the temperature reached by the joint components during the heating cycle. The first step in understanding where heat travels during cooling is to compare the thermal resistances of the joint components. Figure 3.7 shows a schematic of a Squishbot1 joint during cooling. The energy source is the solder. The heat associated with fusion must be lost by the solder in order for it to solidify. The temperature of each component at the start of the cooling cycle correlates to the energy that a component must lose before the solder solidifies. Equation (3.4) shows that the temperature difference between two components drives the heat flow between the components. As a result, components that did not reach the melting temperature during heating serve as heat sinks during the cooling cycle. The two paths for energy to exit the solder are (i) through convection to the environment, and (ii) through conduction to the 'heat sink' elements.

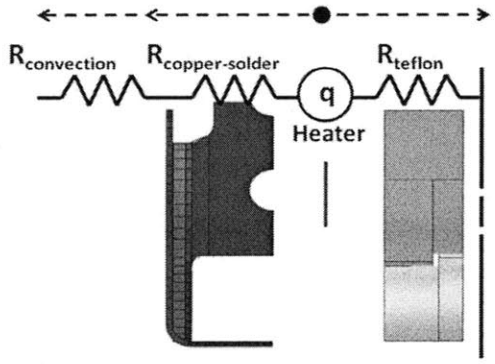

Figure 3.7: Squishbot1 heat paths through thermal circuits during joint heating.

The fact that certain elements act as heat sinks should be exploited to reduce the cooling time. It is important to take advantage of the heat sinks because in mm-scale joints little heat is

loss to the environment in the near vicinity of the joint due to the low natural convection coefficients and the small convective surface areas. The convection rate may be improved by enlarging the surface area or adding fins, however, this is not easy given size requirements and fabrication constraints. The elements that serve as heat sinks see a temperature rise during the cooling cycle. As a result, the more times the joint is activated with short rest times, the less efficient they are as heat sinks.

To obtain a lower bound on the cooling time, consider (i) the solder's latent heat of fusion and (ii) the energy that must be lost to solidify the solder. The heat of fusion dominates given the solder has not been superheated. This energy, Q_{solid}, must be lost to either the environment or the 'heat sink' components, and is calculated using Equation (3.11). In transient problems the resistances of components vary with time. This time dependence is due to the fact that the temperature rise first occurs at the contact surface and then travel along the length of the component. The time dependence may be ignored in components with low characteristic times, because the increase in resistance occurs in a small portion of the heating cycle. However, in the Teflon, for example, the heat does not travel throughout the length of the component during the heating step. The heating time and the characteristic time of the component may be used to calculate the Fourier number of the part. The Fourier number is used to estimate the temperature response of a slab during heating [22]. In order to estimate the cooling time, the designer can look at the temperature response of the high characteristic time component for the heating cycle and estimate the length of the material that sees a temperature rise. This length is then used to calculate the resistance of the material during cooling. The temperature gradient across the affected length is the difference between the melting temperature and the initial temperature of the component. This is a higher bound estimate of the heat flow into the component during cooling. In reality, the resistance continues to increase as the energy is absorbed by the Teflon. This heat transfer rate, q_{sink}, may be used to estimate the lower bound on the cooling time of the joint. An estimate for the time to solidify the solder, t_{solid}, is shown in (3.12), where q_{sink} represents the sum of the heat transfer rate into 'heat sink' components and the convective heat transfer rate.

$$Q_{solid} = (m \cdot c \cdot (T_l - T_s) + m \cdot H_f) \tag{3.11}$$

$$t_{solid} = \frac{Q_{solid}}{q_{sink}} \tag{3.12}$$

3.4.4.1 Cooling Step Insights

Although the use of the first order models does not yield exact cooling times, they may be used to obtain insight into what may be done to reduce the cooling time.

(1) Minimize the energy that must be lost during the cooling cycle. This is in line with reducing the energy input during the heating cycle. The larger the amount of solder in a joint, the greater the energy of fusion. The larger solder mass translates to longer cooling times. The cooling energy may also be reduced by minimizing the mass of the joint components and ensuring that the solder is not overheated.

(2) Given the low convection coefficients and small surface areas, convection is limited in these joints. Components with high characteristic time scales may be used as 'heat sinks' during the cooling process. Ideally, the heat sink only sees a temperature rise close to its contact surface. The smaller the length of heated material, the smaller the resistance to heat flow from the solder during cooling.

3.4.5 Overall Activation Cycle

The thermal design of the joint must take into account the heating and cooling parts of the activation cycle. Some insights point to similar approaches that reduce these times and some that are counterintuitive. In general it is clear that one should reduce the amount of solder, as this scales with the required energy input and output. Reducing the number of components in the critical path, as well as their mass, is also beneficial for the same reason.

The Biot number and characteristic time scales of the joint components give insight into the materials behavior during cooling and heating. In many heat transfer problems, materials with low characteristic times are often ideal for reducing cycle time. Given the limited convection area, it is beneficial for the non-critical path components to have a high characteristic time so that they do not reach the melting temperature. This temperature gradient between the solder's melting temperature and the heat sink components helps drive the transfer heat from the solder. This type of insight demonstrates the power of first order models; they are useful but not always sufficient. More accurate modeling is useful for fine tuning of joint performance and obtaining exact heating and cooling times.

3.4.5.1 Cycling

It is important to note the role that cycling plays in the thermal performance of the joint. In the preceding sections, the joint performance has been discussed given a certain set of starting conditions. These conditions may be different every time the joint is activated. The joint component's initial temperatures differ depending on the time since the joint was last activated, the duration of the heating cycle was, and how long the cooling cycle was. There are different cycling approaches that might be considered to achieve the desired mechanism performance. First order models become tedious at this point since they require that the heating and cooling times be recalculated with different starting conditions every step. At this point it is useful to setup an FEA model where the designer may easily cycle the joint using different cycling approaches to either conserve energy or achieve the fastest cycle time.

3.4.6 Detailed FEA Model

Finite Element Analysis should be used to optimize the joint design and the cycling approach. This detailed modeling should be done after the first order models have been completed as they provide a faster and more efficient means to converge on a preliminary design. Once the initial design has been set, FEA modeling is useful in obtaining more precise heating and cooling times, as well as observing the joint performance during cycling.

In this research, the CosmosWorks feature of SolidWorks was used to analyze the PCM activated joints. The program chosen by the designer must have the ability to model the heat of fusion of the solder.

FEA models of specific joints are used throughout this thesis to corroborate the predictions of the first order models. Chapters 4 and 5 contain detailed design of two case study joints and comparison of first order models to FEA simulations. These finite element models provide insight into the heat distribution within the joint.

3.4.6.1 Advantages and Limitations

The first order models were built upon several assumptions. One of the main assumptions was one-dimensional heat transfer. This is a reasonable first order assumption; however, it is an assumption and so it does not yield error-free estimates. The FEA model shows that the problem

has important 3-dimensional characteristics, which are apparent in components with lower thermal diffusivities.

First order models were used to calculate a lower bound on the energy that is required to melt the solder, the unlocking time and locking time. This estimate was "good enough" to make decisions that improve joint performance. An FEA model provides the designer with a more accurate activation time. The first order models are only able to give an estimate based on a set of starting conditions. Once the FEA model is setup, it is easy to cycle the joint several times. The program uses the results of the previous cycle as starting conditions for the next cycle. This capability is incredibly useful when comparing different cycling approaches. More specifically this ability to model several cycles helps in determining which approach uses the least amount of energy and which one gives the fastest activation times.

An FEA model is limited by the accuracy of the inputs. An estimate of the convection coefficient must be used. The value of this coefficient depends on several aspects including: the robot's position, its traveling speed, and the surrounding environment. Guidelines for natural convection indicate that the convection coefficient is typically between 5-10 W/m^2K [22]. The designer should determine the convection coefficient that seems most accurate for their ambient conditions. In this thesis $10W/m^2K$ has been used because the motion of the robot may help in increasing the heat loss to the environment.

3.4.6.2 Heat of Fusion

A short section on modeling of the heat of fusion is necessary before describing in detail how to setup an FEA model of a PCM activated joint in CosmosWorks. In some programs there might be a place to input this material property along with the materials melting point, such that the software takes the heat of fusion into account during simulation. In CosmosWorks this is not a formal option; however, there is a work-around to include the effect of the heat of fusion. The heat of fusion is added as a spike in the specific heat capacity of the material at the material's melting point [24]. Essentially the specific heat capacity is chosen to be temperature dependent. A graph is created to show that the heat capacity is at its nominal value at all temperatures except at the melting point, at which point the heat capacity is reported as the sum of the nominal value plus the heat of fusion of the material. Figure 3.8 shows the heat capacity graph versus temperature that was used in the software program.

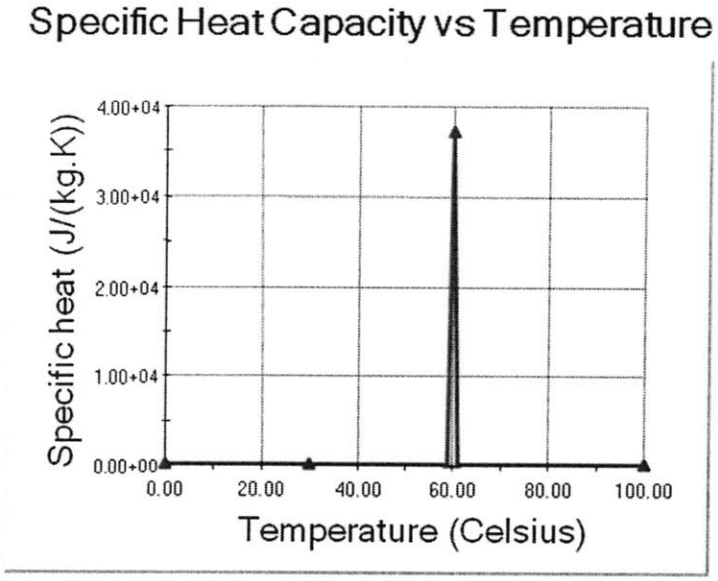

Figure 3.8: Modeling of heat of fusion in CosmosWorks. Heat of fusion is modeled as a spike in the material's specific heat capacity at the material's melting point.

With this approach to modeling the heat of fusion, there are a couple issues that must be considered. If the time step of the simulation is too large, the program may miss the heat of fusion spike completely, therefore modeling the solder melting process inaccurately. The program may consult the heat capacity at temperatures below and above the melting point, reading the nominal value, and missing the heat of fusion of the material entirely. Figure 3.9 depicts how sampling might miss the heat of fusion spike. There are two approaches to dealing with this situation; one is to decrease the time step of the simulation. Unfortunately this approach increases the modeling time. Another approach is to widen the spike in the specific heat capacity. By widening the spike, one increases the chances of the heat of fusion being captured by the simulation. This approach may overcompensate, or undercompensate, for the heat of fusion, depending on the size of the time step. Figure 3.10 shows how the two approaches help to deal with the problem. A combination of these approaches is the best solution, although the solution is not perfect and neither is this modeling approach. A designer must always check the simulation results to see if they make sense. The heat of fusion spike is an easy way to include heat of fusion into a CosmosWorks model.

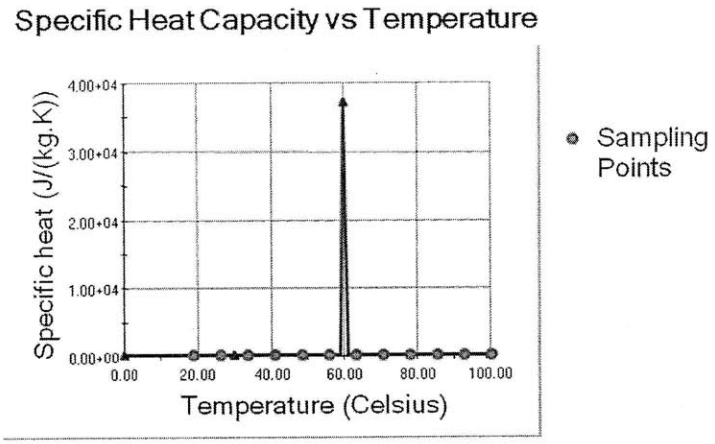

Figure 3.9: Graphical representation of sampling of heat capacity for a material by CosmosWorks. If the problem's time step is too large the temperature of the solid at sampling will be above and below the heat of fusion spike, model will not account for heat of fusion.

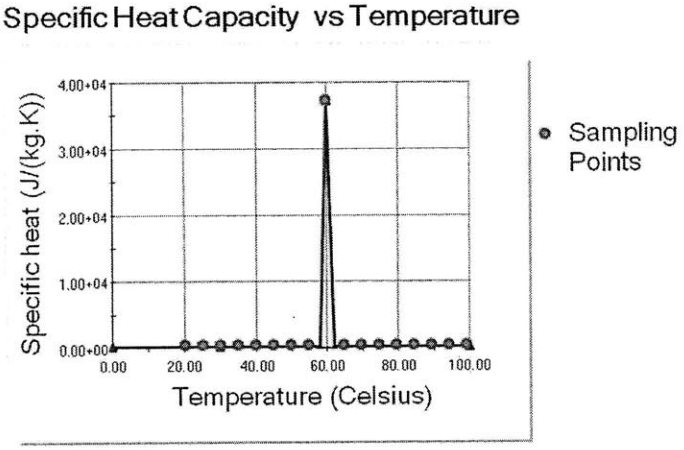

Figure 3.10: Graphical representation of sampling of heat capacity for a material by CosmosWorks, with shorter time steps and a wider heat of fusion spike.

3.4.6.3 Model Parameters

A transient study allows the designer to choose the time step length as well as the total time for the simulation. Both of these parameters are important. The shorter the time step, the greater the accuracy of the simulation. The length of simulation impacts the number of cycles the joint experiences.

Next, define the different materials in the joint, paying particular attention to the accuracy of the material's thermal properties. At this point, the solder's heat capacity should be made time

dependant so that the heat of fusion is captured. The next step is to set the model constraints, starting with the initial temperature of the components. The heat power constraint on the heater face is then added. At this point, if the designer wants to examine the cycling of the joint, the thermostat box must be selected. The thermostat plays the role of the sensors on the joint. The sensor determines when the heater is turned on and off. The thermostat should be modeled in the position of the sensor. The thermostat set points are determined by the designer according to the cycling approach they plan to use. It is recommended that the solder not be heated more than a few degrees above its melting point. Overheating increases the activation energy required as well as the heating and cooling times. Finally, the faces where convection plays a role are selected and given a convection coefficient.

Once all the parameters are set the simulation may be run. A helpful way to analyze the results is to probe the different materials at a given point and then plot their temperatures with respect to time. The graphs, like those shown in Figure 3.11, highlight the temperature changes of the components with cycling. Particular attention should be paid to the 'heat sink' components whose temperature continues to rise after the heater has been turned off as the solder energy flows into them. Figure 3.11 shows the temperature of a point on the solder as well as a point on a 'heat sink' element, which in this case is Teflon.

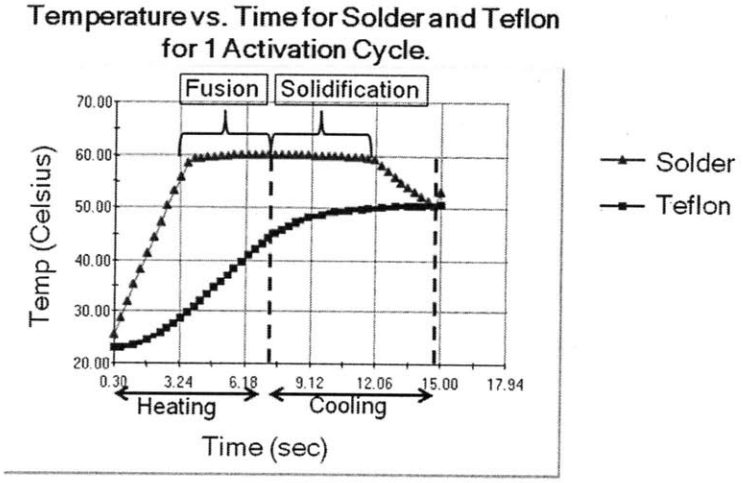

Figure 3.11: CosmosWorks result graph. Solder and Teflon were probed and their temperature graphed over time. The heating and cooling times of the solder, as well as the fusion and solidification times are highlighted.

In Figure 3.11, the heating and cooling times for a given cycle are highlighted. It should be noted that these change as the number of cycles increases, this occurs because the initial

temperature of the components is different every time the joint is cycled. The positive slope of the solder curve represents the heating step; the temperature is increasing because the heater is inputting energy into the system. The cooling step is characterized by the negative slope in the solder's curve, when the solder is dumping heat into its surroundings. The energy expended is calculated as the product of heater power and the heating time. Figure 3.12 shows the temperature response graph for a joint that is cycled two times. The thermostat was set so that the heater was on between 50°C and 60°C degrees. Understanding these charts should begin to highlight how the different cycling approaches influence cycle time as well as the energy required from the battery. The heating time of the second cycle is less than that of the first cycle because the components had an initial temperature of 50°C as opposed to room temperature. The cooling time increases because the difference in temperature between the solder and the Teflon is reduced; the heat transfer rate into the Teflon is lower.

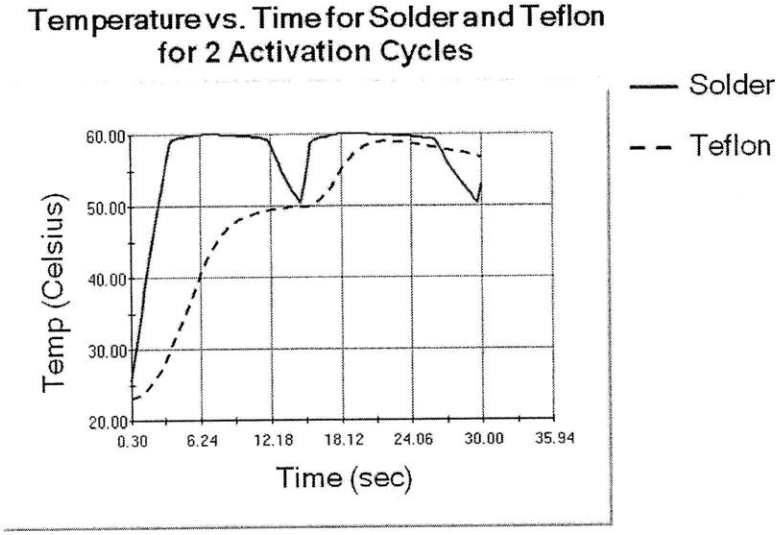

	Cycle 1	Cycle 2
Heating Time	6.9 s	4.2 s
Cooling Time	7.8 s	10.8 s
Total Time	14.7 s	15.0 s

Figure 3.12: CosmosWorks result graph for two activation cycles. Cooling and Heating times are quantified in the table below for each of the cycles.

3.4.6.4 Cycling Approaches

In order for the mechanism to perform different configurations have to be achieved at different times. Therefore, the joint cycling approach is determined by the function of the

mechanism. Given the cycle constraints imposed by the mechanism function, the designer has two variables to play with: (i) temperature set points and, if possible (ii) time between activation cycles. If energy is of greatest concern the designer might find that keeping the joint at a certain starting temperature might be more efficient than allowing the joint to cool down beyond a certain point between cycles. This approach certainly reduces the heating time; however it increases cooling time as the 'heat sink' components reach a higher temperature which decreases the temperature gradient between them and the solder during cooling. The time between activation cycles affects the temperature of the components at the beginning of a cycle, and may be used to tweak heating and cooling times. These decisions are case specific, so the designer should determine what the main constraints for their mechanism are and then adjust these variables, if possible, to try to optimize the joint performance.

3.5 Thermal Energy Sources

Resistive heaters are widely available in varied geometries and capabilities. They produce heat via Joule heating induced by running a current through an internal wire. The rate of energy generated, $\dot{E}_g$, by the heater is set by the current passing through, I, and its resistance, R_{heater}; it is calculated using Equation (4.1) [21]. Therefore, the heat generation is easily set using current control. Cartridge heaters are too large to use in cm-scale applications, however, small strain gages are well-suited for use as miniature heaters. Strain gages have been used as low temperature heaters for years because they are widely available, inexpensive, durable, and reusable. The power output of the strain gages is easy to control [25].

$$\dot{E}_g = I^2 \cdot R_{heater} \tag{4.1}$$

Vishay 062AK EA series strain gages were chosen for heating the joints in Squishbot1. These strain gages, shown in Figure 3.13, have a 120 Ohm resistance and a footprint of 4.06x6.90 mm. At each joint, two Vishay strain gages were used in parallel to reduce the total resistance to 60 Ohms, and enable heating on both sides of the joint. Squishbot1's power constraints allotted 0.7 Watts of power to be spent in heating each joint.

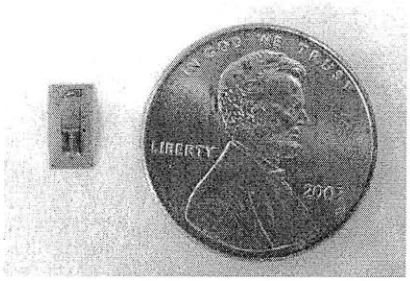

Figure 3.13: Vishay 062AK EA series strain gage. This strain gage was used as the heater mechanism in Squishbot1.

3.6 Sensors

Sensors are required in solder-activated joints for two reasons (i) to measure the temperature of the joint and (ii) to determine whether a joint has been actuated. The most critical sensor to have is a temperature sensor on the joint; this may be any small temperature sensor such as a thermistor or thermocouple. A sensor is necessary for the controller to know when to turn the heater on and off. Temperature sensors may reduce the cycle time by ensuring that the solder is heated to just above the melting point, thereby reducing the time and energy required to cycle the joint. They may also indicate when the heater must be turned on to maintain the joint at a certain temperature.

The temperature of the joint may be used as an indicator of joint locking and unlocking. In reality, it is only an indicator of whether the solder is melted or not. To unlock a joint, the solder is melted and then the joint is actuated while the solder is cooling to ensure the joint is unlocked once the solidus temperature has been reached. Therefore, a joint may be locked or unlocked at the solidus temperature. A strain sensor on the joint would be used to confirm the current state of the joint. If the robot begins to actuate and a strain is detected in a supposedly locked joint, then the joint should be reactivated to lock it. This sensor would prevent the robot from performing an undesired task when a joint fails to lock or unlock.

Currently Squishbot1 is equipped with thermistors. However, the plan is to integrate polymer-based piezoresistors and MEMS piezoresistors that gather thermal (to know if the PCM is solid or liquid) and strain information (robot motion and displacement) within the robot.

CHAPTER

4

CASE STUDY I. SQUISHBOT1

4.1 Project Introduction

Squishbot1, shown in Figure 4.1, is the first implementation of solder-activated joints in a cm-scale robotic mechanism. The robot uses a single spooler actuator, which to the back stage and pulls on the front stage using a string. The two stages are connected by three legs which splay out when the stages are brought together. Joints are used to connect the legs to the stages, and to divide the legs into two solid parts. Using three solder-activated joints, the mechanism may achieve multiple one-DOF mechanism states. Figure 3.2 shows a CAD image of Squishbot1 identifying its different components. Squishbot1 was developed as a proof of concept robot to demonstrate how single actuator cm-scale mechanisms may be built and actuated to perform a multiplicity of tasks using PCM-activated joints. The robot was developed under the Chemical Robots DARPA Challenge.

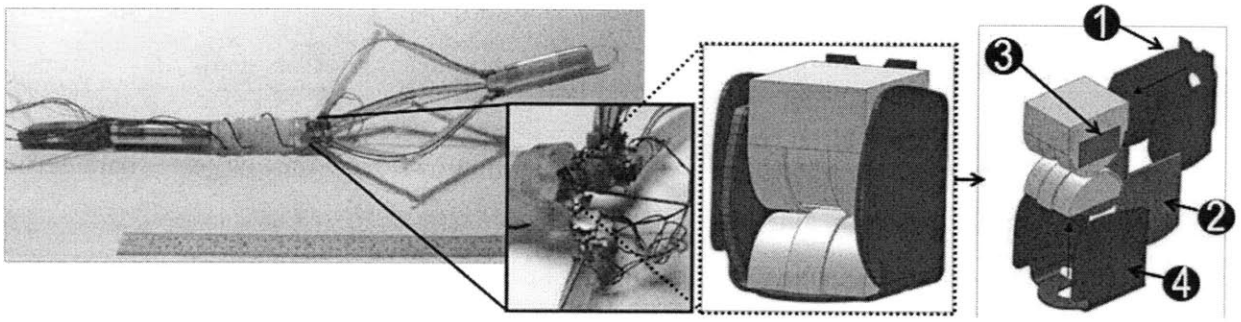

Figure 4.1: Squishbot1 – A single actuator robot. The first inset shows three solder-locking joints. The second shows a solid model of one of the rolling flexure locking joints to wherein u-shaped copper elements (1 & 4) are attached to the sides of the top and bottom joint elements. The flexure joint, a CORE joint, uses flexures to keep the top and bottom half-cylinders in contact. Rolling of the top half-cylinder over the bottom is constrained when the solder (2) between their side plates is solidified. Current is run through a strain gage (3) within the joint to melt the solder.

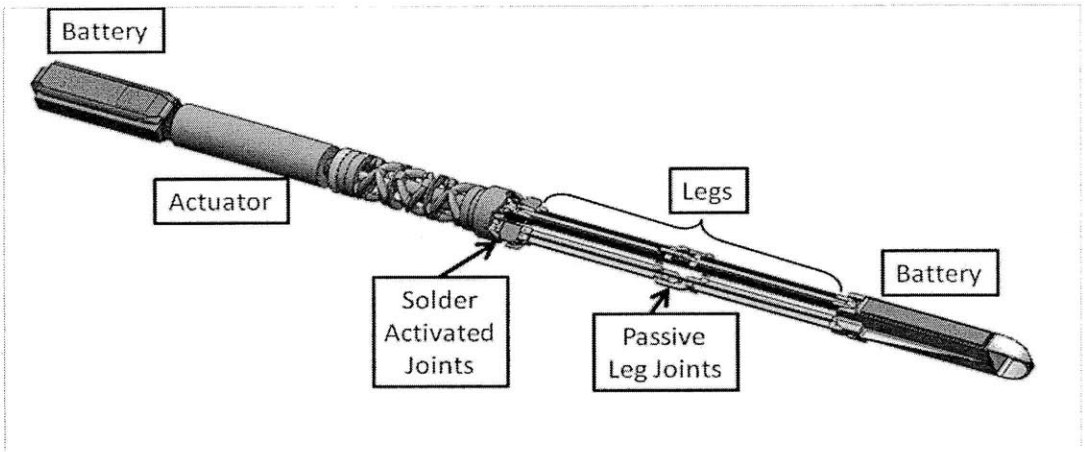

Figure 4.2: Squishbot1 CAD model with labeled components.

4.1.1 Chemical Robots Program

The Chemical Robots (ChemBots) program is funded by the DARPA Defense Sciences Office. The goal of the program is to develop a new class of soft, compliant, meso-scale robots that may enter confined spaces through small openings and perform various tasks. These types of robots would allow military operations to gain access to denied or hostile space. The purpose of the robot is to give war-fighters a way to perform tasks in these hostile and hard to reach spaces safely, covertly, and efficiently [26]. To develop this new class of robots, DARPA asked for proposals from academic institutions and corporations detailing how they would create compliant robots. To gage the progress of each team, DARPA instituted performance parameters for these robots; the parameters are listed in Table 4.1.

Table 4.1: ChemBots Program Phase 1 Success Metrics [26].

1) Travel a distance
2) Traverse an arbitrary-shaped opening much smaller than the largest characteristic dimension of the robot itself;
3) Reconstitute its size, shape, and functionality after traversing the opening;
4) Travel a distance and perform a function or task using an embedded payload.

4.1.2 SQUISHbot Team

The SQUISHbot (Soft QUIet SHape Shifting Robot) team is one of the teams participating in the ChemBots program. The team is comprised of four MIT labs: Prof. Hosoi's group, Prof. McKinley's Non-Newtonian Fluid Dynamics Research group, Prof. Culpepper's

Precision Compliant Systems Lab, and Dr. Iagnemma's Robotic Mobility Group; and an industry partner, Boston Dynamics. After considering the ChemBots performance parameters and the limitations of small-scale actuators, the SQUISHbot team developed the one-actuator plus tunable stiffness approach to creating compliant robots. Tunable stiffness allows for the robot to be comprised of 'soft' materials which may then be tuned to become stiff, achieving different one-DOF mechanism states. Materials are considered to be soft when they can achieve large deformations, on the order of the component's size scale, without yielding

The team worked on this vision in two parallel paths (i) developing materials with tunable stiffness using active fluids as activators and (ii) demonstrating that a one-actuator mechanism could perform a variety of tasks. The focus in the Precision Compliant Systems Lab (PCSL) was to work with Boston Dynamics to create a cm-scale mechanism with a single actuator. Tunable stiffness was achieved using active fluid locking joints. Figure 4.3 shows the development path that led to the creation of Squishbot1. Previous work demonstrated locking joints using MR fluid [3]. Boston Dynamics then implemented the idea of locking joints into a mechanism scheme. The tripod scheme was chosen because it enables the robot to achieve large dimension changes. This scheme was demonstrated by Boston Dynamics using thermo-rheological activated joints. This first mechanism was constructed largely out of metal and was unable to fit in a 1.5cm hole. The next iteration was to adapt the robot design so that it could be made in the cm-scale. The PCSL redesigned the robot at the cm scale. This lab then developed the concept of solder-activated joints, as well as the guidelines for how to design these effectively. The resulting robot, Squishbot1 is able to fit through a 1.5cm hole, has minimal metal parts, and uses solder activated joints effectively to crawl, steer, and lift its front end.

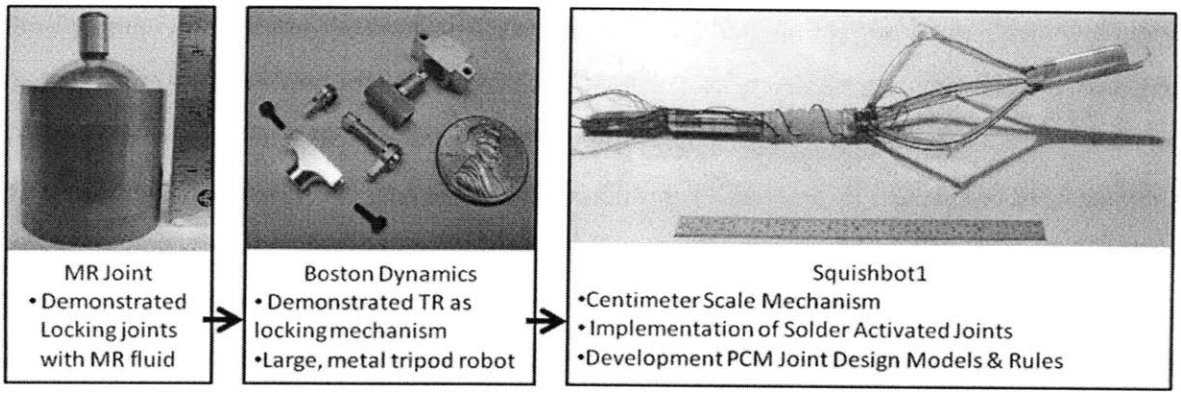

Figure 4.3: Active Joints Development Path.

4.1.3 Scope

Squishbot1 is used as a case study to demonstrate how to use the presented guidelines and insights to design and optimize solder activated joints. These rules were developed as Squishbot1 was being created. This mechanism provides an ideal platform to explore the efficacy of the models provided. In some respects, the models show that because Squishbot1 was developed while the rules and insights were not completely understood, it does not possess the optimal locking mechanism design. Chapter 5 discusses a second case study that was built using the completed solder-activated joint design theory. The focus of this chapter is to analyze the design of the joints of Squishbot1 using the insights, rules, and models described in Chapters 2 and 3. These design models predict the performance of the joints and highlight the areas where the design may be improved.

4.2 Overall Robot Description

The focus of this thesis is the design of the active joints in Squishbot1. A quick introduction of the overall robot design is presented because it plays a role in the joint design. The active joints in Squishbot1 had to enable actuation of the mechanism to perform several tasks using a single motor. The robot had to crawl, steer left and right, lift its front end, have a large deformation in one of its dimensions, and transverse through a 1.5 cm hole without a tether. Table 3.2 summarizes the functional requirements for Squishbot1. In order to perform all of these tasks, the original tri-pod scheme had to be redesigned to use flexural joints instead of the existing pin joints. The pin joints could not be fabricated or assembled at the millimeter-scale. Efficient solder-activated joints had to be developed, so that they could be activated several

times with a limited power supply. The available actuator, energy source, and kinematic design of the robot were considered in the design of the active joints, as well as the material constraints set by the ChemBots challenge.

Table 4.2: Squishbot1 Functional Requirements and Constraints.

Power Supply	2 - 150mAh batteries[+]
Minimum Range	5 meters without tether
Minimum Speed	4.2 mm/sec
Cross-Section Diameter	Travel through 1.5 cm hole
Functions	Steer Left and Right, Lift front end

+ Li-ion polymer battery, model GMB051235 from the Guangzhou Markyn battery company.

4.2.1 Actuator and Energy Source

The actuator and the energy source choices were limited by the size constraints. Both of the components had to be able to fit through the 1.2cm hole. The chosen actuator, a Maxon RE6 motor, was adapted by Boston Dynamics with a 221:1 gear train and spooler mechanism that enabled it to exert 5N of pulling force while reeling in a string. The final actuator mechanism measured 12mm in diameter and approximately 38mm in length. Table 4.3 lists the final actuator mechanism specifications. Appendix B contains the motor's full specification sheet.

Table 4.3: Squishbot1 Actuator Specifications

Maxon RE6 Motor	
Diameter	6 mm
Power	0.3 W
Efficiency	54%
With Spooler Mechanism	
Diameter	12 mm
Length	38 mm
Pulling Force	5 N

The batteries chosen to power the robot were Li-ion polymer batteries model GMB051235 from the Guangzhou Markyn battery company. Table 4.4 lists the Squishbot1 battery specifications. The batteries dimensions are 36x12.5x5.2mm and they provide 150mA-hours each. Appendix C contains the full specification sheet for the Markyn batteries. Squishbot1 utilizes two of these batteries, one located behind the actuator and the other at the front end as shown in Figure 3.2.

Table 4.4: Guangzhou Markyn model GMB051235 battery specifications. Squishbot1 utilizes two of these batteries.

Weight	4 grams
Dimensions	36x12.5x5.2mm
Power	150mA-hours
Nominal Voltage	3.7 V

4.2.2 Tripod Approach

The tripod approach was chosen because it allowed the robot to perform all of the desired maneuvers and resulted in an approximate 5:1 expansion of the mechanism's diameter when the legs are splayed. Figure 4.4 shows the kinematic diagram for Squishbot1. To create this configuration in a cm-scale, flexural components were used. These were chosen over traditional joints as they lend themselves to better assembly and are not subjected to frictional losses occurred in pin joints [10].

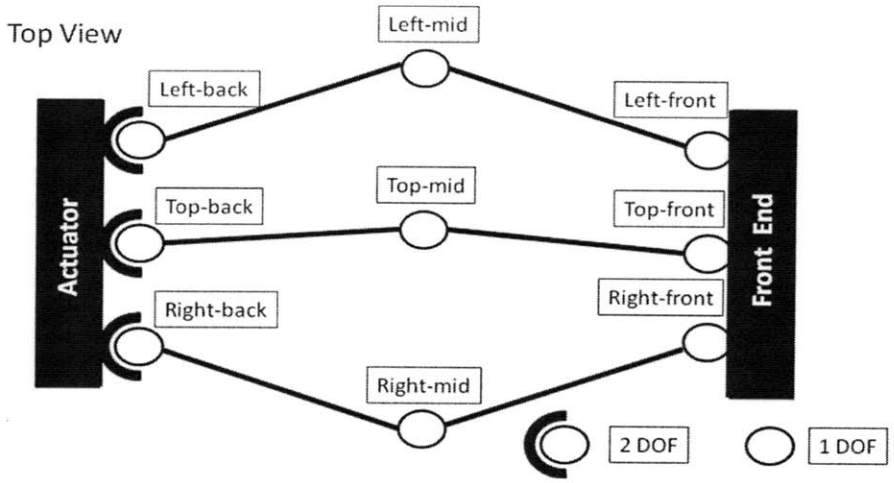

Figure 4.4: Squishbot1 mechanism kinematic diagram. Diagram specifies the required DOF of the mechanism's joints.

The middle joints connecting the two leg segments had to have approximately 180° of range for the robot to crawl, fit through the 1.5cm hole, and achieve the largest diameter increase possible. Large range is hard to achieve in flexural mechanism because these operate by using the compliance of members to achieve motion. A single flexure blade would have been able to achieve this range of motion, but would not have been able to support the loads required to lift the front end of the mechanism. To address this issue, a new flexural mechanism was developed that utilizes two 'bones' which meet in the middle of the leg. The bones are kept in contact using two flexural blades on either side. The bones guide the motion of the blades and support the loads by constraining the blades from twisting. Figure 4.5 shows CAD models of the assembled leg design as well as an exploded view of the different leg components. The final piece of the leg is a mechanical stop on the bones which prevents the leg from flexing in the undesired direction. The legs were designed to simplify their assembly; the design utilizes a single flexural blade with a slot down the middle in which the bones are inserted. The flexure blades were milled out of blue-tempered spring steel shim stock. The blades were then given an initial curvature by rolling them around a 9mm diameter cylinder; this initial curvature pre-loads the legs enabling them to propel the mechanism forward. The hard stops prevent the pre-load from bending the legs in the opposite direction. Figure 4.6 shows the pre-load on the flexure blade. The leg bones were 3D printed.

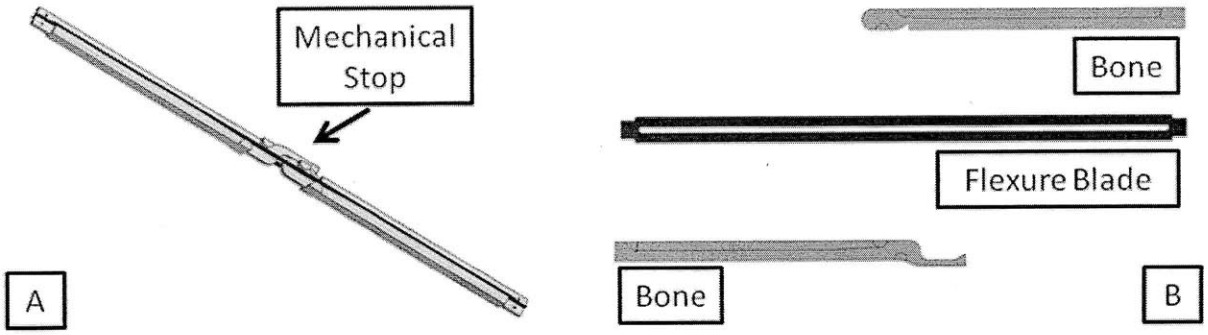

Figure 4.5: CAD models of the Squishbot1 leg assembly. (A) Shows the assembled leg and (B) presents a top view of the three components of the leg.

Figure 4.6: Flexure beam is curved around 9mm diameter cylinder, to preload the flexure. The preload propels the mechanism forward when the string is released.

The flexure blades were required to provide enough restoring force to be able to extend the legs once the string was released by the actuator. The top blade had to be stiff enough to be able to lift the weight of the battery. Beam bending equations may be used to calculate the force necessary to achieve small displacements, however, given the large displacement of the blades these equations did not apply. The initial radius of the flexures also had to be taken into account in the calculations. Given the complexity of these equations, it was decided to experimentally measure the stiffness of the flexure beams. The critical dimensions of the flexure blades are shown in Figure 4.7. A force gage was used to measure the force necessary to deflect an assembled leg by 180°. Table 4.5 lists the dimensions used for the top and side legs of Squishbot1 as well as the measured force.

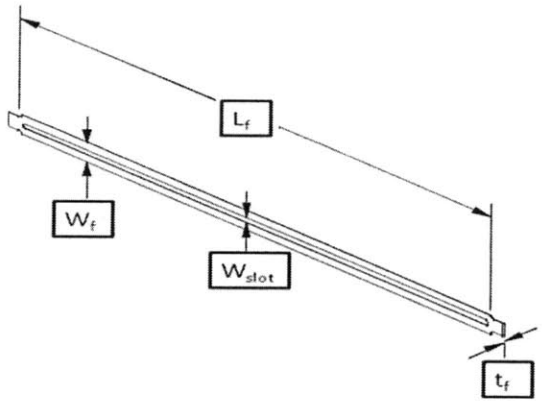

Figure 4.7: Leg flexure beam with dimension labels.

Table 4.5: Squishbot1 leg flexure beam dimensions, and measured force required to deflect assembled leg 180°.

	L_f	W_f	W_{slot}	t_f	Force$^+$
Top Flexure	90.8 mm	4.50 mm	1.10 mm	0.102 mm	0.34 N
Side Flexures	90.8 mm	3.60 mm	1.10 mm	0.127 mm	0.16 N

+Force necessary to deflect assembled leg by 180°. The force was measured using a force gage.

4.2.3 Material Constraints

The ChemBots program seeks to create a new class of compliant robots, as opposed to traditional robots which are considered to be 'hard' and to have limited DOF. Squishbot1's main purpose was to demonstrate that cm-scale single actuator mechanisms could perform a variety of tasks using solder-activated joints. Squishbot1 also sought to explore the use of soft materials as robot components. As such, the SQUISHbot team decided to limit the use of metals as much as possible, and instead used plastics which could be considered to be a step closer to 'soft' materials. The flexural elements used in Squishbot1 are also more compliant than the traditional hard components that they replaced.

4.3 Squishbot1 - Solder Design

4.3.1 Mechanical Considerations

A locked joint must sustain the actuation load without unlocking. In Squishbot1, the various one-DOF mechanism states were achieved by locking a joint in the compressed position

(string reeled in), then allowing the flexure blades to straighten the unlocked legs. The locked joints' holding torque had to exceed the loading torque exerted on the joint by the motor. The highest torque on the joints is observed when the joints are locked in their extended position and the motor exerts 5N of force on the front stage. Equation (4.1) is used to calculate the holding torque, Γ_l, of a joint, where F_{motor} is the motor's max force output, given in Table 4.5. The loading arm, l_{arm}, depends on where the active joints are located within the mechanism.

$$\Gamma_l = F_{motor} \cdot l_{arm} \tag{4.1}$$

Once the joint locking torque is calculated and the loading mode and yield stress of the solder established, Equation (3.2) is used to calculate the minimum locking area, A_{plate}. The minimum locking area depends on the distance between the locking mechanism and the loading torque, l_{plate}.

$$A_{plate} = \frac{\Gamma_l}{\sigma_{yield} \cdot l_{plate}} \tag{4.2}$$

When choosing a solder, the ease of soldering and the cycling that the solder must be considered. For Squishbot1, 60/40 solder was chosen as the starting point given its availability, low melting point for a lead-tin solder, and the ease of soldering of lead-tin solders to copper. The combination of lead-tin solders on copper was chosen because the joints would be cycled many times during Squishbot1's lifetime and these two materials have a high wetting ability. A copper lead-tin solder joint also has one of the highest yield stresses [5]. The high yield stress of the 60/40 solder allowed room for alloying the solder to lower its melting temperature, and still maintain a high yield stress to support the loads.

4.3.2 Thermal Considerations

In order to choose the best solder to use in Squishbot1, it was critical to understand the power available to melt the solder. This constraint depended on the power that could be drawn from the battery to be used by the heater. For Squishbot1, 700mW of power were allotted for each heater to use in melting the solder. Therefore, the chosen heater had to melt the solder using only this power within a reasonable amount of time, around 10-20 seconds. The heater had to fit within the joint space as well. Vishay 062AK EA series strain gages were selected to be used as heaters. They have a 120 Ohm resistance and a footprint of 1.6x1.6 mm^2. At each joint, two strain gages were used in parallel reducing the total resistance to 60 Ohms. This parallel configuration allowed for heating the joint on both sides. Reducing the electrical resistance of the

heaters increases the current running through them and decreases the voltage across them. This reduction in voltage is necessary to protect the strain gages from burning up.

4.3.2.1 Melt Energy and Heating Time Calculation

For Squishbot1 60/40 solder was chosen as the starting point because it is widely available and its properties are well-known. This solder has a composition that is close to the eutectic composition of lead-tin solders (63% tin and 37% solder). The 60/40 composition yields one of the lowest melting points for pure lead-tin solders, 190°C. Using Equation (2.4), and the thermal properties of 60/40 solder listed in Table 4.6, it was estimated that melting 0.5 grams of this solder from room temperature (23°C) requires approximately 33 Joules. Equation (2.4) is discussed in detail in Chapter 2. Given the heater power, P_{heater}, and the solder melt energy, Q_{solder}, it is possible to estimate melting time, t_{melt}, via the relation in Equation (4.4).

$$Q_{solder} = m \cdot c \cdot (T_l - T_i) + m \cdot H_f \tag{4.3}$$

Table 4.6: Lead-Tin 60/40 solder properties.

Property	Expression	Value
Density	ρ	8.6 g/cc
Shear Strength	σ_{yield}	39 MPa
Heat of Fusion	H_f	37 J/g
Specific Heat Capacity	c	0.173 J/g°C
Solidus Temperature	T_s	183 °C
Liquidus Temperature	T_l	190 °C

$$t_{melt} = \frac{Q_{solder}}{P_{heater}} \tag{4.4}$$

Power limitations made it necessary to limit melting power to 0.7W, which yields an unlocking time of at least 47 seconds. The long melting time clarified the need to alloy the solder and thereby tune melting temperature for better performance.

4.3.2.2 Alloying to Reduce Melt Energy

To alloy the lead-tin solder, Table 4.7 was consulted which lists the general trends in mechanical properties and thermal properties of the solder when it is alloyed with certain

elements. For Squishbot1, indium and bismuth were considered as they lower the melting point of the solder. The wetting ability of pure indium and bismuth to copper is poor; therefore, they were combined with 60/40 solder to overcome this limitation. The alloys considered as possible additions to the 60/40 solder are listed in Table 4.8. These were alloys that were easy to obtain through distributors, and have been designed to have low melting points.

Table 4.7: Trends in Lead-Tin solder properties with addition of alloys[+].

Element	Strength	Ease of Soldering	T_{Melt}	Creep Strength
Indium	↓	↓	↓	↓
Bismuth	↓	↓	↓	↓
Antimony (<6%)	↑	↓	≈	↑
Silver (<5%)	↑	↑	↑	↑

[+]Symbols indicate whether adding the element to lead-tin solders increases (↑), decreases (↓), or has little effect (≈) on the properties.

Table 4.8: Possible alloys to lower 60/40 melting point.

Alloy	Composition by %	T_{Melt}
Chip Quik	10-30 In, 10-30 Pb, 7-13 Sn	58°C
Bismuth Alloy	52.5 Bi, 32 Pb, 15.5 Sn	95°C
Indalloy 117	44.7 Bi, 22.6 Pb, 19.1 In, 8.3 Sn, 5.3 Cd	47°C

When the materials in Table 4.8 are combined with 60/40 solder, the solder's melting temperature decreases. The unlocking temperature of the three custom mixes was determined experimentally. A shear joint was created by nesting one copper rod within a copper cylinder and then soldering the two together. The joint was heated until it unlocked under its own weight. The average radial gap between rods was 175 microns and the axial overlap was 1.27cm. Two k-type thermocouples were used to measure the temperatures on the (i) outer surface of the joint and (ii) at the heater. A Mitutoyo 543 indicator was used to detect joint motions that signaled an unlocking event. Figure 4.8 shows the experimental setup. Table 4.9 lists the temperatures of the heater and the outer thermocouple when release of the inner joint was observed. These results provide rapid, useful estimates of melting temperature for first order performance models.

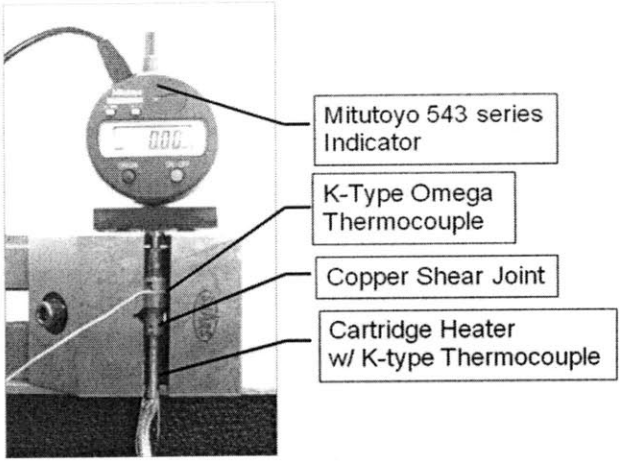

Figure 4.8: Experimental Setup used to determine the unlocking temperature of the 60/40-alloy mixtures.

Table 4.9: Measured unlocking temperatures of 60/40-alloy mixtures.

Solder Composition	Heater Temperature	Outer Joint Temperature
60/40 solder	202.2 °C	168.6 °C
60/40 with Bismuth Alloy 203	139.4 °C	105.5 °C
60/40 with Chip Quik	102.6 °C	86.7 °C
60/40 with Indalloy 117	69.7 °C	59.4 °C

It was elected to alloy the 60/40 solder with "Chip Quik" as this lowered the melting temperature to a point that was easily achieved with the selected heaters. Chip Quick is nontoxic, unlike "Indalloy 117" which contains cadmium. Given the lower melting temperature and assuming similar latent heat of fusion and specific heat capacities as 60/40 solder, the melt energy for the alloy was calculated to be 21.5 Joules, with 700mW of heater power the lower limit on the melting time is 31 seconds. The time to melt has been reduced by 35% by decreasing the melting temperature of the solder through alloying. This first order estimate does not take into account the heat of fusion and specific heat capacity change that occur when alloying.

4.3.3 Squishbot1 – Solder Design Improvements

4.3.3.1 Solidification Energy

When choosing the solder alloy for Squishbot1, the solidification energy of the solder-alloy combination was not considered. The amount of energy that the solder must lose to solidify

depends on the difference between the liquidus and solidus temperatures and the latent heat of the solder. Given an energy loss rate set by the joint design, this energy determines how long it takes to lock the joint, which is an important parameter in joint performance. The Squishbot1 solder design should have considered not only the unlocking temperature of the alloys, but the locking temperature as well. This information together with the latent heat of the solder alloys would have yielded the best choice of solder considering both melting time and solidification time, resulting in the shortest overall cycle time. The latent heat of fusion of the solder alloys is hard to measure and is not available for the mixture of 60/40 solder and the different alloys.

4.3.3.2 Solidus Temperature

The easiest way to obtain the solidus temperature is experimentally. The 60/40-ChipQuik alloy combination was soldered onto a 10mm by 10mm, .254mm thick copper piece. A k-type thermocouple was attached to the backside of the copper to measure the temperature of the setup. Using a soldering iron the alloy was melted. A copper wire was used prod the alloy to determine when it solidified. The testing setup is shown in Figure 4.9. The measured solidus temperature for the mixture was 56°C.

Figure 4.9: Experimental setup used to measure the 60/40-ChipQuik alloy solidus temperature.

4.3.3.3 Cycling

Cycling was overlooked during the solder design for Squishbot1. It was not until the completed joints were cycled, that it was discovered that the alloy combination would fail after approximately 20 activation cycles. Once this failure mode was observed, it was discovered that indium solders should not be soldered directly to copper. The problem arises because copper and indium diffuse into one another; this may cause failures in applications that are subjected to thermal cycling. These failures are due to brittle intermetallic formations caused by the diffusion.

In applications with thermal cycling, such as Squishbot1, this problem is exacerbated because the rate of diffusion of indium into copper increases with temperature. A solution for these thermal cycling applications is to plate the copper with at least 1.27 micrometers of nickel [27].

4.4 Squishbot1 – Joint Design

4.4.1 Kinematic Design

The Squishbot1's kinematics dictated the design of the solder activated joints. The first step was to create a kinematic diagram of the mechanism, identifying the DOF that each joint must possess, shown in Figure 4.4. For crawling, a tripod robot's legs have to have three one-DOF joints that are aligned to allow motion along the radial direction. When the tripod robot must steer or lift, the legs have to be able to move perpendicular to the radial direction. Normally, this would call for two-DOF joints at both the back and front stages, however, due to the compliance of the flexure legs one two-DOF joint connecting each leg to the back stage suffices.

A table listing all the required one-DOF mechanism states should be created. The table should highlight which joints have to be locked in the compressed position in order to achieve each task. Table 4.10 lists the four tasks that Squishbot1 must perform, and identifies which joints may be locked to achieve the motions. It is desirable to minimize the number of activated joints that a mechanism requires. For Squishbot1, it was decided that the back joints should be locked to minimize the length of the heater cables.

Table 4.10: Squishbot1 one-DOF mechanism states and the possible active joints required to achieve these states.

One DOF State	Description	Possible Locked Joints
Right Turn	Right Leg Locked Compressed	Right: back, mid, OR front
Left Turn	Left Leg Locked Compressed	Left-back, mid, OR front
Lift Front End	Top Leg Locked Compressed	Top-back, mid, OR front
Crawl	No legs locked	No locked joints
Locked - Extended	All Legs Locked Extended	Three Joints must be locked: • Right: back, mid, OR front • Left: back, mid OR front • Top: back, mid OR front

Once the location of the active joints was determined, the multiple-DOF joints were separated into one-DOF joints in order to simplify the design of the locking mechanism. In the case of Squishbot1, only the radial degree of freedom had to be locked, therefore, having separate joints was optimal. Figure 4.10 shows the final kinematic diagram for Squishbot1.

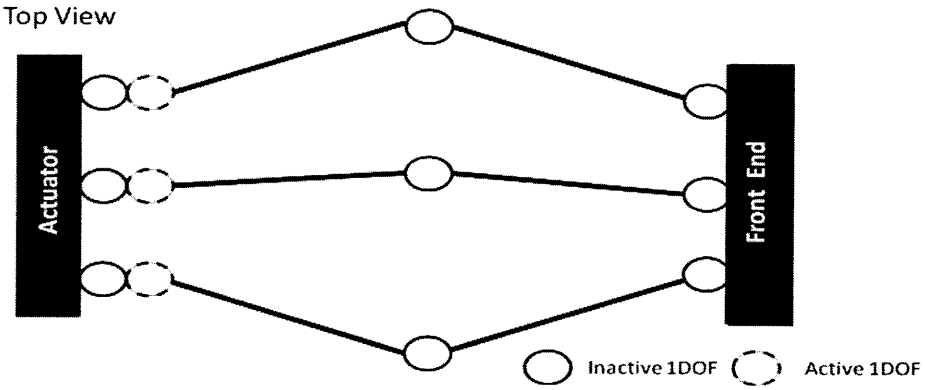

Figure 4.10: Squishbot1 final mechanism kinematic diagram. Diagram shows active joints with dotted circles. It also lists where multiple joints are used.

The final kinematic consideration is the joints' range of motion and locking range. These parameters determine which type of joints may be used and the general geometry of the locking mechanism. For this tripod configuration, the base joints demand a range of motion of 90° to allow the legs to fully compress. The mechanism steers by locking one of the side legs in the compressed position. Releasing the string allows the other two legs to straighten, forcing the robot to steer in the direction of the locked leg. The largest degrees per step are achieved when the leg is locked at its fully compressed position. Therefore, the joints had to be locked 90° from center for optimal steering and lifting. In order for the robot to traverse through a hole, the legs had to be locked in their extended configuration, at 0° from center.

4.4.1.1 Joints

Compliant rolling-contact element (CORE) joints were chosen to connect the legs to the stages [28]. CORE joints are a type of cross-pivot joints. Haringx and Young were among the first to study the mechanics of cross-pivot joints as constructional elements in the 1940s [29]. CORE joints were designed to support large compressive loads through the contact of the two half cylinders. Flexural blades are attached at alternating sides of the cylinders to allow the cylinders to rotate relative to each other while forcing them to maintain contact. This rolling contact reduces the wear and friction of the joints [28]. CORE joints may rotate 90° from center

in both directions and may be stacked perpendicular to each other enabling the leg to have the necessary two-DOF, as shown in Figure 4.11. To simplify the locking mechanism design, the locking plates were attached to the two cylinders and the joint was locked by soldering the two plates together, loading the solder in shear. Figure 4.12 shows the CAD model of a Squishbot1 active joint, with the locking mechanism plates.

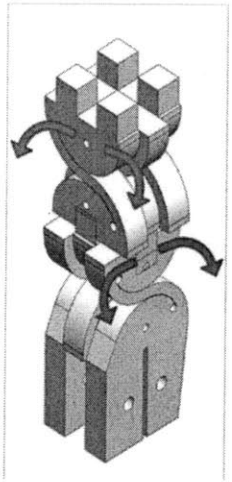

Figure 4.11: Squishbot1 CORE joints stacked perpendicular to each other to achieve two DOF.

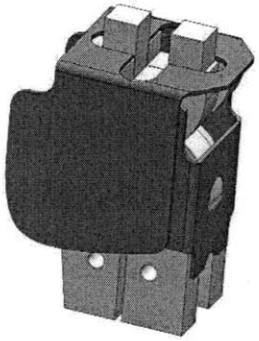

Figure 4.12: Squishbot1 active joint CAD model, with locking mechanism.

4.4.2 Mechanical Design – Locking Mechanism

The first step in the mechanical design of the locking mechanism is to calculate the minimum contact area required to lock the joint. This area is dictated by the yield stress of the chosen solder and the torque on the joint, as calculated by Equation (3.2). For Squishbot1, 60/40-ChipQuik alloy was chosen as the locking PCM. The shear yield stress for this alloy combination depends on the amount of Chip Quik used, as well as the yield stress of Chip Quik. The best way to calculate the actual yield stress of the joint is experimentally. However, the yield strength of

60/40 solder may be used to calculate the lower bound on the contact area. This is an acceptable first order estimate, as long as the designer keeps in mind that this is the ideal yield stress and the actual yield stress is lower. Table 4.11 lists the Squishbot1 values for the variables required to calculate the minimum contact area. Using this information, it was found that the minimum contact area for a Squishbot1 joint is 2.9mm^2. In Squishbot1, the joint was locked from both sides; this meant that the minimum contact area for each side was 1.5mm^2. Given the lower yield stress of the alloy and the need for reliability, an area larger than the minimum area is desirable to ensure locking of the joint. However, the larger the contact area, the larger the amount of solder that is required; which translates into higher melt and solidification energies. There is a careful balance between reliability and using more solder than necessary. Other parameters such as space, fabrication, and assembly need to be considered before deciding on the final shape of the locking mechanism.

Table 4.11: Squishbot1 values required to calculate the minimum contact area of the locking mechanism.

Variable	Squishbot1 Value	Description
F_{motor}	5.0 N	Force applied by motor to compress the legs.
l_{arm}	47.8 mm	Moment arm between joint and applied force.
Γ_l	0.24 Nm	Loading torque on the joint.
σ_{yield}	39.0 MPa	Shear yield stress 60/40 solder.
l_{plate}	2.1 mm	Moment arm between joint and locking mechanism.
A_{plate}	2.9 mm^2	Minimum contact area between plates.

Squishbot1 had to fit through a 1.5cm hole; therefore, all three joints had to fit in a 1.5cm diameter stage. This constraint limited the size of the CORE joints to be 3.9mm wide by 3mm thick. Figure 4.13 shows a CAD model of the stacked joints in the back stage, the assembly has a 14mm diameter. At this scale, fabrication and assembly played a large role in the design of these joints and locking mechanisms. The joints were made out of a plastic, given the material constraints set by the ChemBots program. The joints were designed in three layers, each layer comprised of one third of the cylinder thickness and one flexure blade. The layers were assembled alternating the position of the flexures using alignment holes in the cylinders. A

copper wire was threaded through the alignment holes to ensure the layers were aligned; finally the layers were glued together using super glue.

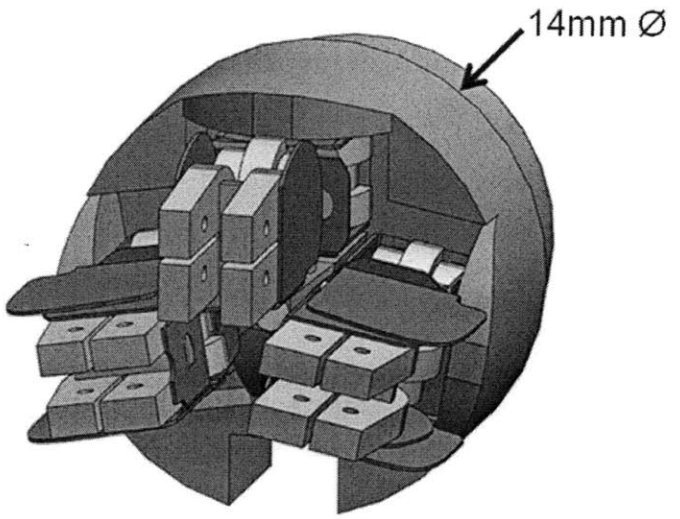

Figure 4.13: Squishbot1 back stage with assembled two-DOF joints. The joints farthest from the stage use the copper pieces to lock. The joints attached to the stage use the copper plates to prevent parasitic displacements.

The layers were cut using a laser cutter from a 1mm thick Teflon sheet. This method of machining resulted in flexures with the necessary thickness and was quicker than micro-milling these pieces. Teflon was chosen because it is a plastic that may be exposed to high temperatures without any damage. It was necessary that the joints would not melt when exposed to the unlocking temperatures of the solder.

The locking mechanism was constructed out of copper because of its wetting ability to lead-tin solders. To ensure that the joint would lock, even if the leg was not fully compressed or extended, the locking area was designed to allow the joint to lock anywhere between 0° and 90°. An explode view of the active joint assembly is shown in Figure 4.14. Plate A attaches to the top cylinder and remains stationary, while plate B slides as the bottom cylinder rotates.

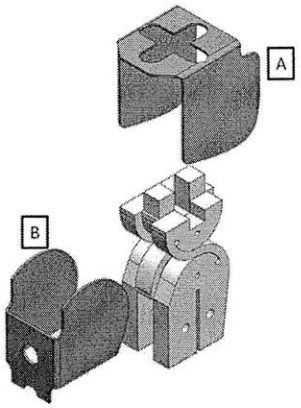

Figure 4.14: Exploded view of a Squishbot1 active joint. Locking plate A attaches to the top cylinder and remains stationary, while plate B rotates with the bottom cylinder. Soldering the two plates together locks the joint.

When designing the locking mechanism for Squishbot1, the thermal performance was not considered. The area of the locking plates was set to ensure the joints could lock at any position and they were made as wide as possible for locking reliability. The plates were cut out of .010" thick copper shim stock using a 10,000 rpm mill and a 1mm diameter end mill. Figure 4.15 shows the unfolded shape of the two locking plates as well as one of the jigs used to fold them into their final configuration. The folding jigs were 3D printed. The locking area depends on the locking position, and its average value is a total of 38mm^2.

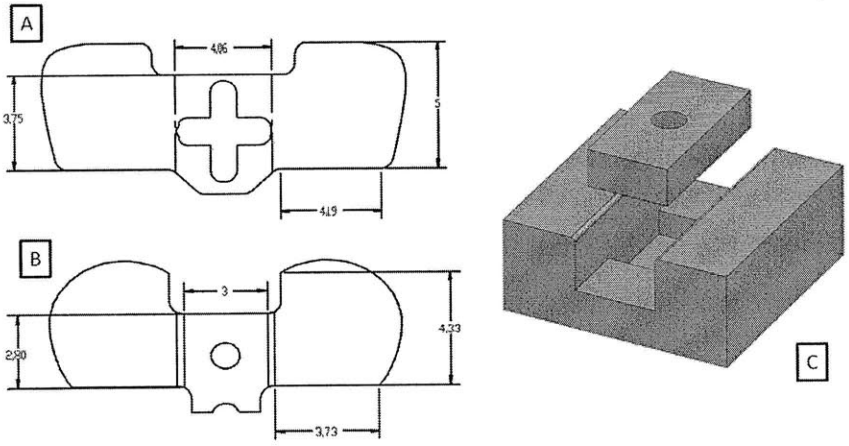

Figure 4.15: Squishbot1 final locking plate design. (A) & (B) Drawings of the locking plates in their flat configuration. (C) CAD model of the jig used to bend the locking plates into their final configuration.

4.4.3 Thermal Design

4.4.3.1 Thermal Circuit

The first step in the thermal analysis and design of the joint is to identify the thermal circuit of the joint and calculate the thermal resistances of each component. Figure 4.16 shows half of a joint of Squishbot1, and highlights the resistances of each component. The joint components are: the Teflon joint, the Kapton heater layer, the inner copper plate, the solder, and the outer copper plate. Table 4.12 lists the dimensions of each component and their conductivity; this information is used to calculate the resistances for each component using Equations (6.5) and (3.3).

$$R_{cond} = \frac{L_{heat}}{A_k \cdot k} \tag{6.5}$$

$$R_{conv} = \frac{1}{A_h \cdot h} \tag{6.6}$$

Heat is conducted through the joint components and convected into the environment. The resistance of the Teflon is calculated for a 1mm thickness to account for the fact that all that interests the designer is the resistance for the heat to travel into the Teflon. The thickness is chosen as an estimate of the portion of the Teflon that the heat travels through during the heating cycle. The estimate was made once the estimated heating cycle time was calculated to be on the order of five seconds. For this cycle time the Fourier number of the Teflon is approximately 0.2. The Fourier number of the component may be used to estimate the temperature response of the Teflon slab based on unsteady conduction analysis. Then the resistance of the thickness may be set as the fraction of the Teflon thickness over which the temperature gradient occurs. Based on models from Mills it was estimated that approximately 3/5 of the Teflon thickness would experience a temperature change over five seconds [22]. This estimate reflects the resistance of the Teflon after the heating cycle, which is used for estimating the heat transfer rate out of the solder during the cooling cycle. In the heating cycle the resistance of the Teflon is simply used to understand the heat flow out of the heater, but it is not used in the estimate of the heating time.

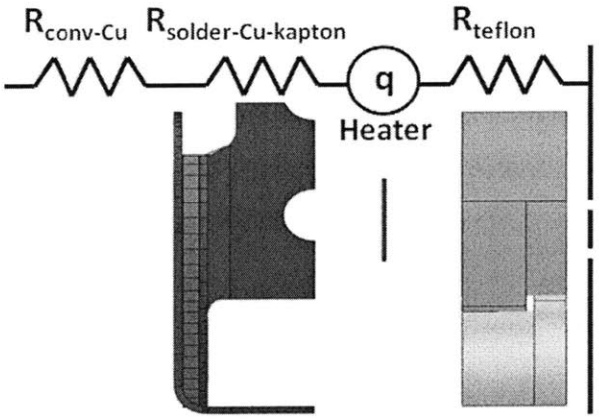

Figure 4.16: Squishbot1 active joint thermal circuit. Analyzing half a joint is sufficient given the thermal circuit is symmetric. The diagram highlights the resistances to heat flow from the heater.

Table 4.12: Squishbot1 component dimensions and calculated thermal resistances.

Component	Conductivity (k) or convection coefficient (h)	Area (A_k, A_h)	Thickness (L_{heat})	Resistance (R)
Teflon	0.251 W/mK	22.0 mm^2	~1.00 mm	~181 K/W
Kapton	0.120 W/mK	4.25 mm^2	0.05 mm	98 K/W
Inner copper	386 W/mK	18.3 mm^2	0.13 mm	.018 K/W
Solder	49.8 W/mK	18.3 mm^2	~0.25 mm	0.27 K/W
Outer copper	386 W/mK	23.9 mm^2	0.13 mm	.014 K/W
Convection	10 W/m^2K	23.9 mm^2		4340 K/W

In order to use thermal circuits for the first order models, the lumped thermal capacity model must hold, which assumes that there is no temperature gradient within each component. This model may be applied if the Biot number of each component is less than 0.1. Table 4.13 lists the calculated Biot numbers for the different parts of the Squishbot1 joint. The calculated Biot numbers are below 0.1, therefore, the lumped thermal capacity model may be applied to the entire joint, and thermal resistances may be used to calculate the heat rate transfer within the joint. It is important to note that 1.6mm was used as the thickness of the Teflon in the characteristic time because one is interested in understanding how long it takes for the entire Teflon slab to reach a constant temperature throughout.

Table 4.13: Squishbot1 component Biot numbers and characteristic time constants.

Component	Biot Number	Diffusivity (α)	Characteristic time (t_c)
Teflon	$6.47\text{x}10^{-2}$	$9.74\text{x}10^{-8}$ m^2/s	$2.71\text{x}10^{1}$ s
Kapton	$4.17\text{x}10^{-3}$	$7.75\text{x}10^{-8}$ m^2/s	$3.22\text{x}10^{-2}$ s
Inner copper	$3.29\text{x}10^{-6}$	$1.12\text{x}10^{-4}$ m^2/s	$1.44\text{x}10^{-4}$ s
Solder	$5.02\text{x}10^{-5}$	$3.35\text{x}10^{-5}$ m^2/s	$1.87\text{x}10^{-3}$ s
Outer copper	$3.29\text{x}10^{-6}$	$1.12\text{x}10^{-4}$ m^2/s	$1.44\text{x}10^{-4}$ s

Finally, the characteristic time of each component is calculated to understand how quickly the joint parts adjust to a temperature. This information provides insight as to how the joint behaves during heating and cooling. Table 4.13 lists the characteristic times and for each of the joint components of Squishbot1.

The resistance of the component quantifies the ease of heat transfer through that component. The joint design rules indicate the desire for a low resistance from the heater to the solder to ensure the heat may easily travel through this path. A high resistance to the other paths is necessary to reduce the amount of heat lost to other parts of the joint during heating. The characteristic time scale of the components indicates that the Teflon adjusts its temperature orders of magnitude slower than the rest of the components. This slow adjustment proves to be helpful in the cooling step.

4.4.3.2 Heating Step

During the heating step the heat travels away from the heater through two possible paths. Figure 4.17 highlights the heat paths during the heating step. The heat may travel through the Kapton layer and the inner copper to the solder, or it may travel directly from the heater to the Teflon. The heater had to be oriented so that the Kapton layer contacted the copper, to avoid shorting the heater coil. The equivalent thermal resistances of these two paths are calculated by summing the resistances of each component along the path. The equivalent resistances are highlighted in Figure 4.17. In the solder path, the heat continues to travel to the outer copper plate through conduction and then to the environment through convection. The convection resistance is orders of magnitude higher than the conduction resistance, therefore, a negligible amount of heat is lost to the environment during heating.

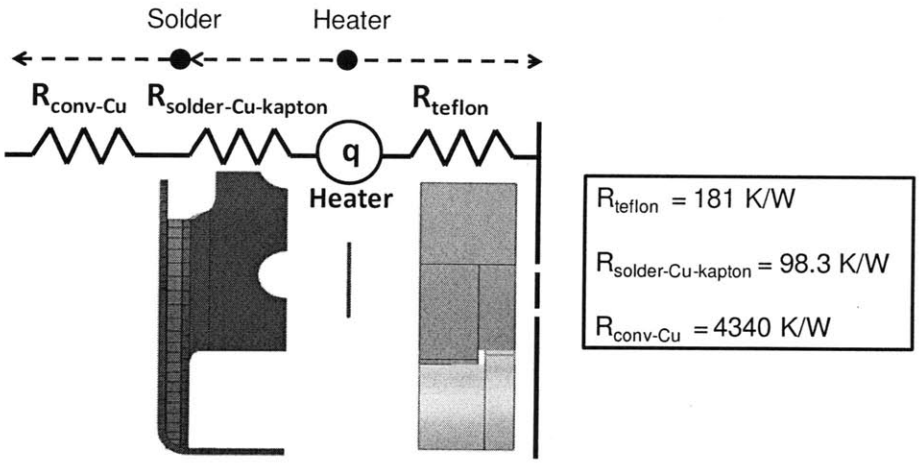

Figure 4.17: Squishbot1 heating cycle heat path. Heat travels away from the heater through either (i) the Kapton, inner copper, and solder or to (ii) the Teflon. From the solder the heat travels to the outer copper and through convection to the environment.

The heating energy lower limit is set by energy required to melt the solder, which is calculated using Equation (2.4). The activation time is calculated using Equation (4.4). Heat transfer rate is driven by temperature potentials; therefore, in a problem where the temperature of the components is changing the heat transfer rate is time dependant. In other words, as the components' temperature increases, the heat transfer rate from the heater to them decreases. Another way to model the decline in the heat transfer rate is to think of the resistance of the components as being time dependant. The longer the heating cycle, the wider the length of component that experiences a temperature rise, the higher the thermal resistance. This time dependency is complex and best calculated using FEA, nonetheless a heating time estimate may be calculated using the melt energy and the heater power. For Squishbot1, the amount of solder used in a joint was estimated, from the modeled volume, to be .04 grams. Given this mass and the .7W of heater power, the lower limit heating time estimate for the 60/40-ChipQuik is 3.7 seconds. This first order calculation gives an order of magnitude estimate of the heating time, it does not account for the energy used to heat the rest of the components. The heating time may be reduced by changing the solder design or the amount of solder used to lock the joint. Characteristic times for the components along the critical path of the solder should be low to ensure that these components adjust their temperature quickly, minimizing the heating time.

A more accurate heating time estimate may be calculated by accounting for the temperature rise in the remaining joint components along the critical path. For components with

characteristic times that are orders of magnitude lower than the estimated heating time for melting the solder, it may be assumed that these components reach the melting temperature of the solder during heating. Table 4.14 summarizes the information used to make a more accurate melting temperature calculation; this estimate takes into account the temperature rise of all of the joint components with low characteristic times. The total energy required to activate the joint is 2.55 J, and the estimated activation time is 5.6 seconds.

Table 4.14: Squishbot1 joint components heat capacity, mass, and temperature rise observed during joint activation. This information is used to calculate the energy required to heat each component to the solder's melting temperature.

Component	Heat Capacity (c)	Mass (m)	Temp. Rise (ΔT)	Energy to Heat (Q)
Kapton	1090 J/kgK	2.98×10^{-4} g	35 K	11.4 mJ
Inner copper	385 J/kgK	2.75×10^{-2} g	35 K	371 mJ
Solder	173 J/kgK	3.93×10^{-2} g	35 K	238 mJ
Outer copper	385 J/kgK	3.60×10^{-2} g	35 K	485 mJ

4.4.3.3 Cooling Step

The cooling time of the joint is dictated by the ability of the joint to conduct heat out of the solder. Figure 4.18 shows that during the cooling step, the solder is the energy source because the solidification energy needs to be conducted out of the solder in order to lock the joint. Heat may exit the solder through two paths (i) conduction through the outer copper plate, and then to the atmosphere through convection and (ii) conduction through the inner copper plate to the Kapton, and then to the Teflon. The equivalent thermal resistances of the two heat paths are highlighted in Figure 4.18.

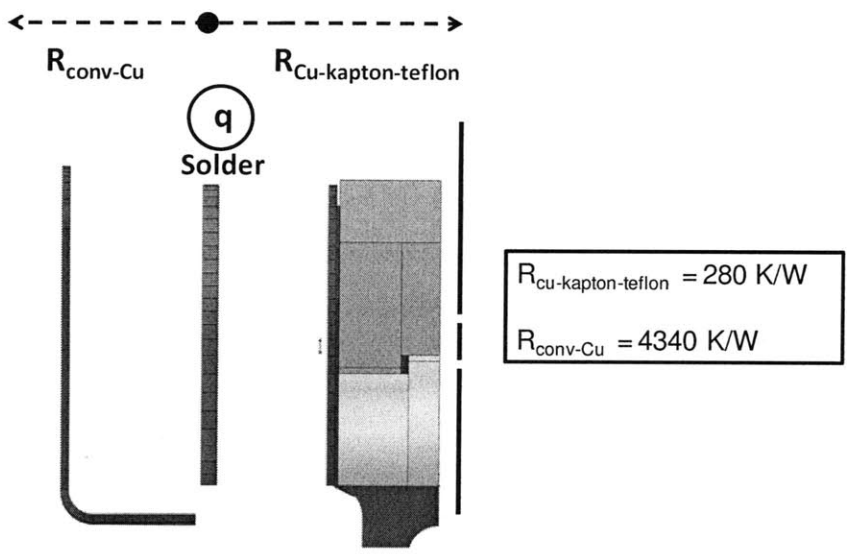

Figure 4.18: Squishbot1 cooling cycle heat path. Heat travels away from the solder through either (i) the inner copper, Kapton and Teflon or (ii) the outer copper then through convection to the environment.

During the making of Squishbot1, it was discovered that high characteristic time components have the potential to act as 'heat sinks' during the cooling cycle. As Figure 4.18 shows, the thermal resistance to the environment is large; if convection was the only way for heat to be lost to then the cooling time would be much longer than observed. The thermal circuit analysis shows that the resistance for heat to travel through to the Teflon is lower than the resistance to the environment. This point would be null if the entirety of the Teflon reached the melting temperature of the solder, because then there would be no thermal potential between the solder and the Teflon. However, since the characteristic time of the Teflon is longer than the first order calculation of the melting time, only a portion of the Teflon experiences a temperature rise. Therefore, the Teflon may act as a 'heat sink' during the cooling process.

It has been argued that lower bound for the cooling time may be calculated using the solidification energy of the solder and the heat transfer rate out of the solder. To obtain a more accurate estimate of the cooling time, the energy that must be lost by the components with low characteristic times may be added to the solidification energy of the solder. The energy loss necessary for the copper pieces to drop their temperature to locking temperature is easy to calculate by assuming that they reach melting temperature during heating. This is a fair assumption given the low characteristic times of these components. The Teflon, however, has a

characteristic time that is an order of magnitude larger than the preliminary heating time. The temperature rise in the Teflon is hard to estimate without an FEA model, or complex calculations.

To calculate the heat transfer rate from the solder to the Teflon, it is necessary to know the Teflon's temperature at the end of the heating cycle. The temperature of the Teflon after heating is different after each cycle because it depends on the length of the heating and cooling steps, and the time between cycles. In the first heating cycle, the short characteristic time components see a temperature rise from 23°C to 58°C. Teflon on the other hand was estimated to see only a temperature rise over the length of 1mm. Therefore, one can model the temperature gradient across the 1mm to be 35°C. The calculated resistance from the solder through the Teflon is 280 K/W. These first order models indicate that it takes approximately 11.2 seconds to solidify the solder. This estimate includes the energy that the copper, Kapton, and solder have to lose to lower their temperature to the solder's solidus temperature (56°C). Detailed FEA models provide a more accurate number; nonetheless, this information may provide a good idea of the performance of the joint and how to improve it.

4.4.4 Squishbot1 – FEA Model

A Finite Element Analysis of the Squishbot1 joints was created to examine the transient behavior of the joint, and to verify the validity of the first order models. The FEA model differs from the first order models in that (i) it does not model heat transfer as one-dimensional, (ii) it does not use the lumped capacity model, it calculates the temperature of each component at every time step and then uses this as the starting condition for the next time step, and (iii) it calculates the temperature reached by each of the components during heating and uses this information to calculate the cooling time of the joint. A model of half of a joint of Squishbot1 was created, specifying the different component materials and a convection coefficient. This convection coefficient is the same value that was used in the first order models, $10 W/m^2$, but again it is an estimate and one of the limitations of the FEA model. The solder's specific heat capacity was modeled as temperature dependant to include the heat of fusion spike at the melting point. The solder's liquidus and solidus temperatures were taken from the experimental data collected; for all other solder properties the values for 60/40 solder were used.

Figure 4.19 shows the half-joint used for the FEA analysis highlighting the constraints placed on the model. The heater face between the Teflon and the Kapton was given a heat power input of 0.7W. The outer surface areas of the outer copper locking layer were given $10W/m^2$ convection coefficients. The analysis was run as a transient analysis. A thermostat was placed on the outer copper layer to shut-off the heater once the temperature reached 58°C. The thermostat's lower bound was set to 56°C, indicating the heater to turn back on once the solder had reached its solidus temperature. The analysis was run for 10 seconds with 0.1 second steps to ensure an accurate result accounting for the heat of fusion.

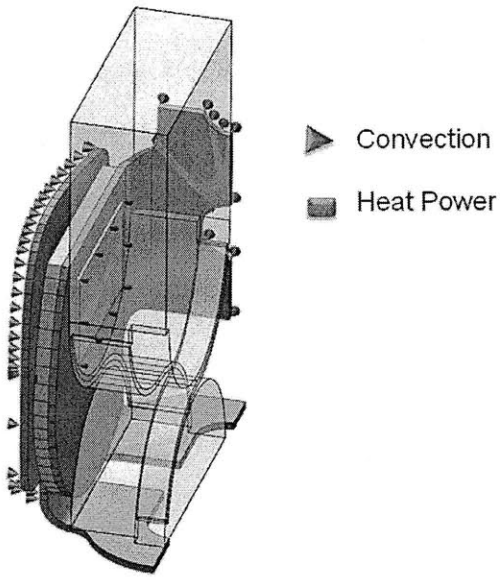

Figure 4.19: Squishbot1 CAD model highlighting the constraints set on the finite element analysis.

The temperature of the solder and the Teflon were probed and graphed over the analysis time to calculate the heating and cooling times, shown in Figure 4.20. The graph shows the temperature of the Teflon at a particular node. The results are compared to the first order calculations in Table 4.16. The activation times for the first-order and FEA models are 5.6 seconds and 5.0 seconds, respectively. The cooling times are 11.2 seconds for the first-order model, and 1.0 seconds for the FEA. The lower FEA cooling time may be explained by examining the Teflon temperature. Figure 4.21 shows the FEA results at the end of the heating cycle. The FEA results at this time show that at the end of the heating cycle, the temperature gradient in the Teflon is occurring across less than 1mm. Therefore, the Teflon resistance is lower than estimated. Another possible source of discrepancy might be the way the heat of fusion was modeled in the FEA program. It may be possible that the heat of fusion that must be lost

during cooling was not entirely accounted for by the program as discussed in Chapter 3. The validity of the models is discussed in more detail in section 6.4.6.

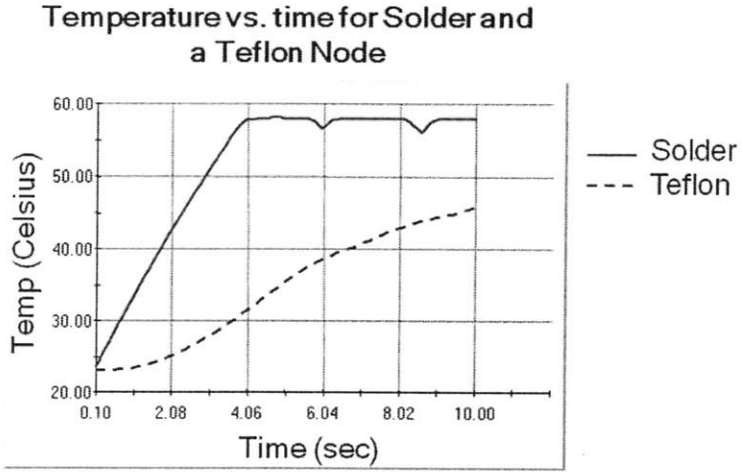

Figure 4.20: FEA thermal transient study temperature vs. time results for a Squishbot1 active joint. Both plots represent the temperature at a particular node of the components.

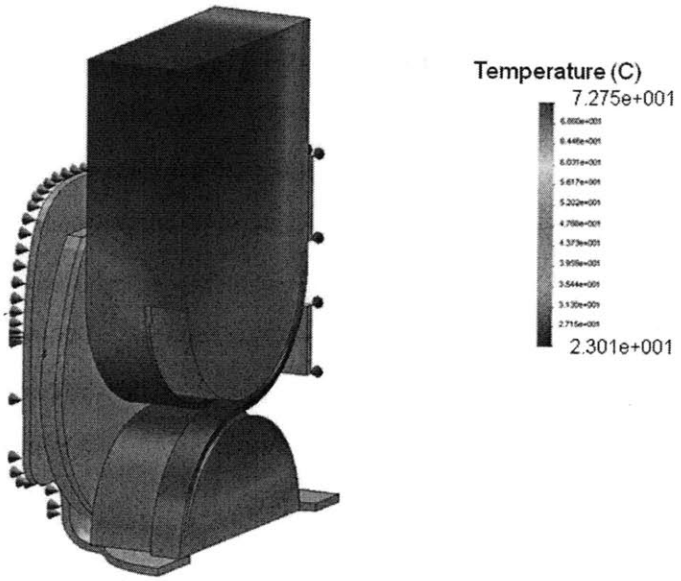

Figure 4.21: FEA results after heating cycle. Results show the temperature of a Squishbot1 joint after solder reaches melting temperature.

Figure 4.20 shows two complete cycles of a Squishbot1 joint. The second cycle begins as soon as the solder reaches 56°C. In cycle two, the starting temperature of the components is

higher than the starting temperature of cycle one. Therefore, the heating time is reduced from 4.7 seconds to 1.2 seconds. Although this cycling approach shortens the heating time, it increases the cooling time from 1.0 second to 1.4 seconds. This increase in cooling time is due to the Teflon reaching a higher temperature at the end of the heating step of cycle two. This higher temperature decreases the thermal potential between the solder and the Teflon, leading to a longer cooling cycle. The activation times for the two cycles are compared in Table 4.15. The thermostat points may be changed in the FEA model to try different cycling approaches.

Table 4.15: FEA heating and cooling times for two joint cycles.

Cycle #	Starting Temp. of solder & copper	Heating Time	Cooling Time
1	23°C	5.0 seconds	1.0 seconds
2	56°C	1.2 seconds	1.4 seconds

4.4.5 Experimental Results

The last step is to validate the FEA and first order models by collecting data on the performance of a Squishbot1 joint. The joint was tested by itself without the rest of the robot in order to match the models. Figure 4.22 shows the different components of joint before assembly as well as the fully assembled joint.

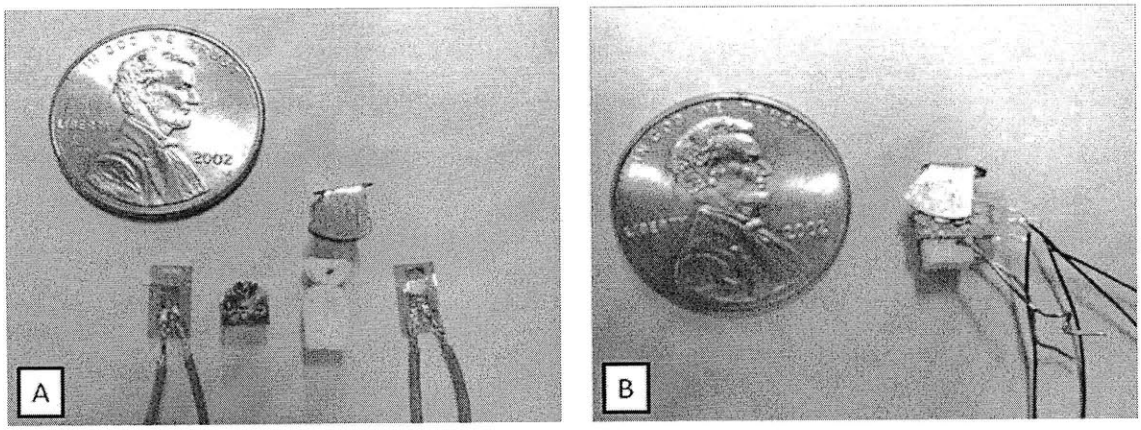

Figure 4.22: (A) Squishbot1 joint parts and (B) assembled joint. The assembled joint was used to experimentally validate the first-order and FEA models.

Before assembling the locking plates, they are wetted with a thin layer of 60/40 solder. The plates are then attached to the joint using super glue and Chip Quik is used to solder them

together. As a result, the joint is locked at the end of assembly. During this assembly process it is hard to control the amount of solder and Chip Quik that is used to lock the joint. The heating time was measured as the time between when the heater was turned on to when the joint was unlocked. The heater was turned off as soon as the joint was unlocked. The solidification time was measured as the time between when the heater was turned off and the joint was locked. The measured heating time was 6.4 sec, while the cooling time was 3.8 sec. Table 4.16 compares the results of the two models to the experimental data.

Table 4.16: Model and experimental heating and cooling times for the first cycle of a Squishbot1 joint.

	Heating Time	Cooling Time
First-order model	5.6 seconds	11.2 seconds
FEA model	5.0 seconds	1.0 seconds
Experimental	6.4 seconds	3.8 seconds

4.4.6 Validity of Models

In order to simplify the first-order models, thermal circuit analysis was used. The first-order model used the initial conditions to calculate the heating and cooling times for the joint. The FEA model takes into account that this problem is in fact transient, and as such the heat transfer rate to the different components depends on the elapsed time. This is the major difference between the two models. Nonetheless, the first-order model result for the heating time is only 0.6 seconds off the FEA model estimate. The cooling time estimate differs by 10.2 seconds. This large difference is due to overestimating the resistance of the Teflon at the start of the cooling cycle in the first order model. This overestimate led to a lower heat transfer rate out of the joint and as a result, a longer predicted cooling time. The first order model does not take into account the convective cooling on the Teflon which lowers its resistance during cooling. The FEA is limited by the size of the time step, which in this case was 0.1 seconds. The heat of fusion is incorporated into the FEA indirectly, and as a result the heat of fusion may be over- or under-estimated by the program. In this case the first order models and experimental results suggest the heat of fusion was not accounted for entirely in the FEA model.

The FEA and the first-order models are only as accurate as their inputs. In both cases several inputs were estimated including: (i) the convection coefficient, (ii) the thermal properties

of the 60/40-ChipQuik combination, and (iii) the amount of solder in the joint. These estimates account in part for the differences between the modeled and measured times. The joints used in the models were composed of only five components. In reality the Teflon consists of three parts that are glued together and aligned using copper wire, as shown in Figure 4.22. The heater and copper pieces are super glued to the Teflon as well. Neither the super glue layers nor the copper wires were accounted for in the models. The glue layers and the gaps between the components create a thermal resistance between each of the pieces. A major source of error is the amount of solder in the joint because it is hard to control how much is used per joint. Finally the heater output was not controlled with a temperature sensor and as a result the temperature of the joints may have been lower or higher than the modeled temperatures.

Overall both the FEA and first order models provide a good estimate of the heating and cooling times of the joint. The first order models allow the designer to quickly calculate the order of magnitude of the performance of the joint. More importantly, the models provide insight on the parameters controlling the joint performance.

4.4.7 Squishbot1 – Joint Design Possible Improvements

The locking mechanism design for Squishbot1 didn't take into account the thermal performance of the joint. The locking plates were designed to be as large as possible to ensure reliability and locking over 90°, while still fitting within the allotted space. A better process would have been to consider the thermal performance of the joint when designing the locking mechanism. Listed are some of the thermal considerations that were omitted:

(1) The locking plate surface area affects the cooling time. The larger the surface area, the greater the resulting cooling rate. The surface area affects the heating time as well. However, as long as the conduction resistance continues to be orders of magnitude lower than the convection resistance, the convection heat loss during heating should still be negligible.

(2) The contact area of the plates determines the amount of solder used in the joint. Therefore, there is an important balance between reliability and the quantity of solder required. For Squishbot1, the contact area was an order of magnitude larger than the calculated minimum contact area. The heating and cooling times may be reduced by using less solder.

(3) The role of the Teflon during cooling was not understood when the joint was designed. Had the 'heat sink' effect been known, the choice of plastic for the joint would have been explored in detail. For future designs the ability of the plastic to act as a heat sink should be exploited to reduce the cooling time.

4.5 Squishbot1 Performance

Squishbot1 was able to locomote along its axis, steer left and right, and lift its front while using one actuator and three solder-activated joints. Figure 4.23 shows the completed mechanism lifting its front battery. The robot was able to crawl at 17.5 mm/s and steer at ~37 degrees/step as shown in Figure 4.24. Once in the robot, the joints were allotted a total 15s cycle time to reconfigure. The robot is able to fit through a 15mm diameter hole by locking its three legs in their extended position and using a prismatic joint to scoot through the hole, as shown in Figure 4.25. Squishbot1 uses anisotropic feet to allow it to advance in the desired direction [30].

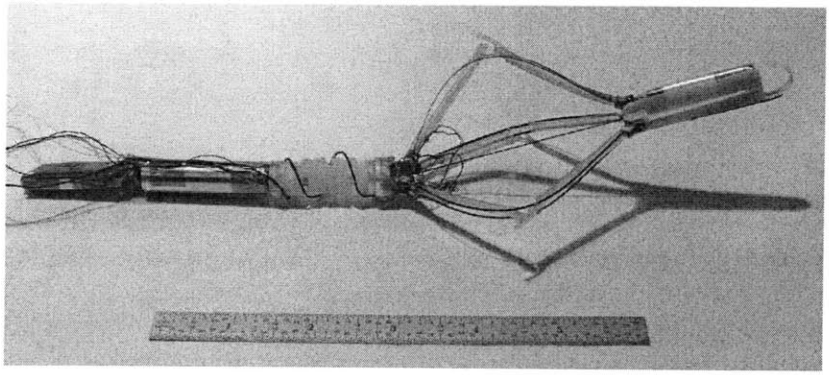

Figure 4.23: Squishbot1 mechanism lifting its front end using solder-activated joints.

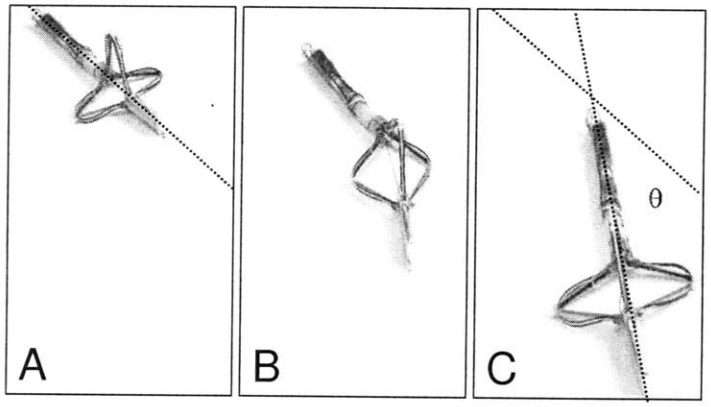

Figure 4.24: Squishbot1 executing a turn. In A, the joints are configured in an axial crawling state. The joint lock/unlock states are reconfigured to a turning state between A and B, and then the robot turns between B and C.

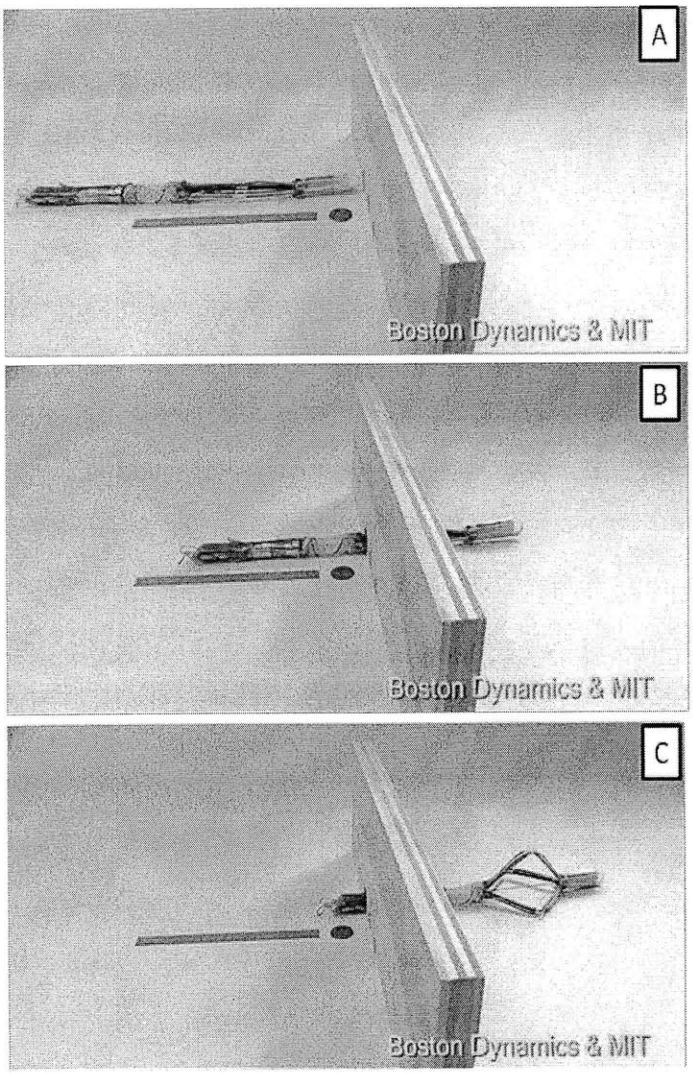

Figure 4.25: Squishbot1 traversing a 20mm hole. In A &B, all the joints are locked in the extended leg position, and a prismatic joint is used to advance the mechanism. In C, the joints have been unlocked and the robot begins to crawl using the tripod structure.

The rules and guidelines for designing solder-activated joints that were developed during Squishbot1 had been applied to future joint designs [30]. One of these designs is detailed in Chapter 5. Squishbot1 demonstrated that single actuator cm-scale mechanisms may perform a multiplicity of tasks by using PCM activated joints. This robot took the SQUISHbot team one step closer to realizing compliant robots with tunable stiffness.

CHAPTER

5

CASE STUDY II. LOCKING TENDONS

5.1 Locking Mechanism Introduction

Squishbot1 was able to crawl, steer, and expand its diameter with a single motor. This robot proved that the single actuator, tunable stiffness approach undertaken by the SQUIShbot team was possible. The single motor design made it possible for the robot to be made at the cm-scale. Squishbot1 also demonstrated the efficacy of solder locking joints and helped developed the rules and insights on how to efficiently design these locking mechanisms.

With the complete set of design rules for solder-activated joints, the team was ready to create the next generation of SQUIShbot mechanisms. The ultimate goal for the team is to develop a new class of compliant robots. As such, the beta mechanism had to be more compliant than Squishbot1. The objective for the PCSL became to create a new locking approach that would enable the control of soft structures with a single actuator. Structures are considered to be soft when they may achieve large deformations, on the order of their size scale, without yielding.

The locking tendons approach is a way to control a variety of restoring structures into different single-DOF mechanism states. Figure 5.1 shows a picture of the final SquishTendons locking mechanism, while Figure 5.2 presents the CAD model of the design with its different parts identified. The tendons in SquishTendons are locked using prismatic joints. Locking the tendons constricts the expansion of the restoring element. The same spooler actuator from Squishbot1 is used to compress the structure. While compressed, the different tendons are then locked using solder. When the string is released, the restoring element expands along the unlocked cables, and remains compressed on the sides that are locked.

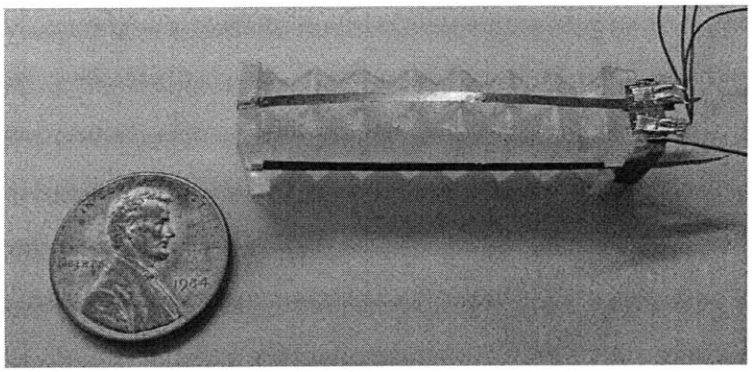

Figure 5.1: SquishTendons final assembled mechanism.

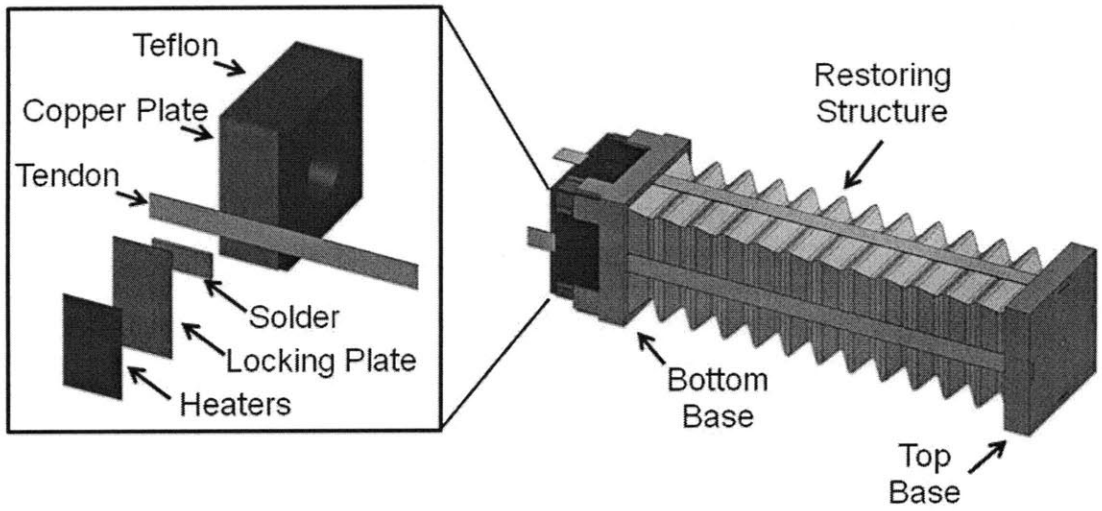

Figure 5.2: SquishTendons CAD model with labeled parts. Left Inset shows an exploded view of the locking mechanism.

The locking tendons approach may be implemented onto a variety of restoring structures. SquishTendons demonstrates that soft structures may be controlled to perform a variety of tasks using a single motor. The mechanism is able to achieve eight one-DOF states.

5.1.1 Scope

This chapter details how the design rules for solder activated joints were used to develop SquishTendons. The goal is to demonstrate the power of these guidelines and models in constructing efficient solder locking joints. The discussion is limited to the design, modeling, and implementation of the locking mechanism. SquishTendons may be applied to a variety of restoring force mechanisms including, but not limited to: the presented 3D printed bellows, a traditional spring, the tripod structure of Squishbot1, and conventional foam. A brief discussion

of the restoring structure used in SquishTendons is presented to provide an example of a soft structure that may be controlled using locking tendons.

5.2 Overall Mechanism Description

The goal for the locking tendons approach was to minimize the energy required to activate the different one-DOF mechanism states, as well as the locking and unlocking times. The SquishTendons were limited by the same heater and power constraints as Squishbot1. The final locking structure has not yet been implemented into a next generation robot.

5.2.1 Locking Tendons Approach

Cables have been used for steering a variety of instruments such as medical devices for many years. Cable steering consists of attaching cables to the tip of a structure and then controlling the position of the tip by pulling on the different cables. Researchers have demonstrated this approach for steering the tips of endoscopes [31]. These cable-steered mechanisms served as inspiration for SquishTendons. However, there are some major differences between the presented locking tendons design and cable steering.

SquishTendons uses a single actuator to control all of the tendons. The tendons slide on the locking plates to create prismatic joints. The locking mechanism, shown in Figure 5.2, uses solder to lock the cables in their compressed position to constrict the soft structure. Unlike previous designs, the SquishTendons design does not actuate the individual cables. Instead, the design uses the cables to restrict the expansion of the restoring structure. The structure must be compressed to achieve the different mechanism states. Figure 5.3 shows SquishTendons in two different one-DOF states.

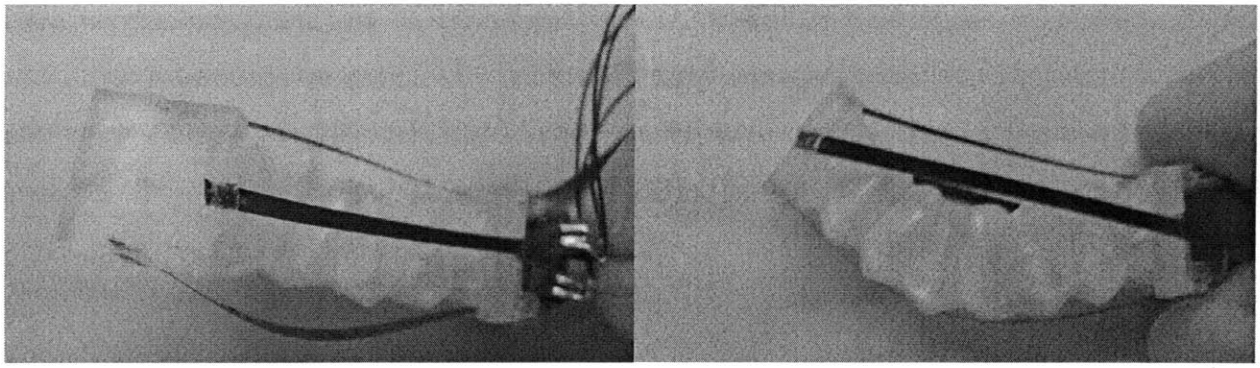

Figure 5.3: SquishTendons in two different one-DOF mechanism states.

Careful consideration of the mechanical and thermal properties of the tendons is necessary for the locking tendon approach to work effectively. The thermal properties of the cable influence the locking and unlocking times and are discussed in detail in the joint thermal design section 5.4.3. Mechanically, the cables must be strong enough to keep the restoring member compressed without failure. The tendons must be able to deflect along with the structure. To achieve large deformations, the cable material should have a high yield stress to modulus ratio. The larger this ratio the more the tendon may bend without yielding. Table 5.1 compares the mechanical properties of the four materials under consideration. The materials are normalized with respect to copper. Copper was chosen as the standard because of its favorable thermal properties and its high solderability. It is important to address other material properties, such as its wetting ability and thermal properties, before making a final selection. In section 5.4.3, the thermal properties of the materials are addressed and the tendon material is selected.

Table 5.1: Yield stress to modulus of elasticity ratio for the different materials considered in the selection of locking plate and tendon material. The values are normalized with respect to copper.

	Modulus of Elasticity (E)	Yield Stress (σ_{yield})	Yield/Modulus Ratio
Annealed Copper	1.0	1.0	1.0
6066 Aluminum	0.63	2.48	3.96
High-Temp Nitinol	0.68	16.8	24.7
1095 Spring Steel	1.82	16.5	9.08

5.2.2 Restoring Member

The SquishTendons mechanism uses a 3D printed compliant bellows structure as a restoring member, shown in Figure 5.4. The bellows has a square cross-sectional area, with an outer 8.8mm side, 0.5mm thick walls, and a 64.5° fold angle when extended. The length of the bellows is 34.3mm, and it is able to compress down to 20mm. The bellows structure was chosen because it supplies a restoring force when 3D printed out of the Connex 500 soft Tango+ material. 3D printing the structure simplified fabrication and allowed for assembly features to be easily incorporated into the structure. The key material properties of Tango+ are listed in Table 5.2, and the full material specifications sheet is included in Appendix D.

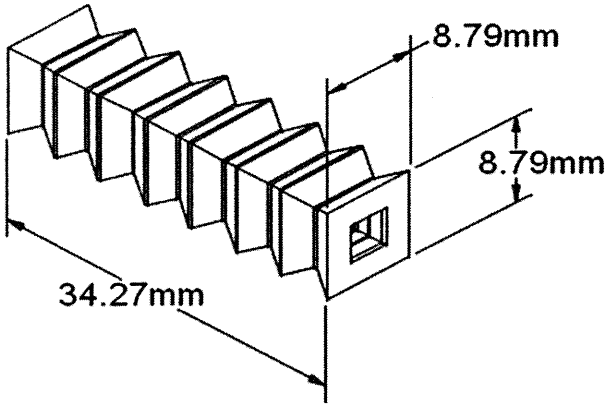

Figure 5.4: SquishTendons' restoring structure drawing with dimensions.

Table 5.2: Relevant mechanical properties of Tango+.

Elongation at break	218%
Modulus of elasticity at 20% strain	0.1 MPa
Shore A Hardness	27 Scale A

5.3 Solder Design

5.3.1 Mechanical Considerations

The yield strength of lead-tin solders is usually higher than the strength of the mm-scale soft structures. Yield strength may be sacrificed, through alloying, in favor of a lower liquidus and solidus temperature. In the case of SquishTendons, the strength of the locked prismatic joint

had to exceed the restoring force of the soft structure. The maximum restoring force is limited by the force output of the spooler motor, which is 5N. The motor must be able to compress the structure to actuate the robot. The minimum contact area for the locking tendons was calculated using the maximum restoring force. Equation (5.1) calculates the minimum contact area, A_{lock}, for the maximum restoring force, $F_{restore}$, and the shear yield stress of solder, σ_{yield}.

$$A_{lock} = \frac{F_{restore}}{\sigma_{yield}} \tag{5.1}$$

For 60/40 solder the minimum contact area for each locking tendon is 0.094mm^2. When alloying the solder to improve its thermal properties the locking area should be larger than the calculated area given the decrease in solder yield strength.

The next step is to consider the ease of soldering and cycling performance of the different alloying elements. This thesis considered the same three alloys from Squishbot1 for SquishTendons because of their availability to the project. During Squishbot1, it was discovered that indium diffuses into copper during cycling, leading to failure of the locking mechanism. This failure mode was not discovered until the completed Squishbot1 mechanism was subjected to a series of activation cycles. To avoid cycling problems, the solder-alloy combinations being considered should be cycled during the solder design phase.

5.3.1.1 Cycling of Solder

Of the three alloys considered in this research, two of them contain Indium. As discussed in Chapter 4, Indium diffuses into Copper creating brittle formations that lead to locking failure [27]. During cycling, bismuth alloys seem to perform better than the indium alloys. The Vishay strain gage heaters used in this research are unable to reach the melting temperature of the Bismuth 60/40 alloy combination. In other applications, when different alloys are being considered, cycling tests should be performed at this point in the design to ensure that cycling is not a problem. From Squishbot1, it was known that the indium alloy combination on copper would begin experiencing locking problems after about 20 cycles.

5.3.1.2 Rules

The mechanical solder design rules were addressed as follows during the design of the SquishTendons:

1. The yield strength of 60/40 solder was used to calculate the minimum contact area necessary for the prismatic joints. The maximum possible restoring force was used in the contact area calculation to ensure that the locking tendons would be able to constraint different restoring structures. Alloying the solder to reduce its melting temperature results in a decrease of the solder's yield strength. When alloying, the contact area should be designed to be larger than the minimum area.
2. The creep strength of the solder was not a problem because the application did not require for the joints to be locked in a loaded position for an extended period of time.
3. Solder activated joints in robotic mechanisms are subjected to phase change cycling, which aggravates oxidation and diffusion problems. Consequently, the wetting ability of the solder is a salient issue. The strain gage heaters used required for the solder's melting temperature to be below 100°C. This maximum temperature constraint eliminated the bismuth alloy. As a result, an indium based alloy had to be used in SquishTendons, despite its diffusion into copper during cycling.

5.3.2 Thermal Considerations

5.3.2.1 Melt Energy and Heating Time Calculation

SquishTendons was designed with the same power constraints as Squishbot1. The maximum power allotted for the strain gage heaters was 700mW. The only way to reduce the heating time was to decrease the melt energy. The easiest way to reduce the energy required to melt the solder is to use less solder to lock the joint. Equation (5.2) shows that the required heating and fusion energies depend on the solder's mass.

$$Q_{solder} = m \cdot c \cdot (T_l - T_i) + m \cdot H_f \qquad (5.2)$$

Table 5.3 compares the melt energies of the two alloys left under consideration. The melting energy was calculated using Equation (5.2) and the measured melting temperatures of the alloys and the thermal properties of 60/40 solder. The energy calculation estimates the amount of energy required to melt 0.1 grams of solder alloy from room temperature. The heat of fusion is the dominant energy in the melt energy calculation because of the small amount of solder and the low liquidus temperatures. A complete analysis would use the thermal properties of each of the alloys in the calculation. These properties were not readily available and were hard to measure accurately without the proper equipment.

Table 5.3: Liquidus temperatures and estimated melt energies for 0.1 grams of 60/40 solder mixed with either ChipQuik or Indalloy117.

	Liquidus Temperatures	Melt Energy[+]
Chip Quik with 60/40	58°C	4.31 J
Indalloy117 with 60/40	47°C	4.12 J

[+] Energy required to melt 0.1 grams of alloy from room temperature (23°C). Energy calculation uses the specific heat capacity and heat of fusion of 60/40 solder.

5.3.2.2 Solidification Energy and Cooling Time Calculation

The cooling time calculation depends on the solidification energy of the solder and the joint's heat loss rate. Therefore, the melting range of the alloys needs to be determined. The larger the melt range, the more energy that must be lost to cool the solder from its liquidus to its solidus temperature. In Chapter 4, section 3.3.2, a simple setup was used to measure the solidification temperature of the Chip Quik 60/40 alloy combination. The same setup was used to measure the solidus temperature of the Indalloy 117 60/40 alloy combination. The solidus temperatures and solidification energies for the two alloys are compared in Table 5.4. The solidification energy was calculated using the heat of fusion and heat capacity of 60/40 solder; it reflects the energy that must be lost to solidify 0.1 grams of solder alloy.

Table 5.4: Melting range and solidification energies for 0.1 grams of 60/40 solder mixed with either Chip Quik or Indalloy117.

	Liquidus Temperature	Solidus Temperature	Melting Range	Solidification Energy[+]
Chip Quik with 60/40	58°C	56°C	2°C	3.74J
Indalloy117 with 60/40	47°C	43.5°C	3.5°C	3.76J

[+] Energy required to solidify 0.1 grams of 60/40 solder-alloy from its liquidus temperature. Energy calculation uses the specific heat capacity and heat of fusion of 60/40 solder.

5.3.2.3 Overall Cycle Consideration

The solidification energy is considered in the solder design because it determines the locking time for a solder given a specific joint design. The solidification energy becomes more important in a cycling application because the heat loss rate during cooling decreases with increasing cycle number. Comparing the melting and solidification energies for the two solder alloys it is observed that both alloys have similar performances. Chip Quik was chosen as the

alloying compound because during testing it was observed that 60/40 solder mixed with Chip Quik adjusted its temperature quicker than the solder mixed with Indalloy117. It is important to note that Chip Quik contains Indium which diffuses into copper during cycling and may lead to a brittle joint. This failure mode should be considered when choosing the locking plate material. If copper is chosen, then a layer of nickel may be added to prevent this diffusion [27].

5.3.2.4 Solder Thermal Design Rules

1. The activation cycle time is directly related to the amount of solder used for locking. Given solder's high yield strength the minimum locking area for a tendon to support 5N of shear force is $0.094mm^2$. SquishTendons' design seeks to balance minimizing the mass of solder in a joint and maintaining joint reliability. This balance is addressed in the locking plate design in section 5.4.2.
2. Alloying lead-tin solders with bismuth and indium lowers the solder's melting temperature and yield strength. Three alloys were considered for reducing the liquidus temperature of 60/40 solder: Indalloy117, Chip Quik, and Bismuth203.
3. Both the liquidus temperature and melting range of the solder alloy combinations were considered in the selection of the solder. The liquidus temperature relates to the melting energy, while the melting range determines the solidification energy. If available the solder alloys' heat of fusion, heat capacity and diffusivity should be considered when selecting the solder, as these properties affect the melting and solidification energies.
4. The Bismuth alloy was eliminated because the chosen strain gage heaters were unable to reach the solder-alloy's liquidus temperature.
5. The final solder selection was made considering both the melting and solidification energies. The Chip Quik alloy was chosen because during testing it was observed that this solder combination adjusted its temperature quicker than the Indalloy117 mixture. Quick changes in temperature indicate a high diffusivity.
6. The melting energy together with the heater output determines the lower bound on the melting time. The heater output was limited to 700mW, which results in an estimated 6.7sec heating time for 0.1 grams of the chosen solder Chip Quik alloy combination.

7. The solidification energy and the joint's heat loss rate govern the cooling time for locking the joint. The locking time may be estimated once the locking mechanism has been designed and analyzed.
8. The diffusivity of the solder-alloy combinations was not measured. It was assumed that all three alloys had a similar diffusivity to that of 60/40 solder, $3.35 \times 10^{-5} m^2/s$.

5.4 Locking Mechanism Design

5.4.1 Kinematic Design

The kinematic design of SquishTendons focuses on the locking joints. The restoring structure has no joints and is assumed to behave as a linear spring. The kinematic diagram in Figure 5.5 shows that the mechanism only needs four prismatic joints to actuate in eight different directions: north, south, east, west, northeast, northwest, southeast, and southwest. Table 5.5 summarizes the tendons that have to be locked to achieve the eight one-DOF mechanism states. All four joints have to be able to lock in order to achieve all the different mechanism states.

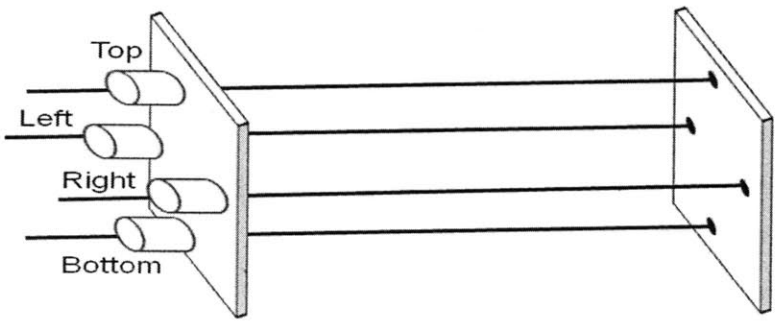

Figure 5.5: SquishTendons kinematic diagram. The locking mechanism is composed of four prismatic joints. Each joint locks one of the tendons.

Table 5.5: SquishTendons one-DOF mechanism states and the locked joints required to achieve them.

Mechanism State	Locked Joints
North	Top Joint
South	Bottom Joint
East	Right Joint
West	Left Joint
Northeast	Top and Right Joints
Northwest	Top and Left Joints
Southeast	Bottom and Right Joints
Southwest	Bottom and Left Joints

A larger amount of one-DOF mechanism states may be achieved by stacking SquishTendons modules, as shown in Figure 5.6. Each module has its own set of tendons, but all the modules are actuated by the same spooler motor. The actuator compresses the set of modules, then, the desired joints in each section are activated. Once the string is released, each module restores to the mechanism state allowed by the locked tendons. Figure 5.7 illustrates a two-module mechanism state. Each module has eight one-DOF mechanism states, as listed in Table 5.5, and together two modules have 64 mechanism states. The number of mechanism states for stacked SquishTendons scales as 8^n, where n is the number of stacked modules. This scaling occurs because for every one-DOF state of one module there are eight different states that may be achieved in the other module.

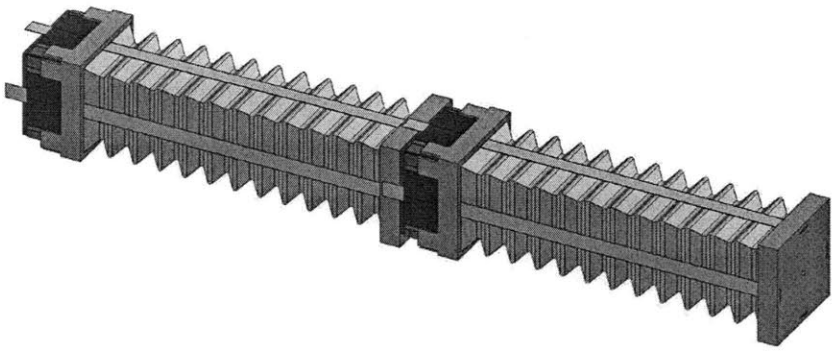

Figure 5.6: CAD model of stacked SquishTendons. Stacking of modules increases the DOF of the mechanism. The stacked modules may all be actuated with a single motor.

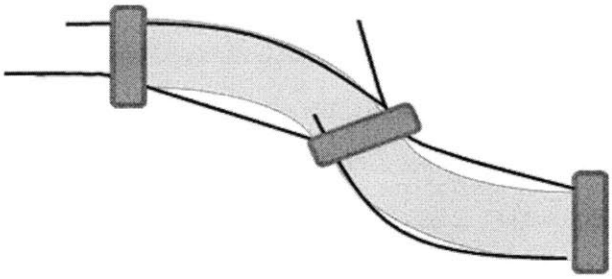

Figure 5.7: Schematic of a one-DOF mechanism state achieved by two stacked SquishTendons.

The final kinematic consideration is the range of motion of the joints and their locking range. The joint range is determined by the length of the tendon. The tendon must be long enough to stay in contact with the prismatic joint when the restoring structure is completely extended and when it is bent at an angle. The locking range of the joint depends on the mechanism functions. For SquishTendons it was desired that the joints lock only when compressed. Being unable to lock in the extended position allowed for the joints to be unlocked without compressing the structure. This unlocking approach reduces the unlocking time by allowing the joints to in the extended position without locking. When trying to solidify the joint to lock a tendon, the structure must remain compressed until the joint is locked. The limited locking range may be achieved by thinning only the portion of the tendon that is in contact with the locking plates when the restoring structure is compressed. Limiting the locking section reduces the amount of solder in the joint.

5.4.1.1 Kinematic Design Rules

1. In the SquishTendons design each joint constrains only one-DOF. Using single DOF locking joints reduces the complexity of fabrication and assembly as well as that of the heat isolation between DOF.
2. All four joints in the SquishTendons design had to be active joints in order for the mechanism to possess eight different one-DOF states.
3. The locking joints are located on the bottom platform because it is closest to the actuator and the energy source. This placement reduces the length of the wiring cables.
4. The locking range of the SquishTendons was set so that the tendons are lockable only when the structure is compressed. The limited locking range reduces the unlocking time for a joint and limits the amount of solder used in the mechanism.

5.4.2 Mechanical Design

The locking strength of the joint depends on the yield strength of the solder and the wetting ability between the solder and the locking plate material. The four tendon materials considered in the SquishTendons design were: copper, aluminum, Nitinol, and spring steel. The wetting ability of aluminum and Nitinol to lead-tin solders is poor. There are solders that have been specifically designed to solder these materials but these solders have prohibitively high melting temperatures for the active joint application [32],[33]. Copper plating may be used to improve a material's solderability. Nitinol and aluminum are not easily electroplated with copper. Steel and copper are solderable with lead-tin solders. Spring steel has a superior wetting ability to indium alloys compared to copper [27]. The material for the tendons and locking plates of SquishTendons is selected in section 5.4.3.1, when the material's yield strength to modulus ratio, wetting ability, and thermal properties are all considered.

The locking strength of the joint depends on the yield strength of the interface between the solder and the base material. The yield strength of this interface for 60/40 solders on both copper and steel is approximately 34.5 GPa [6]. The bond yield strength is 3 orders of magnitude larger than the solder shear strength; therefore the solder strength is the limiting factor. The minimum contact area for a 60/40 solder under 5N of shear force remains $0.094mm^2$.

The next step in the SquishTendons design was to consider the size constraints on the locking mechanism. The entire SquishTendons mechanism had to be able to fit through a 1.5cm hole. This size constraint limited the platforms to a maximum 1cmx1cm cross-sectional area. The footprint of the heaters determined the size of the locking plate. Ideally, the locking plates' area would be close to the minimum contact area to reduce the solder in the joint. However, the strain gages had to be able to fit side by side on the outer locking plate. Two strain gages had to be used in parallel for each joint in order to reduce the resistance of the heaters to 60 Ohms. The lower resistance translates to a higher current and lower voltage input given the 700mW power limitation. The strain gages burned up when the voltage across them exceeded 8-9 Volts. The strain gages' heater grid is 1.6x1.6mm^2. The strain gages were cut using a razor blade to reduce their footprint to 2.8x3.5mm^2. The result is a locking plate with a 6.6x3.5mm^2 area, as shown in Figure 5.8. An extra 1mm of length was necessary for assembly purposes.

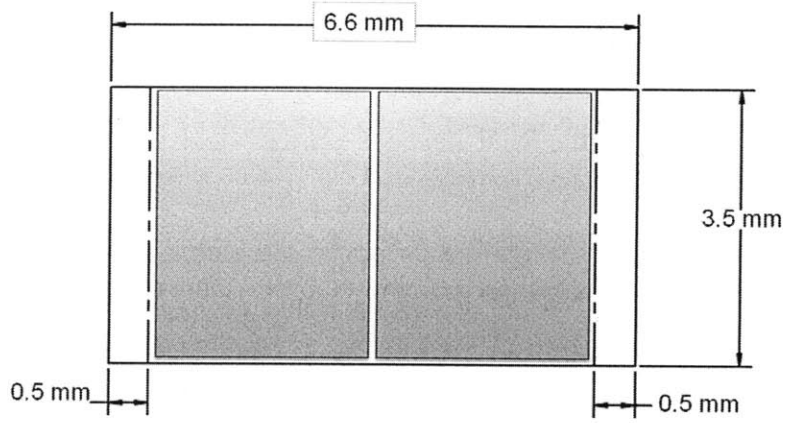

Figure 5.8: Outer Locking plate dimensions. Dotted lines separate the area used for assembly, while the shaded regions indicate the location of the two heaters.

Finally, a successful cm-scale mechanism design calls for fabrication and assembly considerations. Learning from the challenges in making and assembling Squishbot1, the parts for SquishTendons were designed to be as easy to machine as possible. The restoring structure and mechanism bases were 3D printed. The structure and top platform were printed using Tango+, a soft material. The bottom base was printed using DurusWhite, a material designed to have the toughness, flexibility and strength of polypropylene.

The locking plates design does not require the plates to be milled or bent. The outer locking plates are attached onto posts on the base structure. The tendons are super glued to slots on the top platform and run along the outside of the bellows through another set of slots in the

bottom base. Finally, a single cube of plastic is glued onto a recessed pocket on the printed base. This cube serves as a structure to keep the tendons and outer locking plates in contact. The plastic also serves as a heat sink. Table 5.6 summarizes the fabrication methods used for each component. To ensure that the locking plates come into contact with the tendons, the outer locking plate attachment posts were printed at an angle. When the plastic piece is inserted in the middle the outer plates, it provides a preload force keeping the tendons in contact with both plates. The preload mechanism is show in Figure 5.9. The preload angle was set to 5° off the vertical.

Table 5.6: SquishTendons component fabrication methods and material.

Component	Fabrication Method & Material
Top Base	3D Printed – Durus White
Restoring Structure	3D Printed – Tango+
Bottom Base	3D Printed – Durus White
Tendons	Hand Tools – Spring Steel Shim Stock
Locking Plates	Hand Tools – Spring Steel Shim Stock
Copper Plate	Hand Tools – Copper Shim Stock
Teflon Block	Hand Tools – Teflon

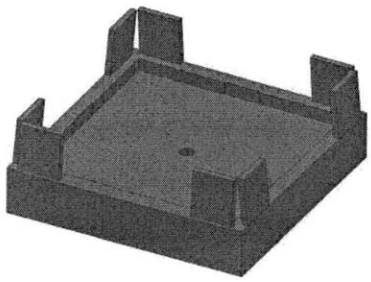

Figure 5.9: CAD model of preload mechanism. The 5° angle on the attachment posts preloads the locking plate against the tendons.

5.4.2.1 Locking Mechanism Mechanical Design Rules

1. The shear strength of the interface between the solder and the base material was compared to the solder's yield strength to determine the weakest face of the locking mechanism. The solder's yield strength is orders of magnitude lower than the interface strength and therefore, it is used to calculate the minimum contact area for the joint. The locking area should be minimized to reduce the amount of solder. The size of the strain gages requires the locking plate to be at least 5.6 mm by 3.5 mm.
2. SquishTendons had to fit through a 1.5cm hole which constrained the mechanism to be 10x10mm^2 in cross-sectional area, with a 14.2mm diagonal.
3. The wetting ability of the base material to lead-tin solders was an important consideration in the design of SquishTendons. Nitinol and aluminum were discarded as possible locking plate materials given their poor wetting ability to lead-tin solders. Both copper and spring steel may be soldered with the chosen solder-alloy combination.
4. The design of the components of SquishTendons simplified fabrication and assembly. 3D printing the restoring structure and bases reduced the number of components and allowed for assembly and alignment features to be easily integrated. The inner locking plates were replaced with a single piece of plastic that served as a support structure and heat sink.

5.4.3 Thermal Design

5.4.3.1 Thermal Circuit

The thermal circuit of the mechanism is used to quickly analyze the joint's thermal performance. The thermal circuit models each piece of the joint as a resistor. The equivalent resistance for each heat path may then be calculated and the heat transfer rate optimized. The thermal resistances depend on the components' conductivity and geometry. Figure 5.10 shows an exploded view of the locking mechanism as well as, the thermal circuit for the design. The resistances for each component may be calculated once the final material is chosen. The heat transfer is modeled as one-dimensional because the heat flow rate perpendicular to the heaters is

orders of magnitude larger than the heat flow in the other two directions. This assumption is verified once the material for the tendons has been chosen.

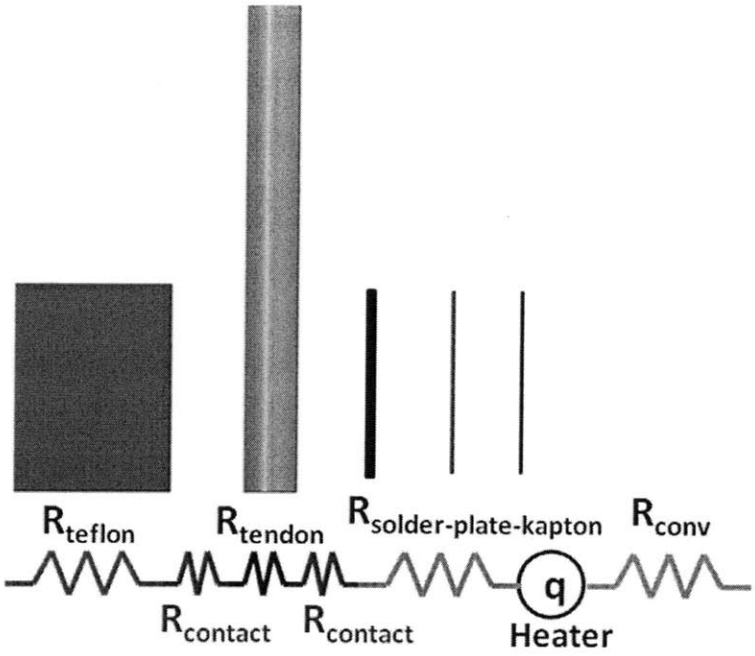

Figure 5.10: Preliminary locking mechanism design and thermal circuit for round cross-section tendons.

Initially the SquishTendons design called for round-cross section cables as the tendons. This resulted in a line contact between cables and the locking plates, as opposed to a surface contact. Line contact has a larger resistance to heat flow. This added resistance is modeled in the thermal circuit as a contact resistance, as shown in Figure 5.10. The preliminary thermal circuit showed that a square cross section cable is a better choice for a tendon. Figure 5.11 shows the updated design and thermal circuit. A square cross-section tendon is modeled as a single resistor. The mechanism states of SquishTendons call for the tendons to curve along the restoring structure. To minimize the load on the locking plates from the deflection of the tendons the width and thickness of the tendons was minimized. The thickness was set to .051mm (.002") by the availability of copper and spring steel shim stock. The width of the tendon was chosen to be 1.5mm. The width was chosen by trying to balance its effect on the heat transfer resistance, the amount of solder used and the load from the tendon on the locked mechanism. The final tendon dimensions are shown in Figure 5.12.

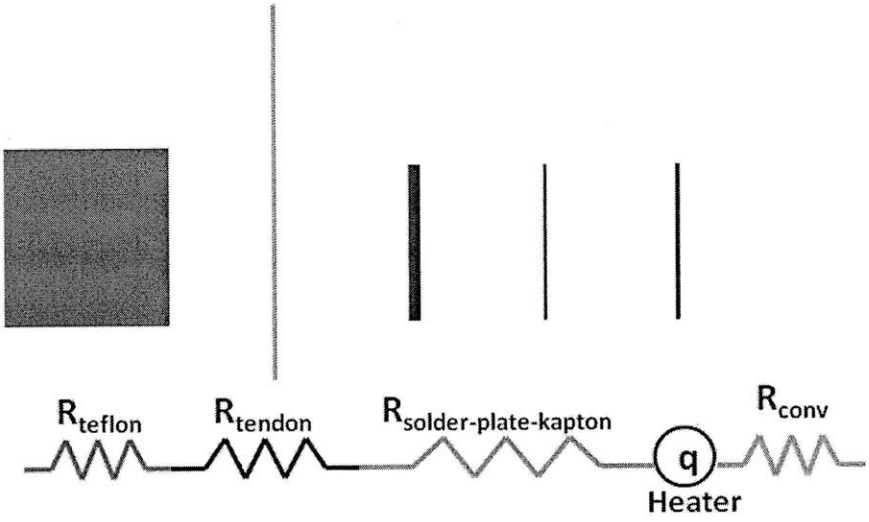

Figure 5.11: Updated locking mechanism design and thermal circuit for square cross-section tendons.

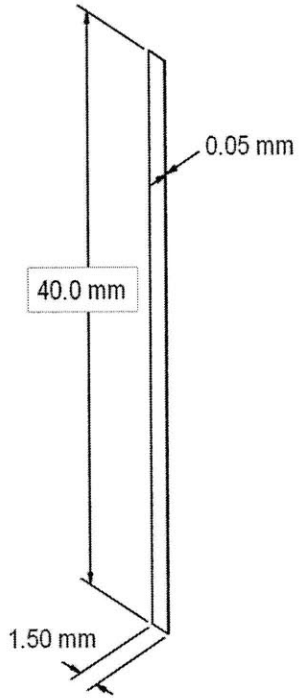

Figure 5.12: Drawing and dimensions of final tendon design for SquishTendons.

With the geometry of the tendons set, the next step was to finalize the tendon material. The two materials left in consideration were copper and spring steel. To make the final decision the thermal and mechanical properties of the materials had to be considered. Table 5.7 lists the conductivity, specific heat capacity and diffusivity of annealed copper and spring steel. The table also shows the values normalized to copper to highlight the difference in thermal performance.

As discussed in the previous chapters, the locking plate material should have a low heat capacity as well as a high conductivity and diffusivity. The low heat capacity reduces the amount of energy required to raise the temperature of the plate to the melting temperature of the solder. The high conductivity and diffusivity improve the heat transfer rate in and out of the solder. Copper has better thermal properties than spring steel, however spring steel has a higher yield stress to modulus ratio and a better solderability to indium based solders. Table 5.8 contains a Pugh chart that was used to select spring steel as the tendon material. Steel was selected despite its inferior thermal properties because of its superior solderability to indium based solders. The dimensions of the outer locking plate, tendons, and solder used in the joint are listed in Table 5.9, along with their calculated conduction and convection resistances.

Table 5.7: Thermal properties of copper and steel, two possible tendon materials. Values are shown normalized with respect to copper for comparison.

	Conductivity		Heat Capacity		Diffusivity	
Annealed Copper	385 W/mK	1.00	.385 J/g°C	1.00	1.12×10^{-4} m^2/s	1.00
1095 Spring Steel	51.9 W/mK	0.14	.461 J/g°C	1.20	1.43×10^{-5} m^2/s	0.13

Table 5.8: Pugh chart comparing copper and steel on their mechanical and thermal properties, as well as their solderability with indium based solders. Copper is used as baseline for comparison.

	Mechanical Properties	Solderability	Thermal Properties
Annealed Copper	0	0	0
1095 Spring Steel	++	+	--

Table 5.9: SquishTendons component dimensions and calculated thermal resistances.

Component	Conductivity (k) or convection coefficient (h)	Area (A_k, A_h)	Thickness (L_{heat})	Resistance (R)
Teflon Support	0.251 W/mK	5.25mm^2	2.50 mm	1897 K/W$^+$
Kapton Heater	0.120 W/mK	19.6mm^2	0.05 mm	21.30 K/W
Outer steel plate	51.9 W/mK	23.1mm^2	0.05 mm	0.042 K/W
Solder	49.8 W/mK	5.25mm^2	0.25 mm	0.956 K/W
Tendon (contact area)	51.9 W/mK	5.25mm^2	0.05 mm	0.184 K/W
Convection	10 W/m^{2}K	23.1mm^2		4329 K/W

$^+$Teflon resistance is only valid for cycle times that are orders of magnitude larger than the Teflon's characteristic time scale.

The ability of Teflon to act as a heat sink was critical to the cooling performance of the Squishbot1 joint. Having learnt that high characteristic time components act as heat sinks during cooling, the design of SquishTendons sought to optimize this ability of the inner plates. The characteristic time of a component is given by Equation (5.3).

$$t_c = \frac{L_{heat}^2}{\alpha} \tag{5.3}$$

Given a set geometry one is left to choose materials with low diffusivities. The diffusivity of a material depends on its conductivity, k, its specific heat capacity, c, and its density, ρ, as shown in Equation (5.4).

$$\alpha = \frac{k}{\rho \cdot c} \tag{5.4}$$

Ideally the thermal conductivity of the material is high enough to facilitate the heat transfer out of the solder but low enough to reduce the heat transfer rate into the plastic during heating. From Table 5.9 it is known that the conduction resistance from the heater to the solder is 43.5K/W and the convection resistance of the outer plate is 4329K/W. The resistance to heat flow into the plastic should be somewhere between these two components. The dimensions of the plastic block were set during the mechanical design to be 8.5x8.5mm^2, with a 4mm diameter hole in the center. The hole was required to allow for the center string; its size was set to increase the surface area exposed to convection while maintaining a high characteristic time scale. Table 5.10 compares three high temperature plastics on their resulting conduction resistance and characteristic times. Torlon was eliminated because its calculated characteristic time was half of that of Peek and Teflon. Teflon was chosen over Peek because it is available in a larger variety of shapes and is less expensive than Peek.

Table 5.10: Thermal properties of the three high temperature plastics considered for the SquishTendons' inner structure/heat sink.

	k	c	P	α	t_c	R_{cond}
Teflon	0.251 W/mK	1.17 J/g°C	2200 kg/m^3	9.75x10^{-8}m^2/s	64.2 sec	1897 K/W
Peek	0.252 W/mK	2.16 J/g°C	1310 kg/m^3	8.91x10^{-8}m^2/s	70.1 sec	1890 K/W
Torlon	0.260 W/mK	1.01 J/g°C	1410 kg/m^3	1.83x10^{-7}m^2/s	34.2 sec	1832 K/W

5.4.3.2 Lumped Thermal Model

Before proceeding to the heating and cooling time calculations the validity of the lumped thermal model was verified. The lumped thermal model requires that the Biot number of the components be below 0.1 for the system the temperature gradient across the component to be less than 5% [23]. Table 5.11 lists the calculated Biot numbers and characteristic times for each of the components in the locking mechanism. The data shows that the lumped thermal model may be applied. The characteristic times highlight that all of the components besides the Teflon, adjust their temperatures quickly and may be assumed to be at the temperature of the solder at all times.

Table 5.11: SquishTendons component Biot numbers and characteristic time constants.

Component	Biot Number	Diffusivity (α)	Characteristic time (t_c)
Teflon	$1.0\text{x}10^{-1}$	$9.75\text{x}10^{-8}$ m^2/s	$6.42\text{x}10^{1}$ s
Kapton	$4.2\text{x}10^{-3}$	$7.75\text{x}10^{-8}$ m^2/s	$3.22\text{x}10^{-2}$ s
Outer Steel	$9.6\text{x}10^{-6}$	$1.43\text{x}10^{-5}$ m^2/s	$1.75\text{x}10^{-4}$ s
Solder	$5.0\text{x}10^{-5}$	$3.35\text{x}10^{-5}$ m^2/s	$1.87\text{x}10^{-3}$ s
Steel Tendon	$9.6\text{x}10^{-6}$	$1.43\text{x}10^{-5}$ m^2/s	$1.75\text{x}10^{-4}$ s

The thermal circuit modeled the joint as one dimensional. This assumption was corroborated by comparing the thermal conduction resistance across the tendon to the resistance along the tendon. The parameters required for this calculation are listed in Table 5.12, along with the calculated resistances. The resistance along the tendon is 10,000 times higher than that across the tendon, which signifies that the one-dimensional model applies. This is not to say that no heat is transferred along the tendon.

Table 5.12: Resistances across and along the length of the steel tendons.

	Conduction Area	Length of area	Resistance
Across Tendon	5.25 mm^2	.05 mm	0.184 K/W
Along Tendon	0.08 mm^2	40 mm	9634 K/W

5.4.3.3 Heating Step

In Squishbot1 the heater energy was able to travel through two paths (i) to the solder and (ii) to the Teflon. To improve the heating and cooling steps in SquishTendons the heater was placed on the outer locking plate as opposed to in between the inner locking plate and the Teflon. During heating, this change resulted in the heat traveling to the solder through the outer plate or to the environment through convection. The heat loss to the environment is orders of magnitude less than the heat transfer rate into the solder given the high convection resistance. Heat reaches the Teflon through the tendon because of the temperature gradient between them; however, the heat must first pass through the solder. Figure 5.13 shows the thermal circuit during heating, highlighting the heat flow paths and the equivalent resistances of the paths.

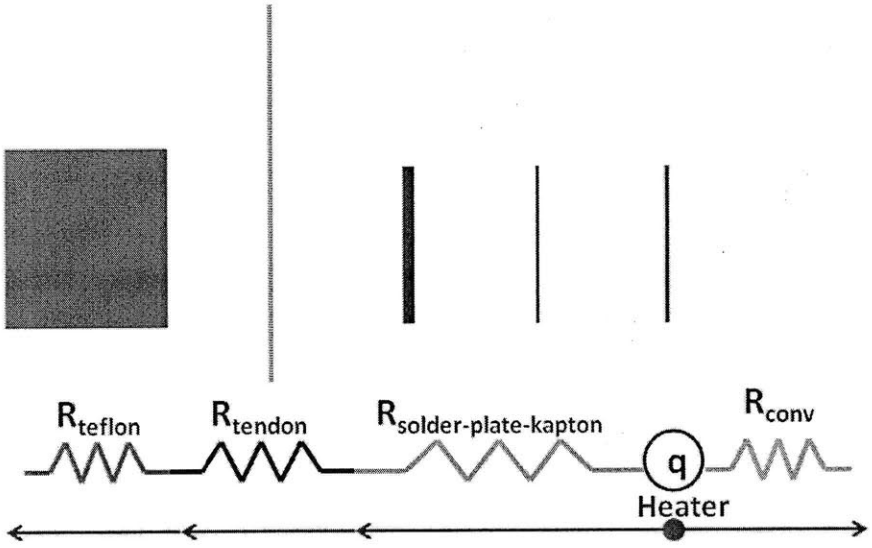

Figure 5.13: SquishTendons thermal circuit during heating.

Another important design feature of SquishTendons is that the amount of solder used in the joint was minimized as much as possible. The amount of solder was minimized by reducing the area of the locking plate and the tendons. It was decided not to use solder between the tendon and the inner plate. Instead the inner plate was used only as a support and a heat sink. The lower bound on the heating time may be calculated by ignoring the heat loss to the environment and the Teflon. The melting energy is estimated as the energy required to melt the solder in addition to the energy required to heat the solder, outer locking plate, and tendon to the solder's melting temperature. Table 5.13 contains the breakdown of the melting energy. Given 700mW of power to each heater, the estimated lower bound on the melting time for this design is 0.82 seconds.

Table 5.13: SquishTendons joint components heat capacity, mass, and temperature rise observed during joint activation. This information is used to calculate the energy required to heat each component to the solder's melting temperature.

Component	Heat Capacity (c)	Mass (m)	Temp. Rise (ΔT)	Energy to Heat (Q)
Kapton	1090 J/kgK	1.39×10^{-3}g	35 K	53.0 mJ
Steel Plate	461 J/kgK	1.05×10^{-2}g	35 K	166 mJ
Solder	173 J/kgK + 37 J/g^{+}	1.13×10^{-2}g	35 K	486 mJ^{+}
Steel Tendon	461 J/kgK	2.73×10^{-2}g	35 K	441 mJ
Copper Plate*	385 J/kgK	3.62×10^{-2}g	35 K	487 mJ

$^{+}$Calculation includes heat of fusion. *Copper Plate is added to the design in the cooling section. The energy to heat it is accounted for in the overall activation cycle section.

The design of the locking mechanism of SquishTendons took into consideration the heating insights as follows:

1. The resistance of the critical path to the solder was minimized to increase the heat rate transfer into the solder. The resistance was minimized by using materials with high thermal conductivity between the heater and the solder.
2. The heat transfer rate into other paths was minimized by placing the heater on the outer locking plate and exposed to air. The low convection area leads to minimal heat loss to the environment; therefore, the majority of the heat is forced to travel through the solder.
3. Throughout the design of SquishTendons, the amount of solder used in the joint was minimized. The locking plates and tendons were made as small as possible, without sacrificing thermal performance, to reduce the solder necessary to lock the joint.
4. The materials along the critical path to the solder were all chosen to have low characteristic times to ensure that they adjusted their temperatures rapidly.

5.4.3.4 Cooling Step

The cooling time for a locking mechanism is determined by the solidification energy and the rate of heat loss out of the solder. The heat loss rate is dominated by the heat loss to the heat sink components. The resistances of the components in transient heat problems are time dependent. The resistance increases as the heat travels through the thickness of the material. For components with low characteristic times, the temperature travels quickly across the entire

component and therefore, the time dependency may be ignored. For the heat sink components, the resistance at the beginning of the cooling step depends on the portion of the length of the component that experiences a heat rise at the end of the heating cycle. The temperature gradient across this affected length drives the rate of heat transfer. In the design presented in Figure 5.11 the contact area between the Teflon and the tendon is limited by the area of the tendon. Given the Teflon's low diffusivity, the heat is not distributed along the face of the Teflon. Therefore, the resistance of the Teflon during cooling increases given the area of the Teflon is limited to the contact area. Figure 5.14, shows how the heat is localized to the contact area. In summary, a large amount of the Teflon volume is being wasted as a heat sink.

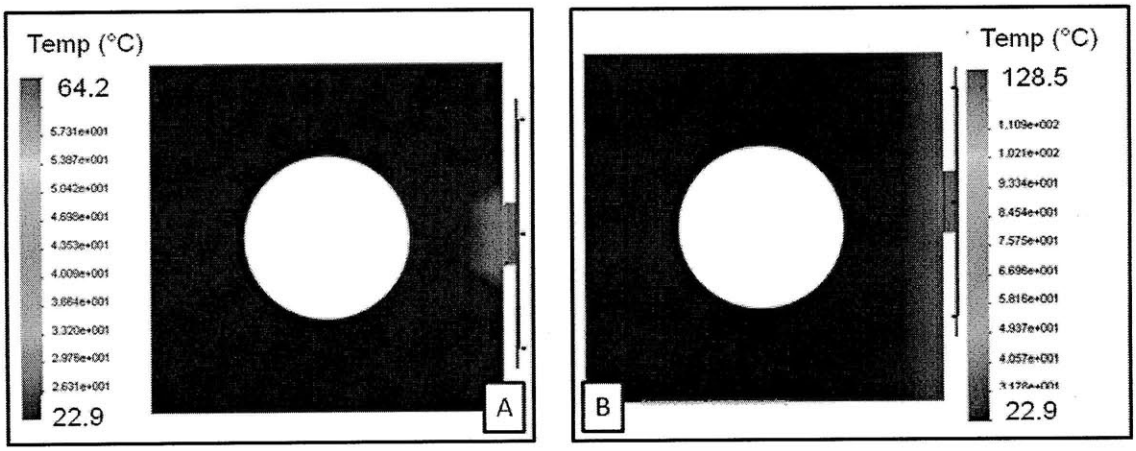

Figure 5.14: Finite Element Analysis of the SquishTendon locking mechanism. (A) 'Hot spot' created when the tendon is put directly in contact with the Teflon. (B) Heat is distributed by the copper plate along the entire Teflon surface area.

To better utilize the Teflon during cooling, it was decided to glue a copper plate to contact faces of the Teflon cube. The copper distributes the heat from the tendons along the face of the Teflon. The finite element analysis in Figure 5.14 shows the effect of the copper plate. For a given amount of energy the depth of Teflon with a temperature rise is less than that of the 'hot-spot', effectively increasing the transfer rate out of the solder. The copper plate increases the heating time because more heat travels to the Teflon as a result of the decrease resistance. However, the copper plate decreases the cooling time. The updated design is shown in Figure 5.15 along with the heat transfer paths during cooling and their resistances. The addition of the copper plate increases the melting energy, the updated heating time calculation is included in the overall cycle section. The energy required to heat the copper plate is listed in Table 5.13.

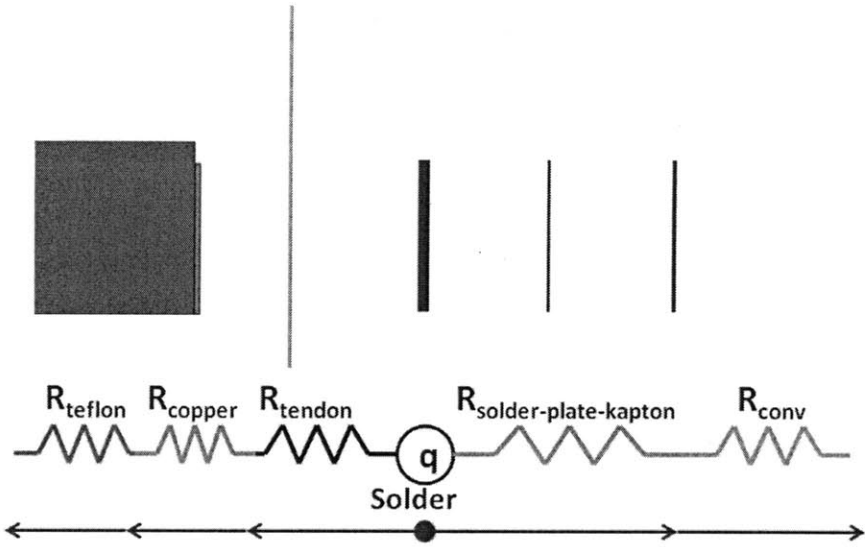

Figure 5.15: Final SquishTendons' locking mechanism design and thermal circuit during cooling phase. Updated model includes the copper plate used to distribute the heat along the surface area of the Teflon.

The cooling rate of the joint depends on the resistance of the Teflon at the end of the heating cycle. The heat penetration depth may be estimated using the Fourier number and the temperature response of a slab with negligible surface resistance. The heating step is approximately 1 second long, and the characteristic time scale of the Teflon is 64 seconds. The calculated Fourier number is .02, which corresponds to a depth penetration of about 2/5 of the length of the Teflon. This gives a resistance of 110K/W. The heat transfer rate into the Teflon is estimated using this resistance and the temperature gradient across the resistance. The model neglects that the Teflon resistance increases during the cooling cycle, effectively decreasing the heat transfer rate into the Teflon. The estimated time is the lower bound on the cooling time. The solidification energy is calculated using equation (5.5).

$$Q_{solid} = (m \cdot c \cdot (T_l - T_s) + m \cdot H_f)_{solder} + (m \cdot c \cdot (T_l - T_s))_{components} \quad (5.5)$$

It was assumed that the low characteristic time components must lose enough energy to lower their temperature from the liquidus to the solidus temperature of the solder. The total heat transfer rate out of the solder takes into account the heat loss to the environment and to the Teflon. Table 5.14 lists the values required to compute the solidification energy. The estimated cooling time was 1.5 seconds.

Table 5.14: SquishTendons joint components heat capacity, mass, and temperature drop observed during joint locking. This information is used to calculate the energy required to cool each component to the solder's solidus temperature.

Component	Heat Capacity (c)	Mass (m)	Temp. Drop (ΔT)	Energy to Cool (Q)
Kapton	1090 J/kgK	1.39×10^{-3} g	2 K	3.0 mJ
Steel Plate	461 J/kgK	1.05×10^{-2} g	2 K	9.5 mJ
Solder	173 J/kgK + 37 J/g^{+}	1.13×10^{-2} g	2 K	422 mJ^{+}
Steel Tendon	461 J/kgK	2.73×10^{-2} g	2 K	25.2 mJ
Copper Plate	385 J/kgK	3.62×10^{-2} g	2 K	27.8 mJ

$^{+}$Calculation includes heat of fusion.

It must be noted that the calculated heating and cooling times are for the first activation cycle. The initial temperatures for each step depend on the cycle number, as well as the time between cycles.

The cooling insights were addressed as follows:

1. The solidification energy was reduced by minimizing the amount of solder in the joint and decreasing the size of the low characteristic time joint components.
2. The ability of high characteristic time components to act as heat sinks is crucial to the cooling process given the high convection resistances. In SquishTendons, the heat sink was optimized by choosing a material with a high characteristic time. The addition of a copper plate on the face of the Teflon allowed for the input heat from the tendon to be distributed along the entirety of the Teflon surface area, avoiding hot-spots that would decrease the cooling heat transfer rate.

5.4.3.5 Overall Activation Cycle

The overall activation cycle was calculated by summing the heating and cooling times. Due to the addition of the copper plate on the face of the Teflon the heating time was recalculated. The melting energy increased by the amount of energy required to raise the temperature of the copper plate from room temperature to the solder's melting temperature. The updated heating time is 1.2 seconds. The first order models predict that the overall activation cycle time is 2.7 seconds.

5.4.4 FEA Model

An FEA model of a locking mechanism is useful for understanding the behavior of the mechanism during cycling. The model may also be used to further optimize the performance of the joint. In the case of SquishTendons, an FEA model was used to validate the first-order calculations. Figure 5.16 shows a CAD model highlighting the convection surfaces and the location of the heat power input into the locking mechanism. The analysis was setup up much like the one in Squishbot1. The thermostat was placed on the solder and was set to stop the heater power once the temperature of the solder reached 58°C, which is the liquidus temperature of the solder. The thermostat was set to turn the heater back on once the temperature reached the solidus temperature of the solder, 56°C. The heat of fusion was modeled as a spike in the heat capacity of the solder.

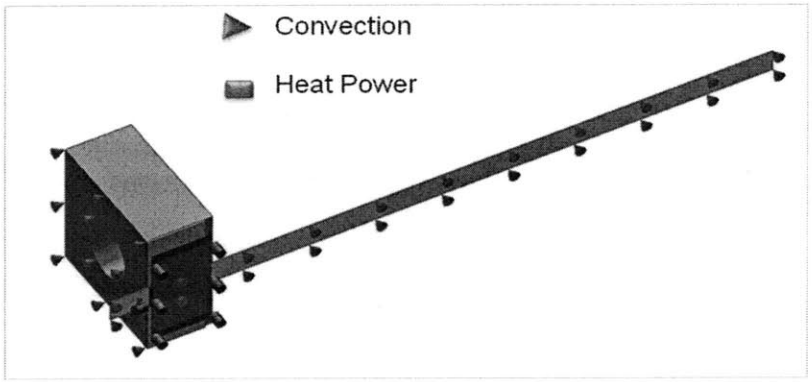

Figure 5.16: SquishTendons FEA model highlighting the heat power surfaces as well as the convective surfaces.

The model was run for three seconds with 0.05 second time steps. The temperature of the solder and a point on the Teflon were graphed versus time in Figure 5.17. The FEA results show the heating time is 1.25 seconds and the cooling time is 0.20 seconds. The discrepancy in the cooling time may be attributed to the fact that the length of Teflon affected by the heating was over estimated. As Figure 5.18 shows, only approximately 1/5 of the Teflon observes a temperature rise, as opposed to the estimated 2/5.

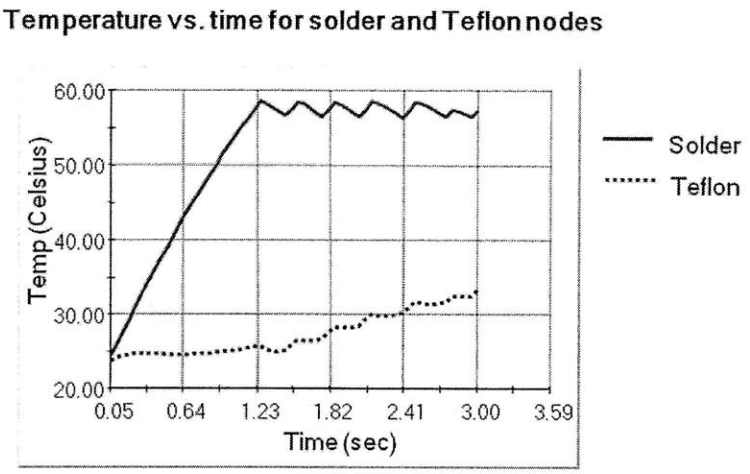

Figure 5.17: FEA thermal transient study temperature vs. time results for a SquishTendons active joint. Both plots represent the temperature at a particular node of the components.

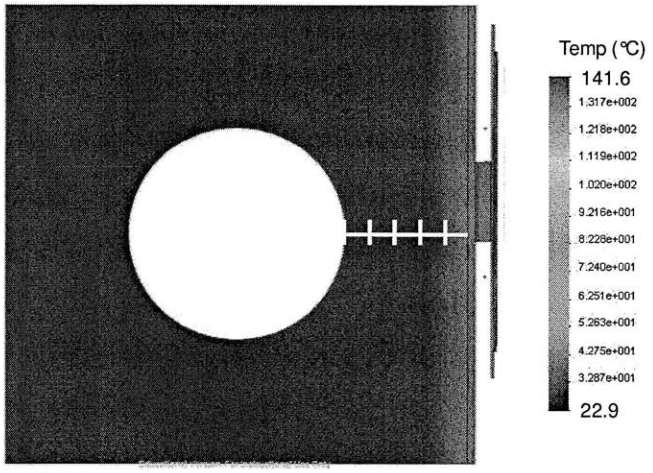

Figure 5.18: FEA results after heating cycle. Results show the temperature of a SquishTendons joint after solder reaches melting temperature. The scale highlights the length of the Teflon that observes an energy rise at the end of the heating cycle.

The FEA analysis captured several activation cycles of the mechanism. The second cycle's heating time is reduced because the starting temperature of the components is higher.

While the cooling time increases with cycle number as the Teflon absorbs more energy. Table 5.15 summarizes the results of the first four cycles.

Table 5.15: FEA heating and cooling times for four activation cycles.

Cycle #	Starting Temp. of solder & copper	Heating Time	Cooling Time
1	23°C	1.25 seconds	0.20 seconds
2	56°C	0.10 seconds	0.20 seconds
3	56°C	0.10 seconds	0.20 seconds
4	56°C	0.10 seconds	0.30 seconds

5.4.5 Experimental results

The final step was to compare both models to the actual mechanism performance. The experimental locking mechanism included the bottom base in addition to the locking mechanism components. The FEA and first-order models only included the locking mechanism components. Figure 5.19 shows the different parts of SquishTendons before assembly as well as the assembled testing mechanism. A single joint was activated and the overall cycle time was measured. The time between when the heater was turned on and when the joint unlocked was recorded as the heating time. The cooling time was measured from when the heater was disabled to when the solder solidified. Table 5.16 compares the first-order and FEA models to the experimental results.

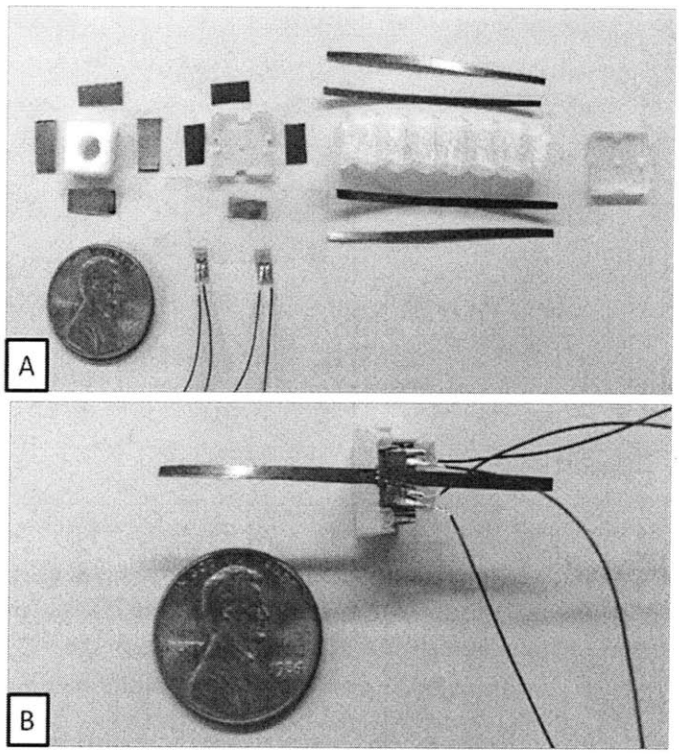

Figure 5.19: (A) SquishTendon joint parts and (B) assembled joint. The assembled joint was used to experimentally validate the first-order and FEA models.

Table 5.16: Model and experimental heating and cooling times for the first cycle of a SquishTendons joint.

	Heating Time	Cooling Time
First-order model	1.17 seconds	1.49 seconds
FEA model	1.25 seconds	0.20 seconds
Experimental	3.30 seconds	2.80 seconds

5.4.6 Validity of Models

The first-order model used the initial conditions to calculate the heating and cooling times for the joint. The FEA model takes into account that this problem is in fact transient, and as such the heat transfer rate to the different components depends on the elapsed time. This is the major difference between the two models. The first-order model result for the heating time is only 0.08 seconds off the FEA model estimate. The cooling time estimate differs by 1.29 seconds. The difference in cooling times may be due to overestimation of the Teflon resistance at the start of the cooling cycle in the first order model. This overestimate leads to a lower calculated heat transfer rate out of the joint and as a result, a longer predicted cooling time. The

FEA is limited by the size of the time step, which in this case was 0.05 seconds. The heat of fusion is incorporated into the FEA indirectly, and as a result the heat of fusion may be over- or under-estimated by the program. In this case the first order models and experimental results suggest the heat of fusion was not accounted for entirely in the FEA model.

The FEA and the first-order models are only as accurate as their inputs. In both cases several inputs were estimated including: (i) the convection coefficient, (ii) the thermal properties of the 60/40-ChipQuik combination, and (iii) the amount of solder in the joint. These estimates account in part for the differences between the modeled and measured times. In addition, the parts of the actual joint were glued together using super glue. The glue layers and the gaps between the components create a thermal resistance between each of the pieces. This resistance was not accounted for in either of the models. The largest discrepancy between the models and the actual joint is the amount of solder. Unfortunately, it is hard to control how much is used per joint and as a result the mass of solder varies from joint to joint. Finally, in the experimental setup the heater output was not controlled with a temperature sensor and as a result the temperature of the joints may have been lower or higher than the modeled temperatures.

Overall both the FEA and first order models provide a good estimate of the heating and cooling times of the joint. The first order models allow the designer to quickly calculate the order of magnitude of the performance of the joint. More importantly, the models provide insight as to what parameters determine the joint performance.

5.5 SquishTendons Performance

SquishTendons was designed using the complete set of rules and models presented in this thesis. As a result, it has an improved performance over the original Squishbot1 design. SquishTendons is able to reconfigure its joints in about 6 seconds, compared to Squishbot1 which requires over 10 seconds. The new tendon design is applicable to a variety of mechanism designs. SquishTendons implemented the tendon locking scheme to a compliant restoring structure. This new mechanism design is a step closer to the desired compliant cm-scale robots. Stacking SquishTendon modules would lead to a mechanism with a large number of DOF with a single actuator.

CHAPTER

6

CONCLUSIONS

6.1 Introduction

Compliant robotic mechanisms at the cm-scale are necessary for applications requiring travel through restricted paths. Search-and-rescue and military operations may use these robots to access dangerous, hard-to-reach places. Additionally, these mechanisms would be useful in medical applications where their compliance would make them less invasive. The challenge in creating these robots is that a compliant robot requires multiple actuatable DOF. Most current robotic designs require an actuator per DOF of the mechanism. At the cm-scale, robots may only afford to carry and power a couple motors, which limits their controllable DOF.

This thesis presents PCM-activated joints as a way to create single actuator, cm-scale, multi-DOF mechanisms. The active joints are locked in combinations that enable different one-DOF mechanism states. All of the mechanism states are actuated with a single motor with a simple control scheme. The multi-DOF nature of the resulting robots allows them to be more flexible in the variety of tasks that they may perform.

6.2 Summary

The successful design and implementation of solder-locking joints into mechanisms requires kinematic, mechanical, and thermal considerations. The design rules, insights, and models presented in this thesis enable the designer to optimize the performance of the active joints.

The design parameters and constraints of solder-activated joints are multi-domain and highly coupled. Therefore, this research focused on developing models, insights, and experimentation techniques, as opposed to intuition and repetition, for designing locking joints

efficiently. The resulting models and guidelines enable a designer to understand (i) the physics that dominate and limit joint performance, (ii) the selection and design requirements for PCMs, and (iii) the use of first-order models to set an initial joint geometry for specific performance characteristics. The first-order models highlight what parameters may be changed to minimize the energy consumption and the locking and unlocking times of the joints.

Active fluids enable the designer to lock the joints without any additional moving parts, which reduces the complexity of the mechanical joint design. These fluids are classified by the means used to cause a change in their rheological properties. The different types of active fluids were compared based on their strength, scalability, and speed. MR and ER fluids were eliminated because of their limited strength at small scales. PR fluids were discarded given their activation times are on the order of minutes. TR fluids provided the strength and scalability necessary to lock joints in cm-scale mechanisms. These fluids lock and unlock the joints through a phase change process. The phase change process may be prohibitively time and power intensive if the TR fluid is not chosen carefully.

Solder's strength and diffusivity make it the best active fluid for locking small joints. The solder interface is often stronger than the mm-scale joint components. As a result, some of the solder strength may be sacrificed, through alloying, to reduce its melting temperature. A decrease in melting temperature results in a decrease in the solder's melting energy. The ability to reduce the melting temperature of the solder is important given that small-scale heaters cannot easily achieve temperatures higher than 100°C. The reduced temperature raise helps protect the other joint materials as well. This thesis presents the details on how alloying may be used to decrease the melting temperature of lead-tin solders. The insights and methods used in this research may be applied to other types of solder. The first order models presented allow the designer to efficiently and effectively compared different solders based on their melting and solidification energies. The ability to compare solders effectively is important given the wide range of solders available to the designer.

This research introduces the designer to the mechanical properties of solder that are relevant for an active joint. The wetting and cycling abilities of a solder are discussed at length because they play a direct role in the joint performance. The phase-change cycling of the solder is particular to this application. As a result, there isn't much information available on the behavior of solders under these conditions. The cycling behavior is best determined through the

experimental setups provided in this thesis. Solutions to common oxidation problems are also presented. The insights and experiments provided enable the designer to narrow the available solders to those with satisfactory mechanical properties before embarking on the solder thermal design.

The design of the locking joints is complicated by the multi-domain nature of the design parameters. This thesis breaks the joint design into the three types of functional requirements: (i) kinematic, (ii) mechanical, and (iii) thermal. The kinematic design of the joint is approached using kinematic diagrams which highlight the constraints on the joint based on the mechanism design. These diagrams enable the designer to quickly decide the optimal location of the joints as well as the number of locking joints that are necessary to control a multi-DOF robot. Finally, rules are provided for determining the locking range of the joint.

The mechanical design section calculates the strength the strength of the joint and explores the fabrication and assembly constraints. Determining the locking strength of the joint is important because it determines the minimum size of the locking area. This information allows the designer to decrease the amount of solder in the joint without losing reliability. Fabrication and assembly considerations are critical given the mm-scale of these joints. The designer must understand the limitations of the available equipment. The insights provided emphasize the benefits of a simplifying the design of the locking mechanism.

The thermal performance of the joint is particular to locking joints and is therefore, described in detail. The transient nature of the problem makes detailed calculations and FEA models time and resource intensive. This thesis presents first order models that enable the designer to make the correct design decisions necessary to improve the performance of the joint. The first order models give order-of-magnitude estimates of the locking and unlocking times for a particular design. Most importantly, they highlight what parameters may be changed to reduce the joint's activation time.

The joint thermal design section uses thermal circuits to highlight the heat transfer modes within the joint. The circuits enable the designer to understand what limits the heat transfer in and out of the solder. This work discovered and exploited the heat-sink ability of high characteristic time components. The heat-sink components reduce the cooling times of the joint by at least one order of magnitude. This research utilized CosmosWorks FEA models and experimental results to corroborate the first order models.

The efficacy of the rules and models was demonstrated through two case studies. The first mechanism, Squishbot1, was designed and created to help develop the design guidelines presented in this thesis. Squishbot1 served as a proof-of-concept mechanism of the solder-locking joints approach. The mechanism is able to steer, crawl, and lift its front end using a single spooler motor. The entire robot is able to fit through a 1.5cm hole. Squishbot1 is able to reconfigure its joints in approximately 10 seconds.

Squisbot1 demonstrated the efficacy of thermal circuits as first order models for joint performance. The models were able to predict the heating and cooling times within an order of magnitude. The unlocking time was estimated within 1 second of the experimentally measured time. It was during the development of Squishbot1that the heat-sink ability of high characteristic time components was discovered. The Teflon in the joints resulted in a 13x reduction of the predicted solidification time. The performance of Squishbot1 also served to highlight when the insights and models had not been used to their full potential in the design of the mechanism.

To improve on the performance of Squishbot1, SquishTendons was designed and constructed utilizing the full set of models and rules. This time, the locking tendons and solder design of the second case study were optimized using the rules and models of this thesis. The resulting mechanism, therefore, has an improved performance over Squishbot1. SquishTendons uses solder-locking joints to control a compliant restoring structure into a variety of single-DOF mechanism states. It is able to reconstitute into a different one-DOF mechanism state in less than 6 seconds. The energy required to unlock a joint is less than 65% of the unlocking energy of Squishbot1.

The SquishTendons locking approach may be applied to a variety of structures. The tendons do not restrict the compliance of the structure and may, therefore, be considered a step closer to the desired cm-scale compliant robots. The insights and rules of this thesis were used to minimize the amount of solder used to lock the tendons without sacrificing reliability. The resulting joints therefore required a reduced amount of energy to be unlocked. The thermal design of the joint exploited the Teflon's heat-sink ability. The resulting cooling time is 16x less than the cooling time based on convection alone. The overall improved performance of SquishTendons demonstrates the value of the insights and models presented in this thesis.

These guidelines may be implemented into the design of active joints that may be used in a variety of mechanism designs. The use of solder-activated joints will enable these mechanisms

to achieve multiple-DOF with a reduced number of actuators. This under-actuated approach does not require a complex control scheme. Including fewer actuators results in (i) less power consumption, (ii) smaller volume, (iii) reduced weight, and (iv) lower cost. These improvements lead to mechanisms with improved performance in applications requiring small, compliant mechanisms. Some of these applications include military operations, search-and-rescue, pipe exploration, and medicine.

6.3 Future Work

This thesis demonstrated that first order models may be used to make design decisions to improve the performance of the joint. The models also provide accurate order of magnitude estimates of locking and unlocking times of solder-activated joints. In this research FEA models were used to corroborate the first order models. These finite element models incorporated the heat of fusion of the solder by making the specific heat capacity of solder temperature dependant. This approach allowed for the fusion energy to be incorporated into a SolidWorks model, however, the experimental results showed that the model under-estimated the heat of fusion of the solder. Despite this shortcoming the FEA models were useful in understanding the joint's thermal behavior. A better FEA model is needed for optimizing the joint performance. A ComSol model is being developed that will allow the designer to input the heat of fusion of the solder directly. The new model will, therefore, provide more accurate heating and cooling time estimates.

The locking tendons approach was demonstrated using the SquishTendons mechanism. The locking mechanism was never implemented into a robot. Future work will focus on implementing locking tendons to achieve a mechanism that may crawl and steer in 8 different directions using a single motor. The current design limits the locking area to ensure that the tendons are only locked in the compressed position. A future design could increase this locking area to allow the tendons to be locked at any state. The locked tendons would then help support shear loads on the structure. This load bearing capability would increase the tasks that the robot may perform. Locking the tendons in the extended position might be used to increase the restoring force of the structure for crawling. Finally the stacked modules approach may be implemented to create a robot with increased DOF.

REFERENCES

[1] M. Telleria, M. Hansen, D. Campbell, A. Servi, and M. Culpepper, "Modeling and implementation of solder-activated joints for single-actuator, centimeter-scale robotic mechanisms," *IEEE International Conf. on Robotics and Automation (ICRA), Anchorage*, AK, 2010.

[2] Vijayan K. Asari, Sanjiv Kumar, and Irwan M. Kassim, "A fully autonomous microrobotic endoscopy system," *Journal of Intelligent and Robotic Systems,* vol. 28, 325-341, 2000.

[3] Maria J. Telleria, Robert Panas, Martin L. Culpepper, "MR fluid activated spherical joint for precision orientation control," *24th American Society for Precision Engineering Annual Meeting*, Monterrey, CA, 2009.

[4] Giles Humpston and David M. Jacobson, *Principles of Soldering*. USA: ASM International, 2004.

[5] Howard H. Manko, *Solders and Soldering*, 2nd edition. USA: McGraw-Hill Book Company, 1979.

[6] AWS Committee on Brazing and Soldering, *Soldering Manual*. Miami, FL: American Welding Society, 1978.

[7] D. Ilic, M. Kilb, K. Holl, H.W. Prass, and E. Pytlik, "Recent progress in rechargeable nickel/metal hydride and lithium-ion miniature rechargeable batteries," *Journal of Power Sources,* vol. 80, 112-115, 1999.

[8] Takeshi Morita, Minoru Kurosawa, and Toshiro Higuchi, "An ultrasonic micromotor using a bending cylindrical transducer based on PZT thin film," *Sensors and Actuators A,* vol. 50, 75-80, 1995.

[9] David A. Henderson, "Novel piezomotor enables positive displacement microfluidic pump," *Presented at NSTI Nanotech,* 2007.

[10] John Speich and Michael Goldfarb, "A compliant-mechanism-based three degree-of-freedom manipulator for small-scale manipulation," *Robotica*, vol. 18, 95-104, 2000.

[11] H. B. Brown, Jr., J. M. Vande Weghe, C. A. Bererton, and P. K. Khosla, "Millibot trains for enhanced mobility," *IEEE/ASME Transactions on Mechatronics,* vol. 7, no. 4, 452-461, 2002.

[12] Yuuta Sugimaya, and Shinichi Hirai, "Crawling and jumping of deformable soft robot," *Proceedings of IEEE/RSJ International Conference on Intelligent Robots and Systems,* Sendai, Japa, 2004.

[13] H. Takonobu, K. Kodaira, and H. Takeda, "Water striders muscle arrangement-based robot," in *IEEE/RSJ International Conference on Intelligent Robots and Systems*, August 2005, pp. 1754-1759.

[14] Mark A. Thrasher, Ali R. Shahin, Peter H. Meckl, and James D. Jones "Efficiency analysis of shape memory alloy actuators", *Smart Material Structures,* vol. 3, 226-234, 1994.

[15] Mark W. Spong, "Underactuated mechanical systems". In B. Siciliano and K. P. Valavanis, editor, *Control Problems in Robotics and Automation,* Springer-Verlag, London, UK, 1997.

[16] Shih-Chi Chen, "A Six-Degree-of -Freedom Compliant Micro- Manipulator for Silicon Optical Bench", M.S. Thesis, MIT, 2003.
[17] Mark R. Jolly, Jonathan W. Bender, and J. David Carlson, "Properties and applications of commercial magnetorheological fluids," *Journal of Intelligent Material Systems and Structures,* vol. 10, no. 1, 5-13, 1999.
[18] Weijia Wen, XianXiang Huang, Shihe Yang, Kunquan Lu, and Ping Sheng, "The Giant Electrorheological Effect in Suspensions of Nanoparticles." *Nature* Materials, vol. 2, 727-730, 2003.
[19] Aimee M. Ketner, Rakesh Kumar, Tanner S. Davies, Patrick W. Elder, and Srinivasa R. Raghavan, "A Simple Class of Photorheological Fluids: Surfactant Solutions with Viscosity Tunable by Light." *Journal of the American Chemical Society*, vol. 129, no. 6, 1553-1559, 2007.
[20] C. Ted Lee, Jr., Kenneth A. Smith, and T. Alan Hatton, "Photoreversible Viscosity Changes and Gelation in Mixtures of Hydrophobically Modified Polyelectrolytes and Photosensitive Surfactants." *Macromolecules*, vol. 37, no. 14, 5397-5405, 2004.
[21] Incropera, DeWitt, Bergman, and Lavine, *Introduction to Heat Transfer*, 5th edition. USA: John Wiley & Sons, 2007.
[22] A. K. Malik, A. Ghosh, and G. Dittrich, *Kinematic Analysis and Synthesis of Mechanisms.* USA: CRC Press, Inc., 1994.
[23] Mills, A. F., *Heat and Mass Transfer.* Concord, MA: Irwin Inc., 1995.
[24] K. Morgan, R. W. Lewis, and O. C. ZienKiewicz, "An improved algorithm for heat conduction problems with phase change," *International Journal of Numerical Methods in Engineering,* vol. 12, 1191-1195, 1978.
[25] D. Moy and A. C. Anderson, "Use of commercial metallic strain gages as low temperature heaters," *Cryogenics*, vol. 23, no.6, 330-331, 1983.
[26] Defense Sciences Office. *Chemical robots program.* Retrieved from http://www.darpa.mil/dso/thrusts/materials/multfunmat/chembots/index.htm
[27] Indium Corporation of America, "Indium/Copper intermetallics," *Application Note 97747.*
[28] Peter A. Halverson, Larry L. Howell, and Spencer P. Magleby, "Tension-based multi-stable compliant rolling-contact elements," *Mechanism and Machine Theory*, vol. 45, 147-156, 2010.
[29] J. A. Haringx, "The cross-spring pivot as a constructional element," *Applied Science Research,* vol. A1, 313-332, 1949.
[30] Nadia Cheng, Genya Ishigami, et. all, "Design and analysis of a soft mobile robot composed of multiple thermally activated joints driven by a single actuator," *IEEE International Conf. on Robotics and Automation (ICRA), Anchorage*, AK, 2010.
[31] Paul Breedveld and Shigeo Hirose, "Design of steerable endoscopes to improve the visual perception of depth during laparoscopic surgery," *Journal of Mechanical Design,* vol. 126, no. 1, 2-5, 2004.
[32] Indium Corporation of America, "Soldering to Nitinol," *Application Note 97759.*
[33] Indium Corporation of America, "Soldering to aluminum," *Application Note 97744.*

APPENDIX

A

AVAILABLE CM-SCALE MOTORS

This appendix presents the information collected by Don Campbell from Boston Dynamics on the performance of off-the-shelf cm-scale motors. The data highlights that a cm-scale robot may only afford to carry a couple of actuators given the size and weight of the motors with over 1N of output force.

		Voltage (V)	phase-phase terminal resistance (ohms)	Output Power (W)	Efficiency (%)	Stall Torque (mNm) / Force (N)	Cont. Torque (mNm) / Force (N)	OD or side of square (mm)	Body Length (mm) *	Mass (g)	Output Force (N)
Maxon											
EC6	310599	6	12.5	1.2	43	0.509	0.232	6	21	2.8	6.25
EC6	250101	12	81.5	1.2	39	0.402	0.241	6	21	2.8	6.49
EC6 Flat	263800	1	68	0.03	22.5	0.0049	0.024	6	3.6	0.35	0.65
EC10	315171	12	1.12	8	80	16	1.2	10	26	13	32.31
EC10	315173	24	3.42	8	81	19.3	1.18	10	26	13	31.77
EC10 Flat	301999	5	52	0.2	29.9	0.176	0.163	10	4.25	0.81	4.39
EC13	305193	18	13.2	6	63	8.13	2.23	13	22	15	60.05
EC13	305199	24	8.93	12	73	23.7	4.79	13	36	25	128.98
RE6	349191	4.5	20.8	0.3	54.5	0.469	0.322	6	16	2.3	8.67
RE6	349192	6	37.2	0.3	54.4	0.465	0.321	6	16	2.3	8.64
RE8	347724	4.2	12.3	0.5	67.4	0.932	0.623	8	16	4.1	16.78
RE8	347725	6	28	0.5	66.3	0.857	0.616	8	16	4.1	16.59
RE8	347727	12	92.2	0.5	66.9	0.925	0.589	8	16	4.1	15.86
RE10	118383	3	8	0.75	67	1	0.789	10	17	7	21.25
RE10	118386	6	20.6	0.75	69	1.25	0.784	10	17	7	21.11
RE10	118397	12	114	0.75	67	1.01	0.746	10	17	7	20.09
RE10	256086	3	8	0.75	64	1	0.784	10	17	7	21.11
RE10	256089	6	20.6	0.75	66	1.25	0.777	10	17	7	20.92
RE10	256094	12	114	0.75	63	1.01	0.741	10	17	7	19.95
RE10	118392	3	2.08	1.5	76	3.12	1.48	10	25	10	39.85
RE10	118396	6	9.09	1.5	76	3.01	1.5	10	25	10	40.39
RE10	118400	12	33.3	1.5	77	3.24	1.54	10	25	10	41.47
RE10	256096	3	2.08	1.5	75	2.49	1.49	10	25	10	40.12
RE10	256101	6	9.09	1.5	76	3.01	1.5	10	25	10	40.39
RE10	256105	12	33.3	1.5	77	3.24	1.54	10	25	10	41.47
Amax12	265374	4.2	10.3	0.75	71	1.55	0.996	12	21	11	26.82
Amax12	265376	8	40.9	0.75	71	1.52	0.978	12	21	11	26.34
Amax12	265378	12	116	0.75	68	1.29	0.841	12	21	11	22.65
Amax12	265389	3	10.3	0.5	61	1.24	0.996	12	21	11	26.82
Amax12	268391	6	40.9	0.5	58	1.01	0.978	12	21	11	26.34

RE13	**118455**	3.6	10.9	0.75	64	1.68	1.25	13	20	15	33.66
RE13	**118458**	6	31.4	0.75	63	1.6	1.21	13	20	15	32.58
RE13	**118570**	3	1.81	1.5	44	3.17	1.06	13	25	15	28.54
RE13	**118576**	9	17.2	1.5	45	3.27	1.28	13	25	15	34.47
RE13	**118578**	12	31.4	1.5	44	3.13	1.25	13	15	15	33.66
RE13	**118512**	3.6	3.5	2	75	5.11	2.84	13	34	21	76.48
RE13	**118516**	7.2	14	2	75	5.27	2.93	13	34	21	78.90
RE13	**118520**	15	53.2	2	76	5.55	2.88	13	34	21	77.55
RE13	**118632**	6	2.19	3	67	11.1	2.35	13	37	23	63.28
RE13	**118634**	7.2	3.53	3	66	10.3	2.35	13	37	23	63.28
RE13	**118638**	15	14.1	3	67	11.1	2.44	13	37	23	65.70
REmax13	**268340**	1.5	1.84	0.75	65	1.6	0.892	13	21	15	24.02
REmax13	**268346**	4.8	17.2	0.75	66	1.77	1.31	13	21	15	35.28
REmax13	**268348**	6	31.4	0.75	65	1.6	0.78	13	21	15	21.00
REmax13	**268357**	3	2.22	2	75	5.35	1.82	13	32	24	49.01
REmax13	**268363**	7.2	14.1	2	75	5.24	2.68	13	32	24	72.17
REmax13	**268367**	15	53.3	2	76	5.53	2.64	13	32	24	71.09
Faulhaber/MicroMo/Smoovy/Arsape											
0308H003B		3	33.8	0.0063	16.5	0.017	0.014	3	8	0.33	0.38
0515G006B		6	15.8	0.43	34.7	0.43	0.2	5	15	1.5	5.39
1202H7.5BH		7.5	16	0.17	32	0.444	0.12	12	2	1.1	3.23
1202H012BH		12	70	0.254	37	0.26	0.12	12	2	1.1	3.23
0620K006B		6	9.1	1.56	57	0.73	0.37	6	20	2.5	9.96
0620K012B		12	59	1.58	55	0.58	0.37	6	20	2.5	9.96
1226S006B		6	2.3	9.6	68	7.19	2.2	12	26	13	59.24
1226S012B		12	5.3	9.3	69	9.21	2.2	12	26	13	59.24
0615N1.5S		1.5	3.9	0.12	52	0.24	0.11	6	15	2	2.96
0615N003S		3	16.2	0.12	50	0.22	0.11	6	15	2	2.96
0615N4.5S		4.5	37.7	0.11	50	0.22	0.11	6	15	2	2.96
0816N003S		3	11.5	0.17	52	0.41	0.15	8	16	3.5	4.04
0816N006S		6	47	0.16	51	0.4	0.15	8	16	3.5	4.04
0816N008S		8	75.7	0.18	50	0.4	0.15	8	16	3.5	4.04
1016N003G		3	8.7	0.24	63	0.64	0.48	10	16	6.5	12.93

1016N006G		6	20.1	0.42	67	0.87	0.48	10	16	6.5	12.93
1016N012G		12	12	0.36	68	0.82	0.48	10	16	6.5	12.93
1024N003S		3	2.3	0.97	79	2.69	1.28	10	24	8.8	34.47
1024N006S		6	10.8	0.81	78	2.34	1.28	10	24	8.8	34.47
1024N012S		12	31.6	1.11	79	2.89	1.28	10	24	8.8	34.47
1219N4.5G		4.5	10.7	0.46	74	1.14	0.6	12	19	11	16.16
1219N006G		6	17.6	0.49	73	1.17	0.6	12	19	11	16.16
1219N012G		12	69	0.5	72	1.19	0.6	12	19	11	16.16
1219N015G		15	131	0.41	70	0.95	0.6	12	19	11	16.16
1224N006S		6	6.6	1.3	78	3.69	1	12	24	13	26.93
1224N012S		12	26.8	1.3	78	3.6	1	12	24	13	26.93
1224N015S		15	42.3	1.3	78	3.62	1	12	24	13	26.93
1224N006SR		6	4.6	1.92	82	5.31	1.8	12	24	13.5	48.47
1224N012SR		12	18.2	1.95	83	5.43	1.8	12	24	13.5	48.47
1224N015SR		15	29.4	1.88	83	5.36	1.8	12	24	13.5	48.47
1319T006SR		6	8.26	1	66	2.91	1.3	13	19	12	35.01
1319T012SR		12	34.6	0.95	65	2.84	1.3	13	19	12	35.01
1319T024SR		24	119	1.1	66	2.89	1.3	13	19	12	35.01
1331T006SR		6	2.83	3.11	81	11.2	3.2	13	31	19	86.17
1331T012SR		12	13.7	2.57	80	9.9	3.2	13	31	19	86.17
1331T024SR		24	52.9	2.66	80	9.76	3.2	13	31	19	86.17
1336U006C		6	4	1.75	68	7.79	4	13	36	23	107.71
1336U012C		12	15.6	1.98	69	8.4	4	13	36	23	107.71
1336U024C		24	63.6	2.02	68	8.39	4	13	36	23	107.71
ADM0620-2R-V3		3	30				0.2	6	9.3	1.4	5.39
ADM0620-2R-V6		6	120				0.2	6	9.3	1.4	5.39
ADM1220-V2		2	4.4				2.4	12	18	9	64.63
ADM1220-V3		3	13				2.4	12	18	9	64.63
ADM1220-V6		6	48				2.4	12	18	9	64.63
ADM1220-V12		12	156				2.4	12	18	9	64.63
ADM1220S-V2		2	4.4				2.4	12	18	9	64.63
ADM1220S-V3		3	13				2.4	12	18	9	64.63
ADM1220S-V6		6	48				2.4	12	18	9	64.63
ADM1220S-V12		12	156				2.4	12	18	9	64.63
AM0820-V-3-18		3	18				0.65	8	14	3.3	17.50
AM0820-V-5-56		5	56				0.65	8	14	3.3	17.50
AM0820-A-0.225-7		2	7.3				0.65	8	14	3.3	17.50

AM1020-V-3-16	3	16				1.6	10	16	5.5	43.08
AM1020-V-6-65	6	65				1.6	10	16	5.5	43.08
AM1020-V-12-250	12	250				1.6	10	16	5.5	43.08
AM1020-A-0.25-8	2	8				1.6	10	16	5.5	43.08
AM1524-V-6-35	6	35				6	15	18	12	161.57
AM1524-V-12-150	12	150				6	15	18	12	161.57
AM1524-A-0.25-12.5	3.5	12.5				6	15	18	12	161.57
AM1524-A-0.45-3.6	2	3.6				6	15	18	12	161.57
LM1247-020-01		13.17			9.26	3.09	12.5		57	3.09
LM1247-080-01		13.17			9.4	3.13	12.5		74	3.13
Firgelli										
LS6	3				5	4	6.35	85		4.00
L12-xx-yy-06-z-w	6						18	50 + stroke	28 to 56	0.00
L12-xx-yy-12-z-w	12						18	50 + stroke	28 to 56	0.00
PQ-12-20-63-A	5					15	22	47 + stroke	19	15.00
PQ-12-20-30-A	5					6	22	47 + stroke	19	6.00
Portescap										
08G61-107	3	11.8	0.7		0.73	0.7	8	20	4.5	18.85
08G61-205C	9	64	0.7		1.01	0.87	8	20	4.5	23.43
08GS61-107	2	12.6	0.5		0.42	0.64	8	17	3.8	17.23
08GS61-105	4.5	30	0.5		0.59	0.64	8	17	3.8	17.23
08GS61-105C	6	48	0.5		0.64	0.66	8	17	3.8	17.77
13BC3C-E	10	22.5	1.7		1.8	1.6	13	28	19	43.08
13BC3C-H	10	14.8	1.7		1.8	1.6	13	28	19	43.08
13BC3C-K	10	10.4	1.6		1.8	1.5	13	28	19	40.39
13BC3C-P	10	5.6	1.7		1.9	1.7	13	28	19	45.78
B0512-050(A)	50	4.27	8		73.6	7.34	13	50	44	197.65
B0512-050(B)	50	17.2	8		73.6	7.34	13	50	44	197.65
P010-64020-02	4.2	20	1		2.6	1.85	11.25	20	9	49.82
P010-62003-02	1.8	3	1		2.6	1.85	11.25	20	9	49.82
NewScale Tech										0.00
SQL-1.5-6					0.2		1.55	6	0.15	0.00
SQL-1.8-6					0.3		1.82	6	0.16	0.00

SQL-3.4-10		100				2		3.4	10	1.7	0.00
SQ-100-N		200				5		12.46	20.57		0.00
SQL-M-1.8-3						0.3	0.15	4.3	13.5		0.15
SQL-M-3.4-4						2	1	7	17.5		1.00
Biometal Helix											
Helix 100			27			0.12		0.4	20		0.00
Helix 150			7.5			0.3		0.5	20		0.00
DPM				* power listed is at peak efficiency of motor for DPM			* cont. torque listed is at peak efficiency of motor for DPM				
JFF-M20S-8Z130		3		0.21	43	0.76	0.17	10	15	4	4.58
JFF-M20S-10100		2.4		0.23	47.7	0.86	0.18	10	15	4	4.85
JFF-M20S-7Z170		2		0.06	37	0.39	0.096	10	15	4	2.59
JFF-M20S-1260		1.5		0.28	43.4	0.62	0.2	10	15	4	5.39
JFF-N30PA-08180		3		0.079	40	0.7	0.16	12	20	7.5	4.31
JFF-N30PA-09210		2.5		0.074	44.8	0.8	0.18	12	20	7.5	4.85
JFF-N30PA-09140		3		0.17	55	1.1	0.26	12	20	7.5	7.00
JFF-N30PA-10140		4.5		0.417	56.9	1.7	0.4	12	20	7.5	10.77
JFF-N20PA-08260		4.8		0.268	43	1.1	0.24	12	15.5	5	6.46
JFF-N20PA-08260		5		0.273	43	1	0.24	12	15.5	5	6.46
JFF-N20PA-13115		2.4		0.35	44.2	1.3	0.28	12	15.5	5	7.54
JFF-N20PA-06310		5		0.137	39.2	0.625	0.2	12	15.5	5	5.39
Canon											
DN12M		5	12.5	0.28		1.15	0.29	12	20		7.81
DN12L		5	5.75	0.89		1.96	0.98	12	30		26.39
LN12		6	3.529411765	1.25		6.4	0.98	12.5	31	17	26.39
LN12 High Power		6	1.898734177	1.32		12.3	0.98	12.5	31	17	26.39

APPENDIX

B

MAXON RE-6 SPECIFICATION SHEET

This appendix contains the specification sheet for the motor used to actuate SquishBot1. The motor is manufactured by Maxon and has a 6mm diameter. The motor was integrated into a spooler mechanism designed by Boston Dynamics to exert 5N of pulling force on the string.

RE 6 ∅6 mm, Precious Metal Brushes, 0.3 Watt

NEW

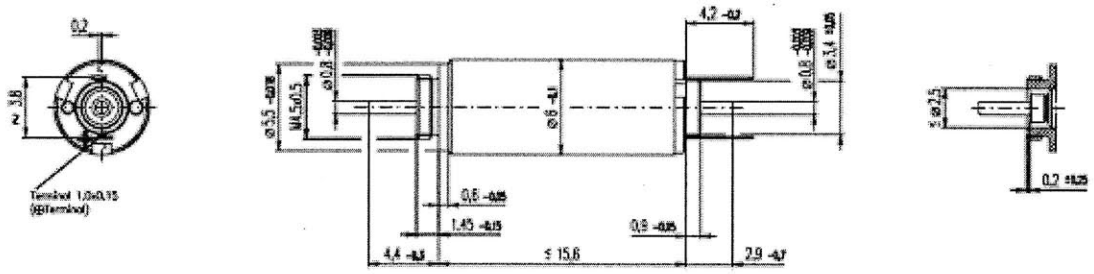

M 2.5:1

Stock program
Standard program
Special program (on request)

			Order Number			
			302018	302019	302020	302021
Motor Data (provisional)						
1	Assigned power rating	W	0.3	0.3	0.3	0.3
2	Nominal voltage	Volt	1.5	3	4.5	6
3	No load speed	rpm	20500	20700	20700	20700
4	Stall torque	mNm	0.368	0.426	0.412	0.409
5	Speed / torque gradient	rpm / mNm	60900	52600	54500	54900
6	No load current	mA	49.3	24.9	16.5	12.4
7	Starting current	mA	576	333	215	160
8	Terminal resistance	Ohm	2.61	9.0	21.0	37.5
9	Max. permissible speed	rpm	23500	23500	23500	23500
10	Max. continuous current	mA	445	239	157	117
11	Max. continuous torque	mNm	0.25	0.27	0.27	0.27
12	Max. power output at nominal voltage	mW	187	221	212	211
13	Max. efficiency	%	51	54	53	53
14	Torque constant	mNm / A	0.639	1.28	1.92	2.56
15	Speed constant	rpm / V	14900	7470	4980	3740
16	Mechanical time constant	ms	10	9	9	9
17	Rotor inertia	gcm²	0.015	0.017	0.016	0.016
18	Terminal inductance	mH	0.01	0.03	0.07	0.12
19	Thermal resistance housing-ambient	K / W	77	77	77	77
20	Thermal resistance rotor-housing	K / W	16.2	16.2	16.2	16.2
21	Thermal time constant windings	s	1.4	1.6	1.5	1.5

Specifications

- Axial play 0.02 - 0.1 mm
- Max. sleeve bearing loads
  axial (dynamic) 0.15 N
  radial (4 mm from flange) 0.6 N
  Force for press fits (static) 10 N
- Radial play sleeve bearing 0.012 mm
- Ambient temperature range -20 ... +65°C
- Max. rotor temperature +85°C
- Number of commutator segments 5
- Weight of motor 2.3 g
- 2 pole permanent magnet
- Ceramic shaft
- Values listed in the table are nominal.
  For applicable tolerances see page 43.
  For additional details please use the maxon selection program on the enclosed CD-ROM.

Operating Range

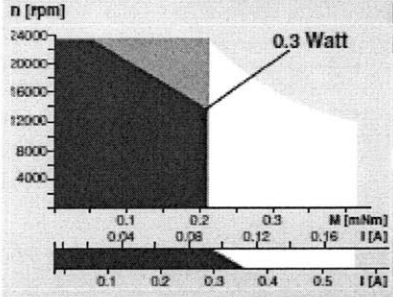

Comments

Details on page 49

Recommended operating range

Continuous operation
In observation of above listed thermal resistances (lines 19 and 20) the maximum permissible rotor temperature will be reached during continuous operation at 25°C ambient.
– Thermal limit.

Short term operation
The motor may be briefly overloaded (recurring).

302021 Motor with high resistance winding
302018 Motor with low resistance winding

maxon Modular System

Overview on page 17 - 21

Planetary Gearhead
Ø6 mm
0.005 - 0.06 Nm
Details page 193

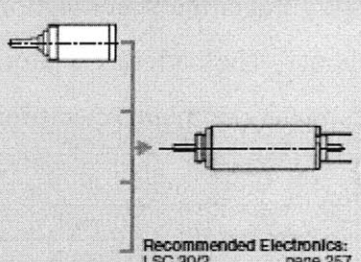

Recommended Electronics:
LSC 30/2 page 257
Notes 17

APPENDIX

C

BATTERY SPECIFICATION SHEET

This appendix contains the specification of the Guangzhou Markey batteries that were used to power Squishbot1. The batteries were chosen because of their size and capacities. Two batteries were used to power the motor, electronics, and heaters in Squishbot1.

No.	Item	Rated Performance		Remark
1	Rated Capacity	Typical	150mAh	Standard discharge（0.2C C_5A) after Standard charge
		Minimum	140mAh	
2	Nominal Voltage	3.7V		Mean Operation Voltage During Standard Discharge After Standard Charge
3	Voltage at end of Discharge	2.75V		Discharge Cut-off Voltage
4	Charging Voltage	4.2±0.03V		
5	AC (1KHz) Impedance New Cell Max.(mΩ)	≤350mΩ		
6	Standard charge	Constant Current 0.5C_5A Constant Voltage 4.2V 0.01 C_5A cut-off		Charge time : Approx 4.0h
7	Standard discharge	Constant current 0.2 C_5A end voltage2.75V		
8	Fast charge	Constant Current 1C_5A Constant Voltage 4.2V 0.01 C_5A cut-off		Charge time : Approx 2.5h
9	Fast discharge	Constant current 1 C_5A end voltage2.75V		
10	Maximum Continuous Charge Current	1 C_5A		
11	Maximum Continuous Discharge Current	1.5C_5A		
12	Operation Temperature Range	Charge: 0~45℃		60±25%R.H. Bare Cell
		Discharge: -20~60℃		
13	Storage Temperature Range	Less than 1 year: -20~25℃		60±25%R.H. at the shipment state
		less than 3 months: -20~40℃		
14	Weight	Approx 4g		Bare Cell
15	Cell Dimension	Length: Max.36mm		Bare Cell Initial Dimension
		Width: Max. 12.5mm		
		Thickness: Max. 5.2mm		

APPENDIX

D

TANGO+ PROPERTIES

This appendix contains the material properties of Tango+, a Connex 500 3D printer resin. This material was used to print the restoring structure used in SquishTendons. The material was chosen because of its compliance.

TangoPlus - FullCure930 / TangoBlackPlus - FullCure980

Property	ASTM	Metric		Imperial	
Tensile Strength at Break	D-412	MPa	1.5	psi	211
Modulus of Elasticity at 20% Strain	D-413	MPa	0.1	psi	21
Modulus of Elasticity at 30% Strain	D-414	MPa	0.2	psi	27
Modulus of Elasticity at 50% Strain	D-415	MPa	0.3	psi	38
Elongation at Break	D-412	%	218	%	218.0
Compressive Set	D-395	%	4	%	4.4
Shore A Hardness	D-2240	Scale A	27	Scale A	27
Ross Flex	D-1052		Above 150,000		Above 150,000
Tensile Tear Resistance	D-624	Kg/cm	3	Lb/in	20
Tg	DSC (-80°C+100°C)	°C	-10	°F	15